Molecular and physiological studies of phytochrome function in light direction sensing in *Physcomitrium patens*

Dissertation

zur Erlangung des akademischen Grades eines

Doktors der Naturwissenschaften (Dr. rer. nat.)

am Fachbereich Biologie und Chemie der

Justus-Liebig-Universität Gießen

vorgelegt von

Silvia Trogu

aus

Cagliari, Italy

Gießen 2023

Table of Contents

1. Introduction

1.1 Photoperception in plants

Light is essential for plant life; accordingly, perception of the light environment strongly influences plant development. As sessile organisms, plants have developed an assortment of photoreceptors for several parts of the light spectrum that enables them to perceive light quantity and quality, periodicity, direction, and polarization (Smith 2000). Phytochromes detect red (R) and far-red (FR) light (Borthwick et al. 1952), whereas cryptochromes (Ahmad et al. 1993), phototropins (Fankhauser et al. 2015), members of the ZEITLUPE (ZTL) family (Somers et al. 2000), and UV RESISTANCE LOCUS 8 (UVR8) (Rizzini et al. 2011) monitor the blue (B) and UV-B range of the spectrum. Members of all these photoreceptor families, except for ZTL, are conserved in both seed and non-seed plants (Imaizumi et al. 1999, Kasahara et al. 2004, Mittmann et al. 2004, Wolf et al. 2010). As will become apparent, phytochromes and phototropins are of particular importance in this project: their biology is summarized below.

1.2 Phytochrome

Phytochromes are particularly prominent photoreceptors in plants, regulating germination, flowering, and much in between, activating and repressing the transcription of thousands of genes: consequently, they are a major focus in plant research (Tepperman et al. 2004, Tepperman et al. 2006, Quail 2010). Although their photochemistry, function, and signal transduction mechanisms have been investigated extensively for nearly a century, these processes are still only partially understood (Cheng et al. 2021).

First detected directly in 1959 in plants (Butler et al. 1959), phytochromes are members of a more widespread family of photoreceptors that is also represented in cyanobacteria (Hughes et al. 1997) and other bacteria (Davis et al. 1999, Jiang et al. 1999), and even fungi (Valadon et al. 1979, Blumenstein et al. 2005, Froehlich et al. 2005).

Plant phytochromes promote and regulate numerous developmental processes throughout the life cycle. Starting from seed germination and photomorphogenesis (Flint et al. 1937, Borthwick et al. 1952, Cheng et al. 2021), phytochromes also control flowering via the circadian clock (Somers et al. 1998, Searle et al. 2004).

Plant phytochrome apoproteins are synthetized in the cytoplasm where they autocatalytically assemble with phytochromobilin (PΦB) produced in the chloroplast, the *A*-ring becoming covalently attached in the apoprotein to form the holophytochrome photoreceptor comprising two ~125 kDa monomers (Vierstra et al. 1982, Furuya et al. 1994, Terry et al. 1996).

Phytochromes exist in two parent states interconvertible by light, namely, the physiologically inactive Pr and the physiologically active Pfr. Pr absorbs maximally in the R region (λ_{max} ~660 nm), which triggers a *cis* to *trans* isomerization in the C15=C16 double bond between the *C* and *D* rings of the chromophore. The formation of short-lived intermediates with the consequent rearrangement of the protein backbone leads to Pfr, absorbing maximally in the FR (λ_{max} ~730 nm) (Eilfeld et al. 1985). Both states also absorb more weakly in the UV/A-blue region (Furuya et al. 1994). Pfr is converted back to Pr upon absorption of FR or by a slower thermal process called dark reversion (Legris et al. 2019). Pfr absorption overlaps that of Pr in the R region, so that even at $Pr_{\lambda max}$ some of the Pfr formed is reconverted back to Pr. Therefore, under continuous R conditions, an equilibrium between the two states Pr and Pfr is established (Hsiao et al. 1984, Mancinelli 1994). Plant development is also regulated by changes in light quality, in particular due to shading by other plants, leading to a low R:FR ratio which favours photoconversion to Pr. This allows ruderal species to initiate a set of developmental responses

called the shade avoidance syndrome in order to reach unfiltered daylight and overtop competitors (Smith et al. 1997, Paik et al. 2019).
In *Arabidopsis thaliana* five phytochromes are known, encoded by *PHYA* to *PHYE*. The family is classified into two groups (I and II) according to their stability in light (Sharrock et al. 1989). phyA is the only type I (light labile) phytochrome and is most abundant in dark-grown seedlings, whereas its levels drop quickly upon exposure to R or white light due to polyubiquitination of Pfr by COP1 and consequent degradation by the 26S proteasome (Deng et al. 1991, Shinomura et al. 1996, Seo et al. 2004). phyB to phyE are all type II (light stable) phytochromes, whereby phyB is the most abundant (Sharrock et al. 2002).

1.2.1 Structure and function

Phytochromes typically comprise a photosensory module (PSM) formed by sequential nPAS, GAF and PHY domains, followed by a PAS repeat domain (PRD) and the histidine kinase-related domain (HKRD) at the C-terminus. The bilin chromophore is attached to a conserved cysteine in the GAF domain (Hughes 2010). Most prokaryotic phytochromes act as histidine kinases in two-component signalling systems involving histidine autophosphorylation and subsequent phosphotransfer to a response regulator. In plant phytochromes, the HKRD lacks the conserved histidine residue necessary for function as canonical histidine kinase (Rockwell et al. 2020). Thus, the HKRD is currently thought to be responsible for dimerization, Pfr-dependent proteolysis, nuclear localization and nuclear photobody (see below) formation (Cheng et al. 2021). Recently, two very different cryo-EM based models of the *Arabidopsis* phyA and phyB dimers as Pr were published. phyA was modelled as a head-to-head homodimer resembling prokaryotic phytochromes, whereas phyB showed instead an unexpected asymmetric mushroom-like structure, which offers a large platform to accommodate various binding partners (Wahlgren et al. 2021, Li et al. 2022).

1.2.2 Localization and signalling mechanism

As already mentioned, phytochromes are synthetized in the cytoplasm as Pr (Pratt et al. 1971, Coleman et al. 1974). Following photoconversion, Pfr is translocated into the nucleus to initiate the light responses, but even this initial step is far from being understood.
The mechanism of phyB nuclear transport is unclear. Since phyB does not contain a nuclear localisation signal (NLS), Pfeiffer et al. proposed that phyB, as Pfr, can be translocated into the nucleus via physical interaction with transcription factors PIFs and/or perhaps other phyB-interacting proteins bearing an NLS sequence. (Pfeiffer et al. 2012). This hypothesis seems to be indirectly supported by a later study showing Pfr-phyB nuclear accumulation being facilitated by the interaction with SPA1 (Zheng et al. 2013). However, one might wonder why this effect is not also found for phyA, which also binds several PIFs like Pfr, but uses a different nuclear importing system.
phyA appears to have an NLS (Nagano et al. 2020), but its nuclear accumulation occurs via association with FHY1. The complex is guided into the nucleus by the action of the NLS present in FHY1, which is recognized by importin α (IMPα) to be then transported along the actin cytoskeleton to the nucleus. (Hiltbrunner et al. 2005, Hiltbrunner et al. 2006, Rosler et al. 2007, Helizon et al. 2018).
Upon import into the nucleus, both phyA and phyB co-localize with downstream signalling components into discrete subnuclear foci known as photobodies or speckles (Sakamoto et al.

1996, Kircher et al. 1999). Photobodies seem to be involved in the regulation of phytochrome-mediated signalling and physiological outputs (Paik et al. 2017, Ronald et al. 2019). However, it has been shown that the isolated phyB photosensory module, when dimerised and localised in the nucleus, generates at least a partial Pfr signal but no speckles (Matsushita et al. 2003). It is clear that the exact functions, composition, and biogenesis of photobodies are still not fully understood. A recent study on phyB photobodies suggests their formation being the result of liquid-liquid phase separation, a process through which a solution separates into two or more distinct coexisting liquid phases (Chen et al. 2022, Lee et al. 2022).

The light signals sensed by phytochromes are transduced to downstream signalling molecules that alter the expression of target genes, finally leading to physiological responses at the cell, organ and whole-plant levels (Quail 2002). These belong to different types of transcription factors (TFs) and play a crucial role in plant development: bHLH-family members (PIFs, HFR1, HEC, and PAR1), basic leucine zipper TFs (HY5 and HYH), transposon derived TFs (FHY3, FAR1, FRS), myb-domain containing TFs (MYB30 and LAF1), B-BOX-containing TFs (BBX4, BBX20, BBX21, BBX22, BBX24 and BBX25), tandem zinc finger PLUS3 (TZP), EIN3 and EIN3-LIKE 1 (Cheng et al. 2021).

Logically, these interactions take place in the nucleus. Nevertheless, significant proportions of phyA and phyB remain in the cytoplasm as Pfr. Cytoplasmic phytochrome has been associated with changes in translation triggered by light (Liu et al. 2012). Indeed, Paik *et al.* reported that both phyA and phyB interact with the cytosolic PENTA1 (PNT1) protein to repress the translation of protochlorophyllide reductase A (PORA) mRNAs. Moreover, physiological responses mediated by *Arabidopsis* phyA are still present even when nuclear translocation is blocked, suggesting an active role of Pfr in the cytoplasm (Rosler et al. 2007, Kami et al. 2012). Cytoplasmic *Arabidopsis* phyA was also recently shown to regulate the release and consequent translation of halted mRNAs from processing bodies (cytoplasmic granules formed by phase separation) (Schwenk et al. 2022). In de-etiolated *Arabidopsis* seedlings light activated phyA and cryptochrome were shown to modulate translation indirectly through the COP1-mediated auxin signalling pathway (Chen et al. 2018). *Arabidopsis* phytochromes also regulate alternative pre-mRNA splicing in response to red light by directly interacting with different splicing factors (Shikata et al. 2014, Xin et al. 2017, Xin et al. 2019, Dong et al. 2020, Yan et al. 2022). As it will be described in this thesis, these effects are, however, only part of the cytoplasmic phytochrome story.

1.3 Phototropin

In higher plants, phototropin photoreceptors mediate directional growth towards light (phototropism), stomatal opening and chloroplast movement. Darwin reported the effect of light on growth direction in his "Power of movement in plants", but it was not until the power of molecular genetics was brought to bear that the photoreceptor was identified (Liscum et al. 1995, Briggs et al. 2001, Briggs et al. 2002, Briggs 2006).

Phototropins are serine/threonine kinases that undergo autophosphorylation in response to UV/blue light irradiation. Phototropins have two light–oxygen–voltage (LOV) domains, named LOV1 and LOV2, and a C-terminal protein kinase domain responsible for propagating the light signal within the cell. Blue light is absorbed by two flavin chromophores (FMN). In darkness, FMNs are bound non-covalently within the LOV domains. Upon blue light irradiation, a covalent

adduct is formed between the FMN chromophore and a nearby conserved cysteine residue. While the function of the LOV1 domain is still unclear, extensive biochemical and biophysical studies shows that LOV2 represses kinase activity in darkness, which is released by the light-inducing disordering of two helices, A'α and Jα, that in turn interact with the kinase domain resulting in receptor autophosphorylation and initiation of the phototropic signal. After illumination ends, the covalent photo-adduct between the flavin chromophore and the cysteine residue decays on the timescale of seconds to hours, returning the domain to its original inactive state with a folded, noncovalently attached chromophore (Hart et al. 2021).

Probably all seed plants contain two phototropins, phot1 and phot2 (Christie et al. 2015). phot1 functions primarily as the photoreceptor for root and hypocotyl phototropism over a broad range of blue light fluence rates (Kutschera et al. 2012, Christie et al. 2015). On the other hand, the action of phot2 in hypocotyl phototropism is restricted to high fluence rates, owing largely to light-mediated increases in protein abundance (Sakai et al. 2001, Christie et al. 2015).

There is presently no crystal structure for a complete phototropin. However, recent small-angle X-ray scattering (SAXS) combined with low resolution molecular modelling have provided insights into the structure of the photoreceptor. In *Arabidopsis*, LOV2-kinase from phot1 and full-length phot2 structural modelling from SAXS data supports a head-to-head dimer mediated by LOV1 (in the full-length molecule) or LOV2 (in LOV2-kinase) (Oide et al. 2016, Oide et al. 2018). Insights into the global structural changes that occur during photoexcitation have also been gained from these data. The N-terminal photosensory region of phototropin (comprising LOV1 and LOV2) is thought to form a closed and inactive conformation with the C-terminal kinase domain in the dark, in which LOV2 acts with adjacent regulatory sequences to repress phototropin kinase activity. Blue light triggers the formation of a covalent adduct between the FMN chromophore and a conserved cysteine residue within LOV2. Adduct formation results in side-chain rotation of an adjacent glutamine residue (Q575) and altered hydrogen bonding with the FMN chromophore. Side-chain rotation of this glutamine is proposed to induce structural changes within the β-sheet surface, leading to displacement and unfolding of the Jα helix flanking the C-terminus of the LOV2 core. Displacement of the Jα helix leads to opening of the catalytic cleft between the N- and C-terminal lobes of the kinase domain to promote ATP binding and initiate receptor autophosphorylation (Christie et al. 2015).

Both phot1 and phot2 are soluble proteins, yet *in planta* studies have shown that are predominantly localized at the plasma membrane (Sakamoto 2002, Kong et al. 2006). Their mode of membrane attachment is still not clearly defined and may involve a still unknown protein partner presumably providing an anchor function.

1.3.1 Stomatal opening

Stomata provide for CO_2 uptake for photosynthesis while restricting water loss through transpiration. Stomatal opening is driven by the swelling of the paired guard cells in response to B light and is mediated by phototropins. This swelling is achieved by increased turgor pressure in guard cells, which is induced by hyperpolarization of the plasma membrane and subsequent K^+ uptake via inward-rectifying K^+ channels. Membrane hyperpolarization is generated by activation of the guard cell plasma membrane H^+-ATPase. The H^+-ATPase is activated in a phototropin-dependent manner by phosphorylation of its C-terminus and subsequent binding of 14-3-3 proteins. Phototropin autophosphorylation leads to H^+-ATPase

activation via BLUS1 activity, a kinase specifically expressed in guard cells. A Raf-like kinase BHP and protein phosphatase 1 (PP1) act as positive regulators of the signalling pathway linking BLUS1 to the H^+-ATPase. However, the signalling events that bridge the photoreceptors and the activation of H^+-ATPase, like the identity of the kinase responsible for its phosphorylation, remain elusive (Inoue et al. 2017).

1.3.2 Chloroplast movement

In order to optimize photosynthesis (maximal light uptake while avoiding photodamage), chloroplasts move to appropriate locations according to ambient light conditions. Chloroplasts relocate towards areas of cells illuminated with low light to maximise light capture (the accumulation response), whereas they escape from the strong light to minimise photodamage (the avoidance response). In most plant species, this response is B light specific and mediated by phototropins (Kinoshita et al. 2001). In *Arabidopsis thaliana* both phot1 and phot2 redundantly mediate the accumulation response, but phot2 predominantly mediates the avoidance response. However, the exact mechanism used by phototropins to regulate the accumulation and avoidance responses remains to be elucidated (Łabuz et al. 2022).
It is known, though, that chloroplast movement is dependent on actin filaments. *In vivo* imaging of actin filaments in *Arabidopsis* revealed that short acting filaments (cp-actin filaments) surrounding stationary chloroplasts are responsible for their movements according to light intensity. In response to strong B light, cp-actin filaments first transiently disappear and then gradually accumulate on chloroplast's front region to allow its movement away from strong light. Weak B light induces cp-actin filament accumulation on the front region without their initial disappearance. B light regulation of cp-actin filaments is dependent on phototropin. phot2 in particular, is a key regulator of their reorganisation under strong light conditions (Suetsugu et al. 2020).

1.3.3 Phototropism

Phototropism enables plants to regulate stem curvature to position leaves for favourable light absorbance. In seed plants, phototropism is induced by UV/blue wavelengths and mediated by phototropins.
Activation of phototropins by lateral light induces a suite of events which creates a gradient of the growth hormone auxin across the elongation zone of the shoot, thereby leading to curvature towards the light. Although early signalling components involved in phototropism have been identified, the signalling events that follow phototropin activation and lead to the establishment of the auxin gradient are still unclear. NPH3 and RPT2, both located at the plasma membrane, were found to interact with phot1 and are essential for phototropism. NPH3 is rapidly dephosphorylated in B light in a phot1-dependent manner, an event which is modulated by RPT2. The PKS family of proteins are also considered as early signal transducers required for phototropism, among which PKS4 is a direct target of phot1 phosphorylation (Christie et al. 2015). Presumably, the hypothetical membrane anchor mentioned above is also a component of the signalling complex.
Auxin transport is brought about by the PIN protein family, mostly basipetally by PIN1 and laterally by PIN3. In a still unclear way, photoactivated phototropin regulates the activity of PIN3 to transport auxin towards the shaded side of the shoot tip. Auxin is then translocated

basipetally via PIN1 to the elongation zone of the shoot. This leads to cell wall acidification through activation of H^+-ATPases in the plasma membrane, increased cell wall plasticity through pH-dependent expansin activity and thus turgor-driven cell extension at the shaded side of the hypocotyl or coleoptile. The result is phototropic curvature (Fankhauser et al. 2015).

1.4 The model organism *Physcomitrium patens*

Due to their simple morphology and a phylogenetic position as a sister linage to seed plants, bryophytes have been used extensively in studying basic processes in plant development (Naramoto et al. 2022). Early genetic investigations used mosses extensively after it was discovered that, unlike seed plants, the predominant phase of the life cycle is the haploid gametophyte, and therefore that mutant phenotypes are directly visible without the need of selfing to gain homozygous lines (von Wettstein 1924, Rensing et al. 2020). More recently, the ability to modify specific sites in the genome of *Physcomitrium patens* ("Physcomitrella") by homologous recombination - a frequent event in most organisms except higher plants - has made this moss useful for investigating molecular function in the plant kingdom (Schaefer et al. 1997). Largely because of these features, the Physcomitrella genome was sequenced, establishing it as a model organism (Rensing et al. 2008, Lang et al. 2018, Rensing et al. 2020). More recently, as described here, CRISPR/Cas9 methods have been added to the Physcomitrella genetic toolbox (Lopez-Obando et al. 2016, Nomura et al. 2016, Ermert et al. 2019, Trogu et al. 2021).

1.4.1 Phytochrome in *P. patens*

P. patens genome encodes seven phytochrome genes: *PHY1* to *PHY4* (Mittmann et al. 2004) as well as the *PHY5a* to *PHY5c* clade (Rensing et al. 2008), more than known in any other species to-date, reflecting whole genome duplication (Li et al. 2015). Physcomitrella phytochromes (*Pp*.PHYs) have plant-typical domain organization (Kolukisaoglu et al. 1993) and show expression patterns reminiscent of *Arabidopsis* phyA and phyB (Mittmann et al. 2004). In the moss *Ceratodon purpureus*, an additional atypical presumptive phytochrome (*Cp.PHY1*) containing a putative C-terminal tyrosine kinase-like domain is present (Thümmler et al. 1992, Hughes et al. 1996). Physcomitrella phytochromes elicit numerous physiological responses including many paralleling those in as well as effects that are unknown in but not necessarily absent from higher plants. Also as in higher plants, sub-populations of *Pp*.phy1 to *Pp*.phy4 and *Pp*.phy5a accumulate in the nucleus upon activation by light, with at least *Pp*.phy1 nuclear import depending on *Pp*.FHY1 (Jaedicke et al. 2012, Possart et al. 2013, Inoue et al. 2016). In particular, *Pp*.phy4, *Pp*.phy2 and *Pp.*phy1 in Pfr were shown to interact with PIF homologs, suggesting a role in regulating gene expression similar to that in seed plants (Possart et al. 2017). In line with this, all four *Pp*.PIF homologs are active when expressed in the *Arabidopsis* pifQ mutant (that is deficient in several PIFs), providing evidence for a similar role in phytochrome downstream signalling in Physcomitrella (Xu et al. 2017). Single PHY and PIF homologs are also present in the liverwort *Marchantia polymorpha*. *Mp*.PIF was shown to accumulate in darkness and to be rapidly degraded in a R-light dependent manner by interaction with activated *Mp*.PHY (Inoue et al. 2016). It is thus likely that PIF-mediated phytochrome signalling existed at the time in evolution even before the bryophyte and

spermatophyte land-plant lineages separated. Other than interacting with PIFs in the nucleus, *Pp*.phy4 participates in regulation of light-responsive alternative splicing directly interacting with splicing regulators PphnRNP-H1 and PphnRNP-F1 in the nucleus (Wu et al. 2014, Shih et al. 2019, Lin et al. 2020).

1.4.2 Phototropin in *P. patens*

In Physcomitrella four phototropin genes (PHOTA1, PHOTA2, PHOTB1, PHOTB2) were initially identified in the genome (Rensing et al. 2008), PHOTA3 has been added to the database subsequently. Their domain organization is identical to that seen in higher plants. They mediate chloroplast movement and side branch formation in blue light (Kasahara et al. 2004). Recently, it was shown that Physcomitrella phototropins (*Pp*.phots) are able to restore the phototropic response to B light when expressed in the *Arabidopsis* phototropin-deficient mutant, implying that the action mechanism is conserved (Kimura et al. 2018).

1.4.3 Directional sensing in non-seed plants

Physcomitrella spores germinate to produce cell filaments known as protonemata. These grow to form a branching, exploratory network of either chloroplast-rich chloronemata or elongated caulonemata, principally according to light and nitrogen availability. Subsequently, specialized side-branch initials appear that undergo a more complex three-dimensional division pattern to form buds that grow into erect, foliate gametophores (Rensing et al. 2020). Protonemata grow towards the light, superficially a similar response to that seen in seed plants and seedlings. The physiology is, however, quite different – and rather intriguing. Firstly, protonemata are single cells, not multicellular organs within which phytohormones can be translocated. Secondly, directional responses are not to B light via phototropin but to R light via phytochrome. These facts have considerable implications.
It is important to recognize that phototropic responses are not only dependent upon light for their induction but also require the transmission of vectorial (that is, directional) information. As described above (see 1.2 and 1.4.1), phytochrome controls the transcription of numerous nuclear genes: unquestionably however, gene regulation cannot transmit vectorial information (for review see (Hughes 2013)). It has been shown that in moss spore germination and protoplast regeneration, cell outgrowth occurs in the direction of the light or perpendicular to the electrical vector (E-vector) of polarized R light (Burgess et al. 1981, Cove et al. 1996). Similarly, protonemal tip cells grow perpendicular to the orientation of the E-vector under polarised R light. (Mittmann et al. 2004). How can any of this happen if phytochrome only controls gene expression? This problem has been studied from numerous perspectives which will be discussed in the following paragraphs.

1.4.3.1 Optics in light directional sensing and the Jaffe/Etzold/Haupt hypothesis

In a single cell, like protonemata, unilateral light direction might be perceived either via attenuation or by a lens effect (refraction) (Hughes 2013). In the case of perception of light direction by attenuation, when the light beam passes through the plant cell, the internal photon fluence rate decreases from the front, where the light enters the cell, to the rear, due to absorption from pigments and scattering (Fig. 1a). In the case of a lens

effect, the light is focused across the cell to a small area on the distal side (Fig. 1b). This is possible because the cytoplasm has a higher refractive index than air (or even water) (Kraml 1994). Lensing effects are implicated in light directional sensing in *Phycomyces* sporangiophore (Banbury 1952, Shropshire 1962, Bergman et al. 1969) and *Synecocystis* (Schuergers et al. 2016). In particular, it was shown that this cyanobacterium uses micro-optics to sense light direction and regulate consequent phototaxis (Schuergers et al. 2016). At this small scale (the *Synecocystis* cell has a diameter of *ca*. 3µm) diffraction effects might be significant too (Chen et al. 2004, Heifetz et al. 2009, Horiuchi 2012).

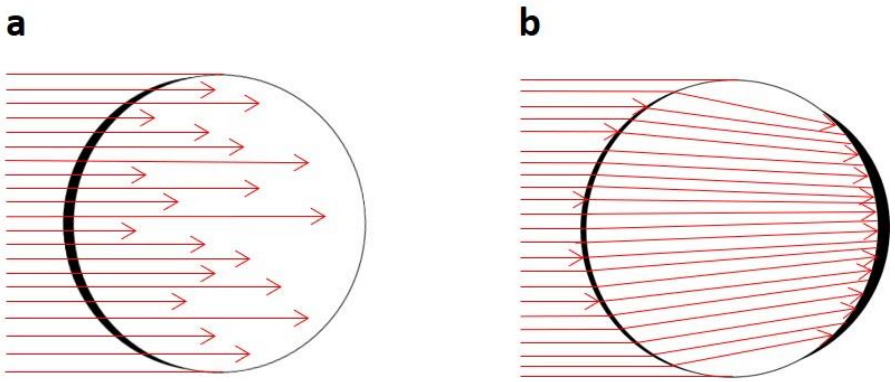

Fig. 1 Schematic of the light paths through a cell irradiated by unilateral, collimated light. a Attenuation; **b** Lens effect. The thickness of the black lines indicates the differences in photon fluence rate at the periphery of the cell.

With either attenuation or a lens effect, light directional could be perceived via different fluences rates in different regions of the cell periphery. How might such fluence rate differences be detected by phytochrome, perhaps via a Pfr gradient? Firstly, the relevant phytochrome molecules must be located at the periphery of the cell. Secondly, their diffusion (freedom of movement) must be restricted, since intermittent light pulses can also induce tropic effects ((Mittmann et al. 2004) see also 4.4.2 below). While this view conflicts with the idea of Pfr as a nuclear transcriptional regulator, it was thought for many years that phytochrome indeed acts as though it is fixed at the plasma membrane (Hughes 2013). This is the Jaffe/Etzold/Haupt model, primarily based on experiments involving chloroplast movement in the zygnemal alga *Mougeotia scalaris* (Haupt 1959, Haupt 1960). In dichroic photoreceptors (like phytochrome), light absorption occurs under preferred E-vector orientations in relation to the electronic transition dipole moment (TDM) of their chromophore: if the E-vector of the exciting beam is parallel to the TDM, the probability for absorption of the incident photon is very high; the probability is very low when the E-vector is perpendicular to the TDM. According to the Jaffe/Etzold/Haupt model, phytochromes are somehow attached at the plasma membrane with the TDMs of Pr oriented parallel to the cell surface. Upon photoconversion to Pfr the TDMs are rotated 90° to become perpendicular to the cell surface (Kadota et al. 1982, Sundqvist et al. 1983, Hughes 2013). This flip-flop dichroism would produce a gradient of Pfr at the surface of a cylindrical cell and might help to

explain even photo- and polarotropism in moss filaments (Haupt 1960, Etzold 1965, Haupt 1970, Hughes 2013).

1.4.3.2 Phytochrome-mediated phototropism

The phototropic reaction in protonemata does not involve lateral cell wall stretching as in higher plants but rather a reorientation of tip cell growth brought about by the rearrangement of the cytoskeleton. In the moss *Ceratodon purpureus*, cytoskeleton inhibitors revealed that actin microfilaments (rather than microtubuli) play a central role. The reaction is rather fast: within 5 minutes of unilateral irradiation, microfilament arrangement becomes loose and the tip starts to expand during the initial "bulging" phase. The actin bundles remain predominantly tip-oriented, whereas the apical bundle-free zone extends slightly. After 10 minutes of irradiation, the actin bundles of the apical dome reorient towards the irradiated apical flank converging towards a small area. After 20 minutes, the reoriented bundles elongate and the convergence disappears, rather forming a hem around what appears now as an empty central region. Finally, after about 30 minutes a new out-growth centre becomes apparent, seemingly established through a directionally-translocated hem/gap structure (Meske et al. 1995, Meske et al. 1996).
In Physcomitrella, knockout lines lacking subunits of the ARP2/3-complex showed severe defects in protoplast regeneration and polar tip growth, together with a compromised response to polarized light (Perroud et al. 2006). As the ARP2/3-complex is the centre of actin filament polymerization, these effects support the notion that directional growth is somehow steered by phytochrome-mediated effects on microfilament initiation. Further studies revealed that the site of actin polymerization is also the target of polymerizing cytoplasmic microtubules, contrary to what was observed by Meske *et al.* These results also showed interesting similarities between cytokinesis and tip growth. In both cases the microtubules are immersed in a meshwork of actin filaments and both are sites of heavy membrane trafficking of vesicles carrying cell wall material (Vidali et al. 2010, Wu et al. 2018). Recently, Bao *et al.* showed that Pp.CDKA in Physcomitrella is involved in the control of photo-, polarotropism and chloroplast movements, possibly by influencing the cytoskeleton organization independently of the cell cycle (Bao et al. 2022).

Phytochromes in Physcomitrella have been summarized above. Although a non-canonical phytochrome in *Ceratodon purpureus* was suggested to mediate phototropism (Thümmler et al. 1992, Algarra et al. 1993), no homolog exists in Physcomitrella. On the contrary, Mittmann and co-workers successively cloned four canonical phytochrome genes in Physcomitrella, showing that *Pp.*phy1 & -3 and *Pp*.phy2 & -4 were closely related both at the sequence level and physiologically, therefore probably representing siblings derived from genome duplication (Mittmann et al. 2004). They targeted each gene to generate knockout lines, revealing a clear phototropic deficiency in *phy4*$^{-}$, implying that primarily phy4 was responsible for mediating this phototropism in wild type protonemata. As no aspect of the phy4 sequence implied a functionality beyond that of higher plant phytochromes, this raised the possibility that these functions might be conserved and even be of general significance (Mittmann et al. 2004).
Jaedicke *et al.* showed on the basis of yeast two-hybrid (Y2H), co-immunoprecipitation and split-YFP studies that a subpopulation of phy4 interacts with phototropins at the plasma

membrane (Jaedicke et al. 2012). This discovery was quite remarkable in several respects. As described above (1.4.3.1), early studies of light-dependent chloroplast movement in the zygnemal algae *Mougeotia* and *Mesotaenium* painted a rather exact picture of phytochrome molecules arranged coherently at the plasma membrane (Haupt 1960, Haupt et al. 1961, Haupt et al. 1962, Haupt 1970, Hughes 2013), an image that had long been overshadowed by the notion of phytochrome regulating transcription in the nucleus. It might seem that the Jaedicke study vindicated plasma membrane-associated phytochrome, but a problem remained, namely that further studies had shown that the response in zygnemal algae was regulated not by a conventional phytochrome but by a novel R/FR photochromic photoreceptor, thus named neochrome (Suetsugu et al. 2005). The domain structure of neochrome showed that whereas its N-terminal region was indeed similar to canonical phytochrome photosensory modules, the rest of the sequence corresponded to an almost complete phototropin. The phy-phot interaction described by Jaedicke et al. was thus an intermolecular mimic of the neochrome. The discovery of a neochrome in the fern *Adiantum* too even provided evidence that such an association was more than a chance occurrence and might offer a general selective advantage (Nozue et al. 1998, Jaedicke et al. 2012).
However, the nature of the phy-phot interaction and its signalling mechanism, like that of phototropin itself, are still not understood despite several putative holophytochrome interacting proteins (HIPs) identified in Y2H and split-YFP studies (Ermert et al. 2016). Nevertheless, the phy-phot complex might represent the physical link to the machinery controlling cytoskeleton organization and light-directed tip growth. Interestingly, a similar interaction at the plasma membrane was also observed between *Arabidopsis* phyA and phot1 using split-YFP methods, suggesting the existence of a conserved phytochrome cytoplasmic pathway in seed plants as well (Jaedicke et al. 2012).

A further aspect of phytochrome-mediated phototropism in Physcomitrella is worth considering here, namely that the response begins within 5 minutes of the stimulus, too fast for transcriptional changes (Meske et al. 1995). Interestingly, even in vascular plants, numerous phytochrome-mediated responses are known that are probably too fast to be regulated via gene expression. In *Mimosa pudica*, *Albizia julibrissin* and *Albizia saman*, changes of ion fluxes allowing leaf movement are dependent on Pfr formation and visible within 10 minutes (Fondeville et al. 1966, Hillman et al. 1967, Koukkari et al. 1968, Satter et al. 1976). In *Sorghum* seedlings, phytochrome-mediated anthocyanin synthesis begins within 1 minute, whereas alterations of the surface potential of *Hordeum vulgare* coleoptiles take place within 30 sec after a R light pulse (Tanada 1968, Oelmuller et al. 1985). In *Vallisneria gigantea*, R light microbeam pulses induce local cytoplasmic mobility within 3 minutes (Takagi et al. 2003). Given that nuclear translocation of phytochrome requires several minutes, as also do effects on gene expression, however they might arise (Kircher et al. 1999, Hisada et al. 2000, Kim et al. 2000), a more rapid, probably cytoplasmic signalling route might be present in vascular plants as well and might share a common mechanism with Physcomitrella.

1.5 CRISPR/Cas9 mediated genome editing

Since its development ten years ago, the CRISPR/Cas9 system is driving a biotechnological revolution that through the precise manipulation of genomes of cultured cells, animals and plants, is accelerating fundamental research as well as clinical and agricultural advances. The CRISPR (clustered regularly interspaced short palindromic repeats) system was originally identified as an adaptive immunity pathway in prokaryotes providing resistance to phage infection and analogous to the RNA interference process found in eukaryotes (Ishino et al. 2018). It has since been modified and adapted for genome engineering leading to the award of the 2020 Nobel Prize in Chemistry to Charpentier and Doudna for its development (Knott et al. 2018, Ledford et al. 2020).

Essentially, CRISPR/Cas9 can be thought of as a programmable restriction enzyme system consisting of two parts: a short, programmable single guide RNA (sgRNA) and a large (~140 kDa) multidomain, multifunctional DNA endonuclease, Cas9 (CRISPR-associated 9). The sgRNA has a specific 20 nucleotide spacer/targeting sequence (crRNA) at the 5' end that specifies the genomic target by Watson-Crick base pairing, linked to a trans-activating (tracrRNA) sequence at the 3' side of the guide sequence necessary for the recruitment and stability of the Cas9 nuclease. This creates an elegant system in which the 20 nucleotides of the crRNA can be changed to program CRISPR/Cas9 to target any DNA sequence of interest as long as it is adjacent to a PAM (protospacer adjacent motif) (Jinek et al. 2012). The PAM sequence is a short, conserved motif (2-5 bp) essential for cleavage by Cas9. Since Cas9 is originally part of the adaptive immune system machinery of *S. pyogenes*, it recognizes a 5'-NGG-3' PAM (where N can be any nucleotide base). The process begins with the Cas9-sgRNA complex searching for a proper PAM sequence before interrogating the flanking DNA for potential complementarity with the sgRNA (Sternberg et al. 2014). During this target recognition process, which can take minutes to hours, Cas9 rapidly dissociates from DNA that does not contain the appropriate PAM sequence: association time depends on the complementarity between sgRNA and adjacent DNA when a proper PAM is present (Sternberg et al. 2014, Knight et al. 2015, Ma et al. 2016, Jones et al. 2017). Once Cas9 has found a target site with the appropriate PAM, it initiates local DNA melting at the PAM-adjacent nucleation site, followed by RNA strand invasion to form an RNA–DNA hybrid and a displaced DNA strand (the R-loop). The first PAM proximal 10-12 nucleotides located in the 3' end of the spacer sequence of the sgRNA defines the "seed region". Mismatches in this region destabilize Cas9 binding and prevent subsequent strand cleavage, although close similarity can lead to off-target binding events (Pattanayak et al. 2013). The complete RNA-DNA complex formation drives conformational changes in Cas9, activating its active state for DNA cleavage through an induced-fit mechanism. Cas9 uses two nuclease domains: a RuvC domain and an HNH domain. Each domain cleaves one strand of the target dsDNA at a specific site 3-4 bp from the PAM sequence to produce a predominantly blunt-ended double strand break (DSB) (Jinek et al. 2012). Cleavage occurs within 1 second, Cas9 remaining tightly bound to the cleaved target DNA until it is displaced by other cellular factors (Sternberg et al. 2014, Gong et al. 2018).

CRISPR's mutagenic ability derives from the action of the endogenous DNA repair mechanisms after the DSB has been generated. DSBs are prevalently repaired by the error-

prone non-homologous end-joining (NHEJ) pathway that often causes random insertions and deletions (indels) at the DSB site, frequently leading to the disruption of gene function due to frame-shift mutations, premature terminations or aberrant splicing variants. On the other hand, in the presence of an external template containing a novel sequence flanked by regions homologous to the target sequence, the homology-dependent repair (HDR) pathway may be initiated to create desired and precise gene modifications through homologous recombination (Pawelczak et al. 2018).

1.5.1 CRISPR applications in seed plants and in *P. patens*

In the middle of the last century, plant breeders began to generate mutations to obtain new varieties by applying genotoxic agents that randomly induce double-strand breaks (DSBs) (Stadler 1928, Stadler 1928). Several decades later, site-specific nucleases (SSNs), such as zinc finger nucleases (ZFNs) and transcription-activator-like effector nucleases (TALENs), were developed to target DSBs to desired, unique positions in the genome (Puchta et al. 1993, Voytas 2013). CRISPR/Cas9-based genome engineering has been applied in crops such as rice (*Oryza sativa*), maize (*Zea mays*), tomato (*Solanum lycopersicum L.)*, cotton *(Gossypium hirsutum L.*), and even banana (*Musa acuminate*) to induce mutations based on non-homologous end joining (NHEJ) (Jaganathan et al. 2018). One major limitation in plant genome editing is the high ploidy and complexity of the genomes that characterize many crops and other plant species. In this regard, the multiplexing ability of CRISPR/Cas9, that is the simultaneous targeting of several genomic loci in a single experiment, is particularly useful and enables the study of gene families or other cases of redundant functionality (Abdelrahman et al. 2021). This is also particularly significant in the case of Physcomitrella, since it has undergone two rounds of whole-genome duplication during its evolution, which has contributed to the expansion of most gene families (Li et al. 2015). Indeed, both Cas9-mediated gene knock-out (KO) with NHEJ and knock-in (with HDR), have proven to be successful in this model organism, including the capability to perform multiplex editing as described here and elsewhere (Lopez-Obando et al. 2016, Nomura et al. 2016, Collonnier et al. 2017, Mallett et al. 2019, Trogu et al. 2021).

CRISPR/Cas9 has its own drawbacks nonetheless, including limitation of available PAM sequences, production of off-target mutations and the relatively large size of the Cas9 nuclease that prevents delivery by virus-based vectors. In order to overcome these problems, Cas9 orthologs have been isolated from different bacteria or generated through protein engineering (Hu et al. 2018, Wada et al. 2022). Several Cas9 variants, like Cas12a, have been applied successfully to edit single and multiple genes in vascular plants (Alok et al. 2020, Wada et al. 2022). In Physcomitrella, the multiplexing ability of Cas12a has also been demonstrated (Pu et al. 2019). However, for some of the new nucleases the PAM sequence is more complex and/or these variants suffer from low efficiency compared with the canonical Cas9 - as is the case with xCas9 and SpCas9-NG tested both in different seed plants and in Physcomitrella (Ge et al. 2019, Wang et al. 2019, Veillet et al. 2020, Wang et al. 2021).

The efficiency of the transfection method and the subsequent regeneration of genome-edited plants can be a strong limitation to CRISPR/Cas9 applications in a broader variety of plants. Several approaches have been used to deliver CRISPR/Cas9 reagents, including plasmids that enable the production of Cas9 and sgRNA(s) or preassembled Cas9-sgRNA complexes (ribonucleoprotein, RNP). Moreover, as with other transgenic approaches in plants, the

presence of the cell wall poses an additional challenge for the delivery of the CRISPR editing components into the plant cell. In this regard, particle bombardment, *Agrobacterium*- and PEG-mediated transfections have proved effective in introducing DNA into plant cells (Laforest et al. 2022).

CRISPR-induced DSBs are predominantly repaired by NHEJ, resulting in random insertions or deletions (indels). This is a disadvantage when a precise genetic modification is required. However, the precise HDR pathway, unlike NHEJ, has very low efficiency in somatic cells used for seed plant transfection, making gene replacement in plants an inefficient and challenging process (Huang et al. 2019, Chen et al. 2022). Alternative to gene replacement, especially when large or complex genomic manipulation is not required, base- and prime editing can also lead to precise modifications without the need of a DSB or donor DNA template. Both have been tested in several plant species with promising results (Hua et al. 2022). Base editors comprise an inactivated nuclease, such as dCas9, fused with an enzyme that can convert one nucleotide into another (Rees et al. 2018). Currently, efficient editing from C to T, and A to G have been achieved in different plant species to interrogate gene function and improve crop traits. However, potential off-target effects when base-editors are used in vascular plants are still a major concern (Hua et al. 2022). In Physcomitrella, on the other hand, cytosine or adenine base editors, in simplex or multiplex mode, can achieve an efficiency up to 55% without apparent off-target mutations (Guyon-Debast et al. 2021).

Prime editing is based on a Cas9-based nickase fused with a reverse transcriptase unit. In the prime editing gRNA (pegRNA), the 5'- sequence specifies the target region and the 3'-sequence contains a primer binding site sequence and reverse transcription template with the desired edit (Anzalone et al. 2019). Prime editing has been tested in several plant species, but the reported efficacy so far has been relatively low (Butt et al. 2020, Hua et al. 2020, Jiang et al. 2020, Lin et al. 2020, Tang et al. 2020, Wang et al. 2021). Similar results were recently obtained in Physcomitrella. In particular, editing frequency and accuracy were shown to vary with the target sequence coded by the pegRNA; no off-target events were detected (Perroud et al. 2022).

1.6 Aim of this study

Alongside the regulation of gene expression, moss phytochromes have the intriguing ability to steer directional responses to unilateral and polarized red light. As transcription and translation are disconnected from directional information, it is impossible for gene regulation to steer directional responses (Hughes 2013). Instead, phototropic growth originates from a cytoplasmic signal probably connected with the reorganization of the actin cytoskeleton (Meske et al. 1995), perhaps via the phytochrome-phototropin interaction at the plasma membrane (Jaedicke et al. 2012).

Although progress has been made, the actual nature of the phytochrome cytoplasmic signalling pathway remains elusive. Functional redundancy masking the phenotype of deletion mutants is one of the obstacles, given that Physcomitrella has no less than seven phytochrome genes with both specific and overlapping functions. This obstacle can, however, be overcome by simultaneously targeting several phytochrome genes in different combinations with the help of CRISPR/Cas9 genome editing. The physiological analysis of different mutants might then help solve the paradox of direction sensing by phytochrome and thereby provide a deeper insight into phytochrome function.

This work aimed to create a phytochrome mutant collection using CRISPR/Cas9 and to investigate the physiology of different mutant combinations under different light conditions. Moreover, to understand the nature of the phytochrome-phototropin interaction better, the phototropin gene family was also targeted to analyse the physiology of the resulting mutants in relation to phy-phot interaction.

Thus, the objectives of this study are to establish multiplex CRISPR/Cas9 mutagenesis and efficient screening procedures in Physcomitrella, to create libraries of phytochrome and phototropin gene family mutants and to analyse these physiologically in order to gain better insight into the steering processes involved in phytochrome-mediated phototropism. Additionally, studies on the mechanism underlying the perception of light direction in Physcomitrella filaments were carried out to clarify the optical origin of the phototropic response. The data generated in the CRISPR/Cas9 experiments, together with the optimization of the mutant screening procedure, broaden our understanding of the CRISPR/Cas9 system in plants and in Physcomitrella in particular, while the multiplex mutants and light experiments provided deep insights into the photoperception system, even allowing tentative conclusions as to the mechanism of phytochrome-mediated direction sensing.

2. Materials

2.1 *Physcomitrium patens*

2.1.1 Wild-type

In phototropic assays conducted prior to this thesis work, it was observed that the WT used to produce the *phy4* KO mutant published in Mittmann *et al.* (*P. patens* (Hedw.) Gransden strain 2004) (Mittmann et al. 2004) had lost its phototropic response in unilateral R, probably due to (epi-)mutations accumulated during >20 years of vegetative propagation in the laboratory. A fresh wild-type line derived from the Gransden strain and kindly donated by Pierre-François Perroud was found to retain phototropic sensitivity, however, and was therefore used in this work.

2.1.2 Mutated lines

Nomenclature of single and double mutants produced via CRISPR/Cas9 editing followed the current rules indicating the mutated gene(s) in lowercase italics. A nomenclature was derived in this work, however, to make the genetic profile of higher-order mutants more readily understandable, whereby the number of mutated genes in a multiplex line is indicated in superscript followed by a minus sign. Wild-type genes still present (in upper case italics) and in-frame mutations (in lower case italics followed by an asterisk) are then given in brackets.

The Phytochrome mutant collection (Trogu et al. 2021) as well as that for phototropin is appended (12.1.1). The following list comprises additional mutants generated later and all the mutants used in physiological assays.

phy^{7-}	(Trogu et al. 2021)
phy^{5-} (phy3 PHY5b PHY5c)*	
phy^{6-} (PHY3)	(Trogu et al. 2021)
phy^{6-} (PHY5b)	(Trogu et al. 2021)
phy^{5-} (PHY1 phy3 PHY5b)*	(Trogu et al. 2021)
phy^{4-} (PHY1 PHY3 PHY5b)	(Trogu et al. 2021)
phy5a^{-}	
phy5a phy5c^{-}	
phy5c^{-} #1	
phy5c^{-} #2	(Trogu et al. 2021)
phy5c^{-} #3	(Trogu et al. 2021)

phy^{7-} (phy5a phy5b*)*	(Trogu et al. 2021)
phy^{5-} (PHY5a PHY5b)	(Trogu et al. 2021)
phy^{6-} (PHY3 phy5a phy5b*)*	
phy^{4-} (PHY1 PHY3 PHY5b)	(Trogu et al. 2021)
phot^{5-} #1	
phot^{5-} #2	
phot^{5-} #3	
photA2^{-}	(Kasahara et al. 2004)
phy5c photA2^{-} #1	
phy5c photA2^{-} #2	

2.2 Buffers, solutions and media

If not stated otherwise, purified water of Millipore-grade was used for all experiments.

2.2.1 DNA methods

High throughput DNA extraction

See Trogu *et al.* in appendix 12.1 (Trogu et al. 2021)

PCR

Taq DNA Polymerase (NEB)
including appropriate
buffer

10x dNTP Mix
2 mM dATP, dTTP, dGTP and dCTP
each

Agarose gel electrophoresis

0.5x TBE buffer
100 mM Tris
83 mM Boric acid
10 mM EDTA (pH 8.0)

Agarose gel
1% (w/v) Agarose
in 0.5 % TBE buffer

EtBr stock solution
20 mg/ml EtBr in H_2O

EtBr staining solution
0.5 µg/ml EtBr in 0.5x TBE

6 x loading dye
0.03 % (w/v) Bromophenol blue
0.03 % (w/v) Xylene cyanol
60 % (v/v) Glycerol

60 mM EDTA
10 mM Tris/HCl

DNA ladder
100 bp / 1 kb marker from NEB
diluted in 6 x loading dye (1:4)

High resolution 15% PAGE gels

See Trogu *et al.* in appendix 12.1 (Trogu et al. 2021)

Plasmid DNA Maxi preparation

STE
0.1 M NaCl
10 mM Tris/HCl (pH 8.0)
1 mM EDTA (pH 8.0)
5 % (v/v) Triton X100
stored at 4 °C

Solution I
50 mM Glucose monohydrate
25 mM Tris/HCl (pH 8.0)
10 mM EDTA (pH 8.0)
stored at 4 °C

Solution II
200 mM NaOH
1% SDS (v/v) (from 10 % stock)
prepared on the day of use

Solution III
3 M Potassium acetate
11.5 % (v/v) Acetic acid
stored at 4 °C

Lysozyme solution
1 mg/ml Lysozyme
10 mM Tris/HCl (pH 8.0)
prepared on the day of use

TE buffer
20 mM Tris/HCl (pH 8.0)
1 mM EDTA (pH 8.0)

RNAse solution
2 µg/ml RNAaseA
in 20 mM TE-buffer

Proteinase K solution
20 mg/ml Proteinase K
in 20 mM TE-buffer

PEG/NaCl
13 % PEG 8000
1.6 M NaCl
dissolved in H_2O

Sodium acetate
3 M Sodium acetate
pH 5.2 – 5.8 (with acetic acid)

Ethanol
pure, stored at 4 °C or -20 °C

Isopropyl alcohol
pure, stored at -20 °C

Kits

QIAprep Spin Miniprep Kit (QIAGEN)

MinElute PCR Purification Kit (QIAGEN)

Gateway BP-Clonase kit (ThermoFisher Scientific)

2.2.2 Plant methods

Physcomitrella cultivation

Standard media based on Ashton and Cove (1977) were used for Physcomitrella cultures. For weekly homogenization of the cultures, a mechanical shredder (T18 basic Ultra-Turrax, IKA, Staufen, Germany) was used.

Solution B (100x)
100 mM $MgSO_4$
dissolve in H_2O
stored at 4 °C

Solution C (100x)
180 mM KH_2PO_4
dissolved in H_2O
stored at 4 °C
pH 6.5

Solution E (100x)
1 M KNO_3
1.4 mM Fe (III)$C_6H_5O_7$
dissolved in H_2O
stored at 4 °C

Solution Ca (100x)
200 mM $CaCl_2 \cdot 2\ H_2O$
dissolved in H_2O
sterile filtered
stored at 4 °C

Solution N (100x)
500 mM Di-ammonium tartrate
($C_4H_{12}N_2O_6$)
dissolved in H_2O
sterile filtered
stored at 4 °C

Hoagland's trace element solution
(TES 1000x)
9.93 mM H_3BO_3
0.23 mM $AlK(SO_4)_2 \cdot 12\ H_2O$
0.22 mM $CuSO_4 \cdot 5\ H_2O$
0.24 mM KBr
0.66 mM LiCl
0.10 mM $Na_2MoO_4 \cdot 2\ H_2O$
1.97 mM $MnCl_2 \cdot 4\ H_2O$
0.23 mM $CoCl_2 \cdot 6\ H_2O$
0.19 mM $ZnSO_4 \cdot 7\ H_2O$
0.17 mM KI
0.12 mM $SnCl_2 \cdot 2\ H_2O$
0.25 mM $NiCl_2 \cdot 6\ H_2O$
dissolved in H_2O
stored at 4 °C

Liquid BCE225 medium (800 ml)
8 ml solution B
8 ml solution C
8 ml solution E
800 µl TES
0.2 % (w/v) glucose
dissolved in H_2O
up to 784 ml with H_2O
sterilised by autoclaving
added through sterile filter:
8 ml solution Ca (100x)
8 ml solution N (100x)

Solid BCE225 medium
liquid BCE225 medium
0.8 % (w/v) agar for plant cultivation

if indicated:
supplemented with antibiotics
overlaid with cellophane foil

PPNH4 medium
Solution A (1x)
Solution B (1x)
Solution C (1x)
Alternative TES (1x)
2.7 mM $C_4H_{12}N_2O_6$
0.5% (w/v) glucose
0.7% (w/v) agar for plant cultivation

Alternative TES (1000x)

220 nM $CuSO_4$
10 mM H_3BO_4
2 mM $MnCl_2$
230 nM $CoCl_2$
190 nM $ZnSO_4$
170 nM KI
100 nM Na_2MoO_4
Autoclaved and stored at 4 °C

Hygromycin stock solution
50 mg/ml hygromycin dissolved in PBS (Invitrogen)

Kanamycin stock solution
50 mg/ml kanamycin dissolved in H_2O
Sterile filtered

Protoplasts isolation, transfection and regeneration

Mannitol solution
8 % (w/v) D-mannitol
dissolved in H_2O
Autoclaved

Driselase stock solution
2 % (w/v) Driselase from *Basidiomycota* (Sigma)
dissolved in mannitol solution
sterile filtered
stored at -20 °C

Driselase solution
0.5 % Driselase (from stock solution) diluted with mannitol solution
Prepared freshly, kept on ice

MES
1% (w/v) 2-(N-morpholino) ethanesulfonic acid in H_2O
pH adjusted to 5.6 with 0.1 M KOH
Autoclaved

$MgCl_2$ stock solution
1 M $MgCl_2$ in H_2O

MMM buffer
0.1% (w/v) MES
9.1% (w/v) D-mannitol
15 mM $MgCl_2$
pH adjusted to 5.6 with KOH
Sterile filtered and stored at 4 °C for up to 1 year

PEG transformation solution
2 g PEG 6000
melt in water bath
1 ml mannitol solution
10 µl $Ca(NO_3)_2$ stock solution
10 µl Tris buffer (pH 8.0)
Mixed by vigorous vortexing
Prepared fresh (2h prior transformation)

Solution D (100x)
1 M KNO_3
45 mM $FeSO_4 \cdot 7\ H_2O$
dissolved in H_2O
stored at 4 °C

PRMB (protoplast regeneration medium, bottom layer)
Solution B (1x)
Solution C (1x)
Solution D (1x)
TES (1x)
5 mM ammonium tartrate
6% (w/v) D-mannitol
0.7% (w/v) agar for plant cultivation
0.5% (w/v) glucose
Autoclaved and cooled down to 50 °C
1 M $CaCl_2$ solution added freshly through a sterile filter to a final concentration of 10 mM

PRMT (protoplast regeneration medium, top layer)	8% (w/v) D-mannitol
Solution B (1x)	0.4% (w/v) agar for plant cultivation
Solution C (1x)	Autoclaved and cooled down to 50 °C
Solution D (1x)	1 M $CaCl_2$ solution added freshly through a sterile filter to a final concentration of 10 mM
TES (1x)	
5 mM ammonium tartrate	

2.3 sgRNAs, oligonucleotides, plasmids and enzymes

2.3.1 sgRNAs

Target genes and crRNA sequences for members of the *PHY* gene family used in the multiplex gene editing are listed in Table 2 of the SI in Appendix 12.1.1.

Table 1. Target genes and crRNA sequences for members of the *PHOT* gene family

sgRNA construct (targeted gene[a])	crRNA sequence (**PAM**)	Specificity Score[b] (%)
PHOTA1 (Pp3c19_10230)	CCGAGTCCTCGGTTAGTAAG **CGG**	100
PHOTA2 *PHOTA2 #2 (Pp3c21_21410)*	CGGGGAGTTCAGGCGTAGAC **AGG** TCCGCGGCTCATGCAAGCGG **GGG**	100 100
PHOTB1 (Pp3c2_10380)	GTAGCTCTGAGGCACCGCGG **GGG**	100
PHOTB2 (Pp3c14_10390)	GGTGCGCCCACTGGGTTGAG **CGG**	100
PHOTA3 *PHOTA3 #2 (Pp3c7_12190)*	AGACGACCTCGCTCGGCAAT **TGG** GTCACCCGAGTGGTTCTAAG **TGG**	100 100

[a]: Identifiers (in brackets) from Phytozome V11 - *P. patens* genome.

[b]: Specificity score data from CRISPOR (Concordet et al. 2018).

2.3.2 Oligonucleotides

Oligonucleotides used in the multiplex *PHY* gene editing published in Trogu et al. are listed in Table 4 of Appendix 12.1.1 (Trogu et al. 2021).

Table 2. Oligonucleotides used in *PHOT* gene editing

Name	Sequence	Description
ST17 FW	GGAAGATGAACTACCGGAAGCTACC	*(PHOTA1)* PCR screening
ST18 RV	CCGGTGCGCTCGACACAT	*(PHOTA1)* PCR screening
ST19 FW	CACCAGCCACGCTGACTGAT	*(PHOTA2)* PCR screening
ST20 RV	CGGCATCCTGAAATGCTCGGAG	*(PHOTA2)* PCR screening
ST21 FW	GCCTATGTCTTCGTCAGCTTCG	*(PHOTB1)* PCR screening
ST22 RV	CCATGGAAGAGGAGCTTTTGC	*(PHOTB1)* PCR screening
ST23 FW	CTGATCTCAAGCCTCAAGAACCC	*(PHOTB2)* PCR screening
ST24 RV	GGCATAGAACTTCCCTCGGC	*(PHOTB2)* PCR screening
ST35 FW	CTGAAATGGCGCCGATGTTC	*(PHOTA3)* PCR screening
ST36 RV	CTGAAATGGCGCCGATGTTC	*(PHOTA3)* PCR screening
ST39 FW	GGACAGGGGAAACCGAGG	*(PHOTA2 #1)* PCR screening
ST40 RV	CAATGTTCTCCGCGACTGC	*(PHOTA2 #1)* PCR screening
ST41 FW	CCAGCTATGGACATGAAGAACGT	*(PHOTA3 #1)* PCR screening
ST42 RV	GCGCCAAATTTACACTACTCTGT	*(PHOTA3 #1)* PCR screening
ST25 FW	GAAGAGCTGAAGCATTCGTCGAT	*(PHOTA1)* Sequencing reaction
ST26 RV	CCTCAGAAACTTGGACGGGTAC	*(PHOTA1)* Sequencing reaction
ST27 FW	GGTCCGTACAGACAGATATGCTG	*(PHOTA2, #1)* Sequencing reaction

ST28 RV	GTCACTCGCGTGATCATTGC	*(PHOTA2, #1)* Sequencing reaction
ST29 FW	ATCCCGCCTCTTCAATCGAC	*(PHOTB1)* Sequencing reaction
ST30 RV	CCCAGTGATCCCCTCTCAGA	*(PHOTB1)* Sequencing reaction
ST31 FW	GCAGACGAGGAGTGTTGTAGC	*(PHOTB2)* Sequencing reaction
ST32 RV	ACTCATCTCCCCTGAGAGCAG	*(PHOTB2)* Sequencing reaction
ST37 FW	TGGCTCGCACAAGGTCAGG	*(PHOTA3, #1)* Sequencing reaction
ST38 RV	TAATCCGTGCCGAGCTCATC	*(PHOTA3, #1)* Sequencing reaction

Oligonucleotides were purchased from Invitrogen.

2.3.3 Plasmids

Table 3. Plasmids used for Gateway cloning and CRISPR/Cas9 editing, in high purity and concentration >1 µg/µl.

Plasmids	**Description**	**Reference**
pAct-Cas9	Cas9 expression plasmid	(Trogu et al. 2021)
pBHRF	Plasmid containing a hygromycin resistance cassette	(Lopez-Obando et al. 2016)
pDONR207	Donor vector for Gateway cloning	ThermoFisher Scientific
pSCOE-fcoCas9	Cas9 expression plasmid with kanamycin resistance cassette	(Nomura et al. 2016)
pAL114	Cas9 expression plasmid with hygromycin resistance cassette	(Trogu et al. 2021)
pENTRsgRNA_PHY1	sgRNA expression plasmid targeting PHY1	(Trogu et al. 2021)
pENTRsgRNA_PHY2	sgRNA expression plasmid targeting PHY2	(Trogu et al. 2021)
pENTRsgRNA_PHY3	sgRNA expression plasmid targeting PHY3	(Trogu et al. 2021)
pENTRsgRNA_PHY4	sgRNA expression plasmid targeting PHY4	(Trogu et al. 2021)
pENTRsgRNA_PHY5a	sgRNA expression plasmid targeting PHY5a	(Trogu et al. 2021)
pENTRsgRNA_PHY5b	sgRNA expression plasmid targeting PHY5b	(Trogu et al. 2021)
pENTRsgRNA_PHY5c	sgRNA expression plasmid targeting PHY5c	(Trogu et al. 2021)
pENTRsgRNA_PHOTA1	sgRNA expression plasmid targeting PHOTA1	This work
pENTRsgRNA_PHOTA2	sgRNA expression plasmid targeting PHOTA2	This work
pENTRsgRNA_PHOTA2 #1	sgRNA expression plasmid targeting PHOTA2	This work
pENTRsgRNA_PHOTB1	sgRNA expression plasmid targeting PHOTB1	This work
pENTRsgRNA_PHOTB2	sgRNA expression plasmid targeting PHOTB2	This work
pENTRsgRNA_PHOTA3	sgRNA expression plasmid targeting PHOTA3	This work
pENTRsgRNA_PHOTA3 #1	sgRNA expression plasmid targeting PHOTA3	This work

2.3.4 Enzymes

Gateway BP Clonase II Enzyme-Mix	ThermoFisher Scientific
Driselase	Sigma
Taq Polymerase	New England Biolabs

Phusion High-Fidelity DNA Polymerase	New England Biolabs

2.4 Growth chamber

Long day conditions, 16h light (Osram L58 W/77, 50 µmol m^{-2} s^{-1}), 8h dark, 22 °C.

2.5 Light sources

R High Power LED Array LED660-66-60 (660 nm) TO-66 (Roithner Lasertechnik, Vienna).

R High Power LED Array LED660N-66-60 (660 nm) TO-66 (Roithner Lasertechnik, Vienna).

FR High Power LED Array LED735-66-60 (735 nm) TO-66 (Roithner Lasertechnik, Vienna).

B LED array Luxeon Blue LXHL (465 nm) (Philips Lumileds Lighting, San Jose, CA).

Green LED (540 nm) safelight.

2.6 Macroscope

Leica Z16 APO zoom system equipped with a CCD-camera (DFX 500, Leica, Wetzlar, Germany) was used.

2.7 Fine chemicals

A. A. Packaging Limited, Liverpool, UK Cellophane discs, 80 mm

Carl Roth GmbH + Co. KG, Karlsruhe, Germany

Acrylamide/Bis-solution 30% (29:1)
Agar Kobe
Sodium hydroxide

Applichem GmbH, Darmstadt, Germany

Agar for plant cultivation
PEG6000
PEG 8000
Ampicillin
D-Mannitol
Tris
Dithiothreitol (DTT)
LB medium
Acetic acid
Bromophenol blue
Glucose monohydrate
Potassium acetate

Kanamycin
Ethidium bromide

Sigma-Aldrich, St. Louis, Missouri, USA
Driselase
Ethanol, pure
MES

Merck KGaA, Darmstadt, Deutschland
EDTA
Triton X100
Sodium dodecyl sulfate (SDS)
Sodium acetate
Sodium chloride

SERVA GmbH, Heidelbergg Deutschland
TEMED
PEG40000

NEB, New England Biolabs Inc.,Beverly, USA
1 kb, 100 bp and 50bp DNA ladder

Fluka Chemie, Buchs, Switzerland
Xylene Cyanol
QIAGEN GmbH, Hilden, Germany

BioRad Laboratories, Hercules, USA
PAGE gel chamber

ThermoFisher Scientific, Massachusetts, USA
Di-ammonium tartrate
Glycerol

3. Methods

3.1 Design of sgRNAs

sgRNAs targeting the 7 *PHY* genes were designed as described in Trogu et *al.* (Trogu et al. 2021). Similarly, sgRNAs targeting the 5 *PHOT* genes were designed as described (Ermert et al. 2019, Trogu et al. 2021).

3.2 Cloning procedure

3.2.1 Gateway cloning

DNA constructs (chemically synthetized by IDT) containing the sgRNA sequence template flanked by *attB* sites for Gateway cloning were dissolved according to manufacturer's instructions to a final concentration of 10 ng/µl. 1 µl of synthetic DNA was then recombined into the Gateway donor vector pDONR207 by BP-reaction according to manufacturer's instructions. The cloning reaction was transformed in chemically competent *E. coli* cells and the following transformants screening performed according to standard procedures (Sambrook et al. 2001).

3.3 Bacteria

3.3.1 Transformation of *E. coli* cells by heat-shock

Chemically competent *E. coli* cells were produced and transformed following the Hanahan method (Sambrook et al. 2001). Cells from -80 °C were thawed on ice for 30 min and mixed with the appropriate amount of plasmid DNA. Following further 30 min incubation on ice, cells were first heat-shocked at 42 °C for 45 sec and then put on ice for 2 min. 250 µl of hand-warm SOC medium was added and cells were incubated at 37 °C on a shaker (180 rpm) for 45 min. Transformations were therefore plated on LB agar plates containing the appropriate antibiotic and incubated at 37 °C overnight.

3.3.2 Small scale plasmid preparation (Mini-Prep)

3 ml liquid LB together with appropriate antibiotic were inoculated with a single *E. coli* colony and incubated at 37 °C on a shaker (180 rpm) overnight. Plasmid DNA was extracted using QIAprep Spin Miniprep kits (Qiagen) according to manufacturer' suggestions.

3.3.3 Large scale plasmid preparation (Maxi-Prep)

250 ml TB together with appropriate antibiotic were inoculated from a small LB + antibiotic overnight culture and incubated at 37 °C on a shaker (160 rpm). Large scale extraction of plasmid DNA was carried out as described (Sambrook et al. 2001). Purity and concentration were determined with a Nano-Drop (NanoVue Plus spectrophotometer from GE Healthcare UK Limited, Buckinghamshire, UK).

3.4 *Physcomitrium patens*

3.4.1 *P. patens* cultivation

Physcomitrella cultures were grown on cellophane-overlaid BCE225 medium under long day conditions. Long-term cultures were transferred to fresh BCE225 medium every 6-8 weeks. To reduce formation of gametophores, cultures were shortly homogenised with the help of an Ultra-Turrax (T18 basic Ultra-Turrax, IKA, Staufen, Germany) once a week.

3.4.2 Cultures preparation for protoplast transfection

After 7-10 days growth, filaments were homogenized as described above (3.4.1) and transferred to a sterile 50 ml tube. The material was left to sink to the bottom of the tube and excess culture medium removed to a total volume of 5 ml. The sedimented culture was therefore plated on cellophane-overlaid PPNH4 medium and incubated in the growth chamber for 6 days prior to transfection.

3.4.3 Protoplast isolation

Protoplasts isolation was carried out as described (Cove et al. 2009) (Trogu et al. 2021). Protoplasts were produced from protonemata by digesting the cell walls with the enzyme cocktail Driselase. Released protoplasts were then washed in an isotonic mannitol solution paying particular attention to minimize turbulence during pipetting and resuspension.

3.4.4 Protoplast transfection and selection

Protoplasts transfection and selection was performed as described (Cove et al. 2009) (Trogu et al. 2021). PEG and heat-shock were used to transfect protoplasts with a total of 20-25 µg of plasmid DNA. Protoplasts were allowed to regenerate on cellophane-overlaid PRMB plates for 1 week. Filaments were then transferred to antibiotic-supplemented medium without mannitol for selection of transfected cells. After another week, regenerants were placed on BCE225 plates without selection and grown further for 2 weeks. Finally, individual regenerants were transferred to wells in microtiter plates.

3.4.5 High throughput genomic DNA extraction

High throughput gDNA extraction was as described (Trogu et al. 2021).

3.4.6 Knockout and off-target screening with high resolution PAGE gels

Screening with high resolution 15% PAGE gels was as described (Trogu et al. 2021).

3.4.7 Physiological essays

3.4.7.1 Gravitropism assay

The effect of light on gravitropism was assayed as previously described (Lamparter et al. 1996) with at least two different mutant lines of each genotype in several independent

experiments. Homogenized protonemata were plated on cellophane-covered agar BCE225 medium and grown for 7–10 days. Approximately 2 mm slices were then placed on vertically-orientated square Petri dishes and grown for 6 days in darkness to generate uniform caulonemata. The plates were then rotated by 90° and either left in darkness or irradiated with 5 µmol m^{-2} s^{-1} of 660 nm R from behind the plate for 3 days (Fig. 2). The filaments were photographed using a zoom macroscope and the tip orientations assayed using ImageJ (Trogu et al. 2021).

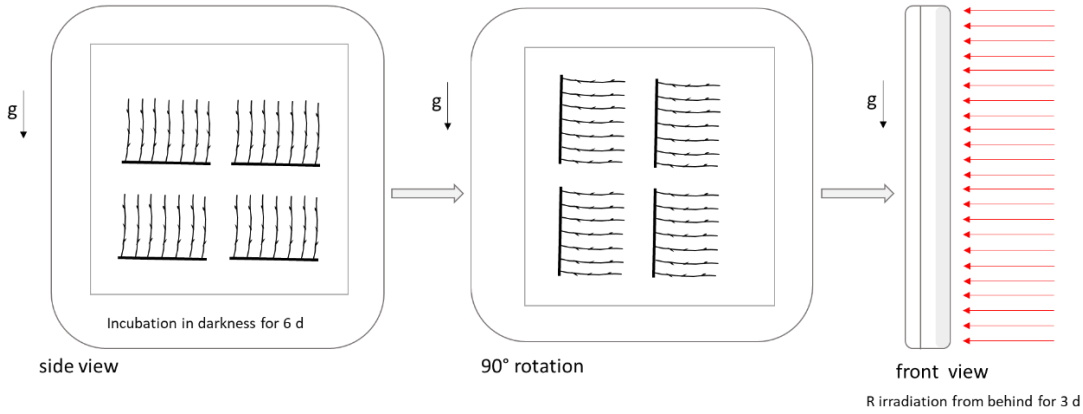

Fig. 2 Schematic representation of gravitropism assay.

3.4.7.2 Phototropism assay

Phototropic responses in the WT and mutant lines were assayed in four or more independent experiments as described (Ermert et al. 2019). Homogenized protonemata were plated on cellophane-covered agar BCE225 medium and grown for 7–10 days. 4 filament slices of *ca.* 2 mm were placed on each half of the cellophane- overlayed squared Petri dish with every line being inclined by *ca.* 35° to prevent shading effects. Plates were then placed vertically in darkness for 6 days to generate uniform caulonemata. To analyse phototropism, unilateral collimated R, FR or B was applied to the vertically positioned plates for 16h (Fig. 3). The different fluence rates used to assay phototropism quantitatively (4.3.2) were obtained using a threshold box, which is made of a series of chambers connected by semi-transparent mirrors oriented in a 45° angle in respect to the light beam so that half of the light passes through and the other half is reflected on the sample. After the light treatment, filaments were photographed using a zoom macroscope and the tip orientation assayed using ImageJ, Excel and Origin.

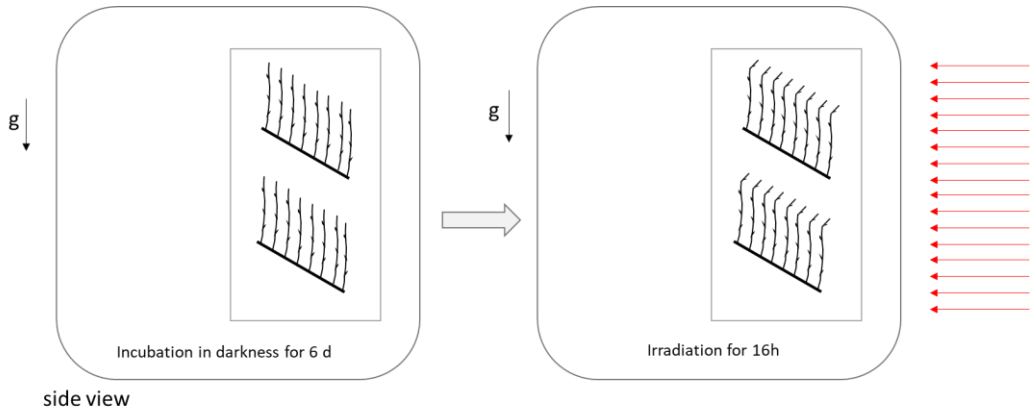

Fig. 3 Schematic representation of phototropism assay under R irradiation. Phototropism assays under unilateral FR, R supplemented with FR and B were carried out in the same way.

For the experiments carried out with WT caulonemata immersed in water or 30% PEG 40000 in water (4.7), filaments were prepared and grown in darkness as described above. Refractive index of the PEG solution was assessed using a refractometer. Caulonemata were then placed in plastic cuvettes filled with water or 30% PEG 40000 and irradiated with unilateral collimated R for 16h. Both experiments, in water and PEG solution, were repeated four times and phototropic responses photographed using a zoom macroscope after the light treatment.

3.4.7.3 Polarotropism assay

Caulonemata were prepared in thin slices as described in 3.4.7.1 and incubated in darkness for 6 days on vertically-orientated square Petri dishes. Polarotropism was assayed as described in Ermert *et al.* (Ermert et al. 2019). Since the plastic lid of the Petri dish was weakly dichroic, it was replaced with a thin glass plate on the day of the experiment. A polarizing filter was placed on top of the plate with the plane of polarization 45° to the vertical axis of the dish. The plate, horizontally placed, was then irradiated from above with 30 nmol m^{-2} sec^{-1} of R for 24h (Fig. 4). Polarotropic bending of filament tip cells was evaluated as described for phototropism experiments (3.4.7.2).

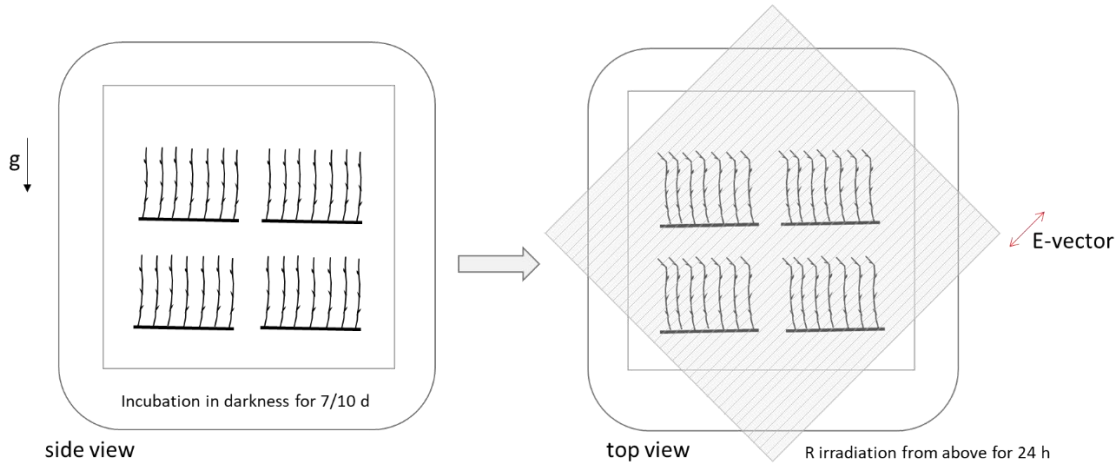

Fig. 4 Schematic representation of polarotropism assay.

3.5 Light measurement

3.5.1 Spectroradiometer

FR and R at very low fluence rates were measured with a spectroradiometer (Ocean optics SD2000) using the manufacturer's software.

3.5.2 PAR meter

A PAR-meter (Skype Quantum Sensor) connected to a microvoltmeter (Voltcraft M-4660A) was used to measure R and B. The dark current was determined by covering the light sensor, then the sensor head was held at the appropriate position in the light beam and voltage was measured. Dark current was subtracted from the voltage measured in the light. The fluence rate in $\mu mol \cdot m^{-2} \cdot s^{-1}$ was derived from the difference and the calibration factor of the sensor provided by the manufacturer.

4. Results

4.1 CRISPR/Cas9 mutagenesis of the phytochrome gene family

Early results from this research were published in Trogu *et al.* (2021) Multiplex CRISPR/Cas9 mutagenesis of the phytochrome gene family in *Physcomitrium* (Physcomitrella) *patens*. Plant Molecular Biology, 107: 327-336 (see Appendix 12.1) and are summarized below.

In this study, multiplex CRISPR/Cas9 mutagenesis was carried out, targeting the seven-member phytochrome gene family in Physcomitrella, aiming to generate single and multiple knockouts for subsequent studies of phytochrome functions related to phototropism.
In preliminary experiments, phytochrome genes in different combinations were targeted by transiently transfecting Physcomitrella protoplasts with separate plasmids carrying Cas9 and a hygromycin resistance cassette together with appropriate sgRNA plasmids.
After transient selection with hygromycin, gDNA was extracted. Initially, this procedure was carried out by breaking the cell walls mechanically followed by CTAB precipitation. Later, an efficient and high-throughput procedure was developed exploiting cellulase rather than mechanical disruption of the cell wall.
Since efficient detection of multiplex indels is a non-trivial process, a PCR-based screening procedure prior to sequencing was developed. Short regions adjacent to each target site were amplified and separated on non-denaturing polyacrylamide gels (PAGE) allowing indels to ± 1 bp to be identified (see Fig. 2 in Appendix 12.1). This mobility-based screen allowed single and higher order mutants to be identified and enabled the efficiencies of different sgRNA constructs in the multiplex transfections to be assessed (Fig. 5b-e & Fig.6b). Possible off-target mutants were also sought by PCR/PAGE: none was found. This result further confirmed that CRISPR/Cas9 editing system is highly specific in Physcomitrella, as shown in other studies (Lopez-Obando et al. 2016, Nomura et al. 2016) using similar methods.

Table 4. Multiplex *PHY* mutagenesis

Transfection	Targets	Total mutants identified
a	2-fold: *PHY2* + *PHY4*	26/75 (35%)
b	2-fold: *PHY5b* + *PHY5c*	38/48 (79%)
c	4-fold: *PHY1-4*	12/60 (20%)
d	6-fold: *PHY1-4* + *PHY5b-c*	28/74 (38%)
e	7-fold: *PHY1-5c*	80/85 (94%)
f	5 + 2-fold: *PHY5a* + *PHY5b* in a quintuple mutant background	47/53 (89%)

Using this system, sibling genes *PHY2* & *-4* and *PHY5b* & *-c* were successfully targeted, obtaining several double KOs in each case (Table 4a-b). *PHY1-4* were targeted obtaining two triple KOs (*phy1 phy2 phy4*), alongside double and single mutants but no quadruple mutant (Table 4c). *PHY1-4* together with *PHY5b* & *-c* were also targeted and the quintuple mutant *phy^{5-} (PHY5a PHY5b)* was obtained along with several lower order mutants (Table 4d, Fig. 5). Subsequently, this protoplast-transfection-based CRISPR system was further optimized by placing the hygromycin resistance gene on the same plasmid as Cas9. With this improved system, all 7 phytochrome genes were targeted simultaneously, successfully generating a

septuple mutant along with several sextuple and numerous lower-order multiplex mutants (Table 4e, Fig. 5a).

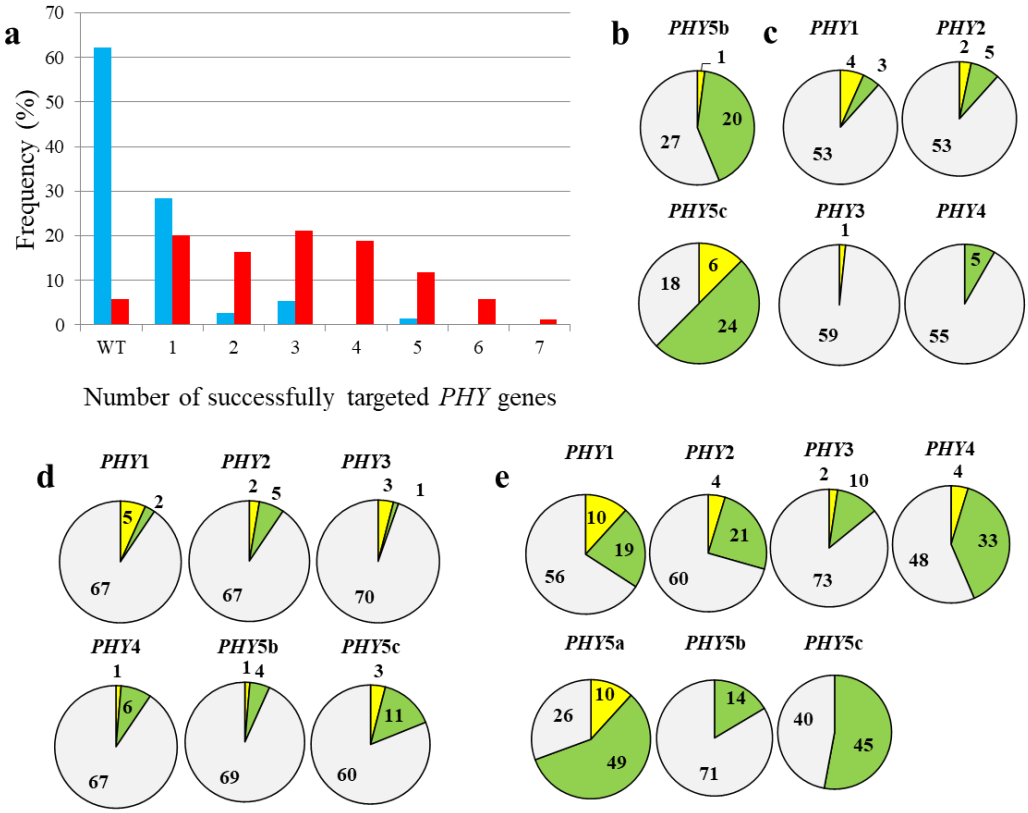

Fig. 5 Cas9-mediated *PHY* multiplex gene targeting. a Frequency distribution of single and multiple mutants obtained in transfections targeting 6 (blue, Table 1d) and 7 (red, Table 1e) PHY genes, the latter exploiting the pAL114 plasmid carrying both Cas9 and the hygromycin resistance cassette. **b, c** Distributions of indels identified for each target in the transfections targeting 2 and 4 PHY genes (Table 1b, c). **d, e** Distributions of indels identified for each target in the transfections targeting 6 and 7 PHY genes (Table 1d, e), respectively. Deletions (green), insertions (yellow), wild-type loci (grey).

Several septuple and sextuple KOs were also generated by targeting the remaining wild-type *PHY5a* and *PHY5b* genes in the quintuple KO mutant generated earlier (Table 4f, Fig. 5).

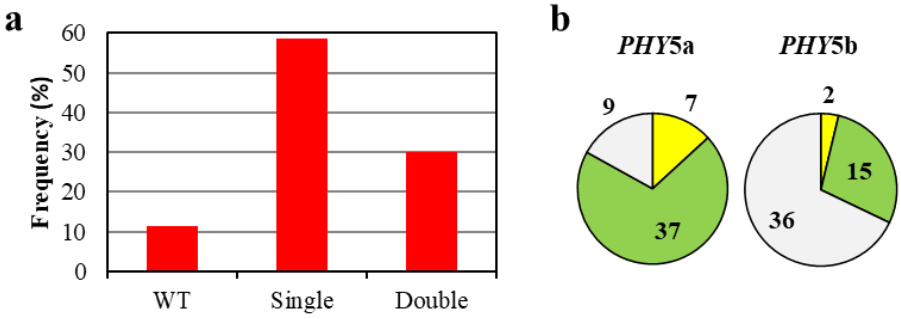

Fig. 6 Retransfection of a quintuple mutant targeting the two remaining WT genes *PHY5a* and *PHY5b* (Table 1f). a Frequency distribution of single and double mutants. **b** Distribution of deletion and insertion events. Deletions (green), insertions (yellow), wild-type loci (grey).

Following the creation of the phytochrome mutant library (SI in Appendix 12.1.1), an additional Cas9-mediated multiplex mutagenesis experiment was performed targeting *PHY5a-c*. This transfection was carried out in order to produce additional mutants for subsequent physiological analysis. Physcomitrella protoplasts were therefore transfected with the optimized pAL114 plasmid and the appropriate sgRNA constructs. Several triple, double and single mutants in different combinations were obtained.

Further aspects of the CRISPR methodology in Physcomitrella were also investigated, including the significance of spacing between paired sgRNA targets and the efficacy of NHEJ and HDR in repairing the chromosome when excising a complete locus (Table 2 & 3 and Fig. 1 in Appendix 12.1).

Additionally, the light-dependent abrogation of gravitropism, a response dependent on the formation of Pfr, was investigated in the septuple *phy*$^{7-}$ mutants and in different lower-order mutated lines (Fig. 7).

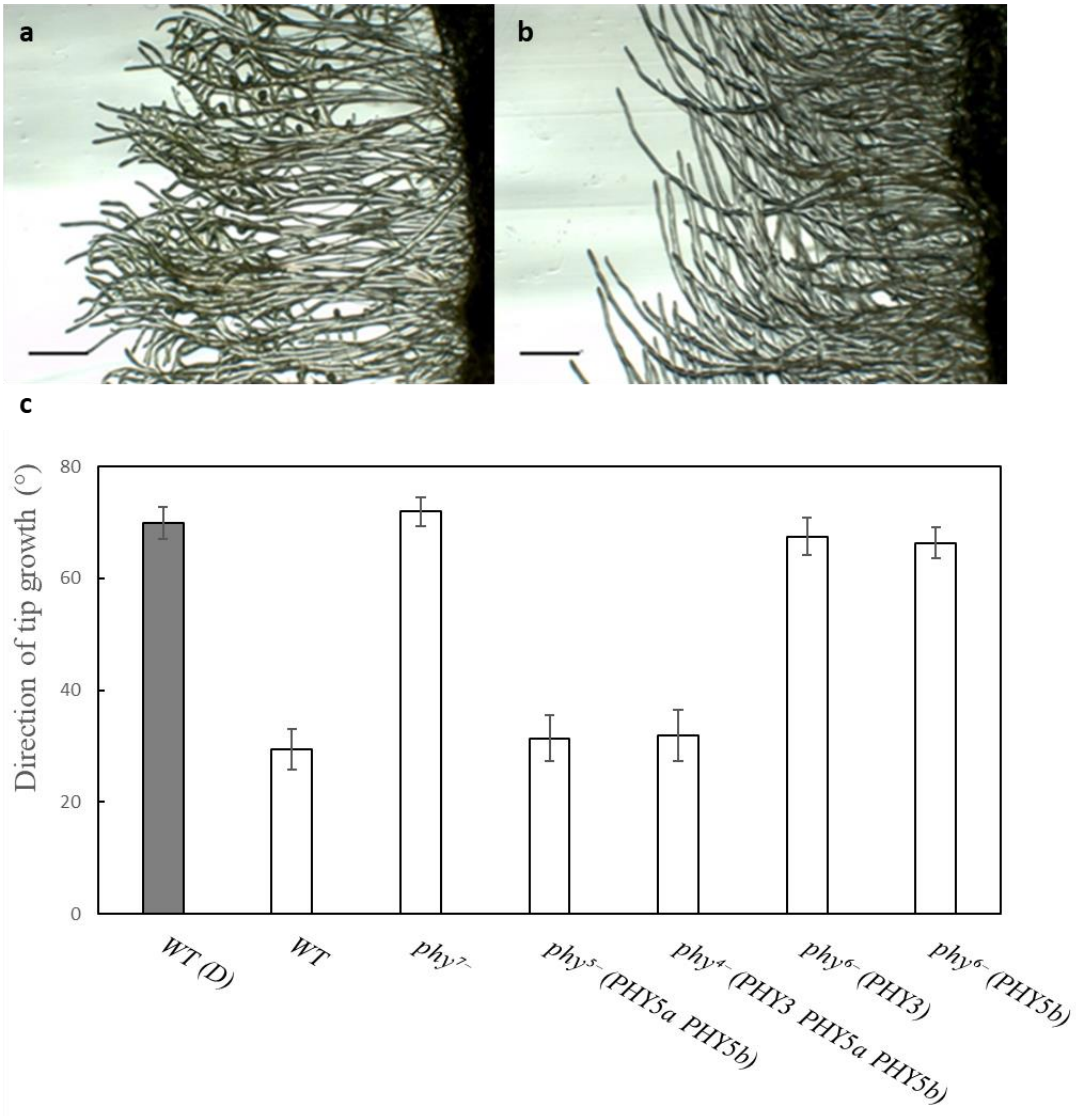

Fig. 7 Phytochrome-mediated abrogation of gravitropism. a WT and **b** *phy*$^{7-}$ lines after reorientation in red light. Scale bars: 1.5 mm. **c** Tip growth direction (mean ± SE) of WT in darkness and of WT and five mutant lines in red light (modified from (Trogu et al. 2021))**.**

The strong negative gravitropism shown by the WT in darkness was inhibited by light, whereas the septuple *phy*$^{7-}$ mutants remained strongly gravitropic, in line with expectations (Fig. 7a-b). The responses of lower order multiplex KOs revealed that gravitropic suppression is primarily controlled by phy5a (Fig. 7c).

4.2 CRISPR/Cas9 multiplex mutagenesis of the phototropin gene family

Double and triple phototropin KO lines, originally generated by Kasahara and co-workers (Kasahara et al. 2004), were previously analysed regarding their phototropism and polarotropism in R light by Jaedicke *et al.* (Jaedicke et al. 2012) The results revealed that both mutated lines were severely affected in their positive R phototropism, the triple KO showing the strongest phenotype. Equivalent polarotropic phenotypes were reported. These observations showed a clear dependency of phytochrome-mediated R photo- and polarotropism upon phototropins, reinforcing the hypothesis that directional sensing in Physcomitrella is carried out by phy-phot complex at the plasma membrane (Jaedicke et al. 2012). In order to analyse the involvement of phototropins in the directional sensing response and to understand better the nature of the phy-phot interaction, Cas9-mediated multiplex gene editing was performed targeting all 5 phototropin genes to generate quintuple *phot*$^{5-}$ mutants.

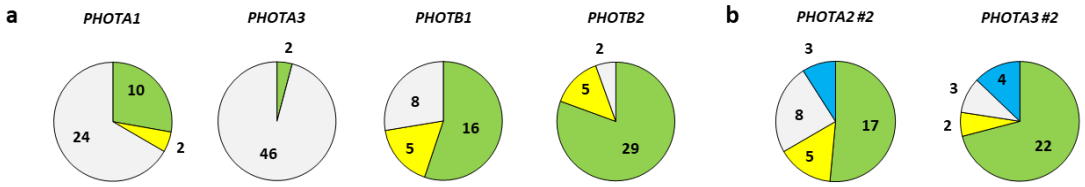

Fig. 8 Distribution of deletion, insertion and insertion-deletion events found for each sgRNA in the transfections targeting Pp.PHOT genes. a Distribution of indels identified in the transfection targeting all five Pp.PHOT genes. sgRNA targeting PHOTA2 induced no mutations, therefore is not shown; **b** Distribution of deletion, insertion and insertion-deletion events found in the retransfection of a triple mutant targeting the remaining wild-type genes PHOTA2 and PHOTA3 with new sgRNA constructs. Deletions (green), insertions (yellow), insertion-deletion (blue) and wild-type loci (grey).

Physcomitrella protoplasts were transfected with the improved CRISPR/Cas9 procedures used to create the phytochrome mutant library (see Appendix 12.1.1). PCR screening revealed that PHOTA1, PHOTB1 and PHOTB2 were successfully targeted. The sgRNAs used induced insertions and, more commonly, deletions as previously seen (Fig. 5b-e & Fig. 6b). However, no line carrying mutations in *PHOTA2* was found and only two carried mutations in *PHOTA3*, suggesting poor targeting efficiency of both sgRNAs (Fig. 8a). Therefore, new sgRNAs constructs (*PHOTA2* #2 and *PHOTA3* #2) were designed and used to target the remaining wild-type *PHOTA2* and *PHOTA3* genes in a triple KO line (*photA1 photB1 photB2*) obtained in the previous experiment. The new sgRNA constructs had efficiencies of 76% and 90% for the sgRNA targeting *PHOTA2* and *PHOTA3*, respectively. Both sgRNAs induced deletions, insertions and insertion-deletion mutation types, deletions remaining more abundant (Fig. 8b). Several quintuple and quadruple KO mutants were thereby produced successfully.

4.3 Vectorial responses of the phytochrome mutants

4.3.1 Phototropism in continuous red light

In order to investigate phytochrome function in Physcomitrella phototropism, phytochrome mutants generated in 5.1 were compared to the WT regarding their phototropic response in R light according to Mittmann *et al.* (Mittmann et al. 2004) and Ermert *et al.* (Ermert et al. 2019). Dark-adapted filaments were grown negatively gravitropically before being exposed to unilateral collimated R at 1.5 µmol m^{-2} s^{-1} (Fig. 3).

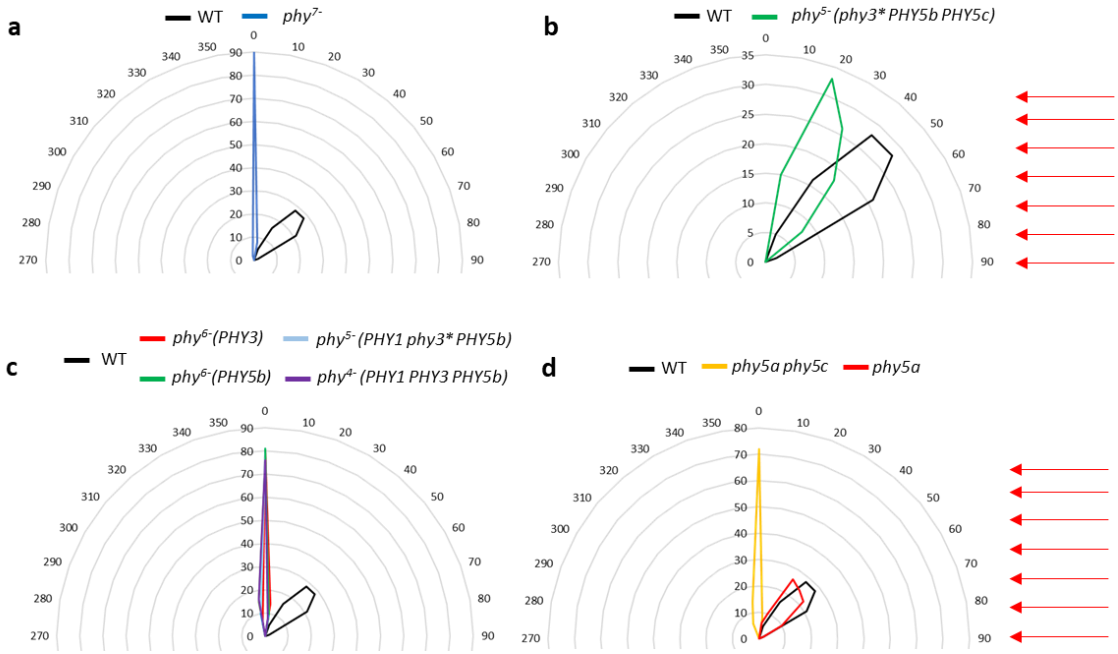

Fig. 9 Phototropic responses of *phy* mutants after R irradiation. a-d Radar charts showing the percentage distribution of bending directions of caulonemata filaments in WT and mutated lines irradiated with unidirectional collimated R light. The direction of illuminations was from the right as indicated by the arrows.

Since directional responses in Physcomitrella are induced by phytochromes, the *phy*$^{7-}$ mutant was expected to have lost the phototropic response. Indeed, *phy*$^{7-}$ lines were aphototropic (Fig. 9a & 11b), whereas WT filaments bent toward the light source (Fig. 9a & 11a). Lower-order mutants were then investigated, some showing positive phototropism. The most interesting example is the quintuple mutant *phy*$^{5-}$*(phy3* PHY5b PHY5c)* in which the response was weakened relative to the WT (Fig. 9b). Several lines were instead aphototropic similarly to the *phy*$^{7-}$ mutants. These findings imply that some phytochromes act redundantly in mediating the phototropic response. Hence, specific combinations of mutated phytochrome genes result in different phenotypes. Indeed, comparing the phenotype of lines containing different combinations of phytochrome mutations, it appears that neither phy1 nor phy3 are involved in the phototropic response (Fig. 9c). On the other hand, all higher-order aphototropic mutants carried hard (frame-shift) mutations in both *PHY5a* and *PHY5c*, suggesting a more prominent role of these photoreceptors in the response (Fig. 9c). This was confirmed by the analysis of the phototropic responses of *phy5a phy5c*$^{-}$ and *phy5a*$^{-}$ mutants. Remarkably, whereas all *phy5a phy5c*$^{-}$ mutants were aphototropic, *phy5a*$^{-}$ showed positive

phototropism, confirming that both phy5a and phy5c photoreceptors are necessary to mediate the phototropic response (Fig. 9d).

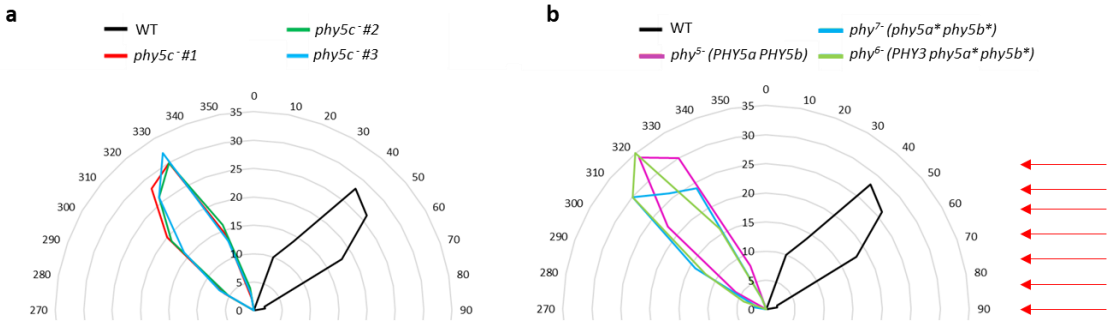

Fig. 10 Phototropic responses of *phy* mutants carrying KO mutations in *PHY5c*. Radar charts showing the percentage distribution of bending directions of caulonemata filaments in WT and mutated lines irradiated with unidirectional collimated R light; **a** WT and *phy5c*⁻ mutants obtained from different transfection events; **b** WT and multiplex mutated lines. The direction of illumination was from the right as indicated by the arrows.

Surprisingly, some mutated lines displayed a negative phototropic response with filament tips bending away from the light source. Amongst higher-order mutated lines, a septuple mutant carrying in-frame mutations in *PHY5a* and *PHY5b* was negatively phototropic, as well as quintuple *phy*$^{5-}$ *(PHY5a PHY5b)* lines and sextuple *phy*$^{6-}$ *(PHY3 phy5a* phy5b*)* (Fig. 10b). *phy*$^{6-}$ *(PHY5b)* lines were instead aphototropic (Fig. 9c). Analysis of three *phy5c*⁻ lines obtained from different transfection events (*phy5c*⁻ *#1, phy5c*⁻ *#2*, *phy5c*⁻ *#3),* proved unequivocally that the absence of the phy5c photoreceptor was responsible for this remarkable phenotype (Fig. 10a & 11c). Clearly, the phototropic response involves some kind of balance between positively and negatively acting phytochromes. The two phytochromes may have different ability to interact with phototropins. Whereas this result reveals that the system is more complicated than has hitherto been expected, the novel insight provided might allow certain aspects that had been ignored in earlier models to be explained.

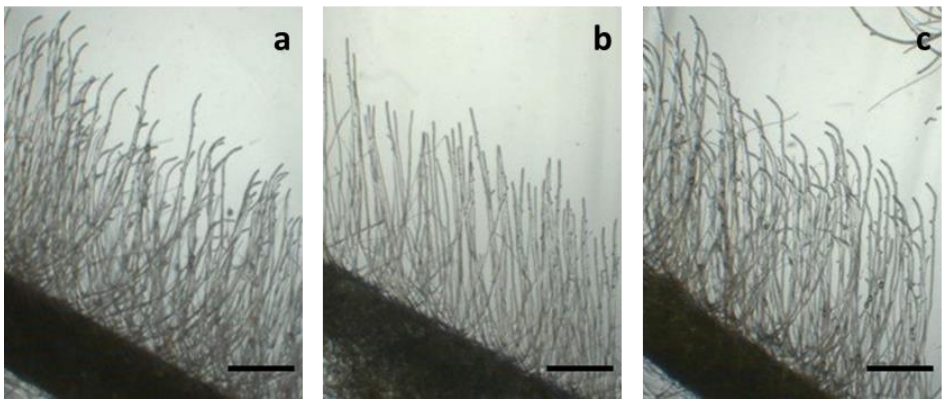

Fig. 11 Physcomitrella caulonemata after irradiation with R at 1.5 µmol · m^{-2} · sec^{-1}. a WT caulonemata with filament tips bending towards the light from the right; **b** *phy*$^{7-}$ remained aphototropic; **c** filaments from *phy5c*⁻ line were negatively phototropic. Scale bars: 1mm.

Table 5. Phototropic response of WT and *phy* mutants at 1,5 µmol m^{-2} s^{-1} R

Line	Mean bending ± SE of tip cell, °	*n*
WT	45 ± 1.4	450
phy7-	0.6 ± 0.3	324
phy5- (phy3 PHY5b PHY5c)*	36.4 ± 1.2	265
phy6- (PHY3)	0.8 ± 0.4	284
phy6 - (PHY5b)	0.5 ± 0.9	250
phy5- (PHY1 phy3 PHY5b)*	-0.4 ± 0.5	250
phy4- (PHY1 PHY3 PHY5b)	0.8 ± 1.7	282
phy5a-	42.1 ± 1.3	210
phy5a phy5c-	-1.3 ± 0.6	320
phy5c- #1	-37.2 ± 1.2	350
phy5c- #2	-36 ± 1.1	350
phy5c- #3	-35.8 ± 1.2	350
phy7- (phy5a phy5b*)*	-35.4 ± 1.5	350
phy5- (PHY5a PHY5b)	-31.2 ± 1	253
phy6- (PHY3 phy5a phy5b*)*	-37.1 ± 1.9	219

Table 6. Mutations profile of the *phy* mutants

Line	***PHY1***	***PHY2***	***PHY3***	***PHY4***	***PHY5a***	***PHY5b***	***PHY5c***
phy7-	-28nt	-4bp	-37bp	-10bp	-23bp	-17bp	-5bp
phy5- (phy3 PHY5b PHY5c)*	5 SNPs	-8bp	-6bp	-10bp	-2bp	0	0
phy6- (PHY3)	+136bp	-8bp	0	+20bp	-13bp	-2bp	-5bp
phy6 - (PHY5b)	-28nt	-4bp	-37bp	-10bp	-5bp	0	-5bp
phy5- (PHY1 phy3 PHY5b)*	0	-8bp	-6bp	-5bp	-7bp	0	-5bp
phy4- (PHY1 PHY3 PHY5b)	0	-4bp	0	+111bp	-4bp	0	-5bp
phy5a-	0	0	0	0	+4bp	0	0
phy5a phy5c-	0	0	0	0	-5bp	0	-5bp
phy5c- #1	0	0	0	0	0	0	-5bp
phy5c- #2	0	0	0	0	0	0	+10bp
phy5c- #3	0	0	0	0	0	0	-5bp
phy7- (phy5a phy5b*)*	+14bp	-8bp	-14bp	-5bp	-9bp	-6bp	-5bp
phy5- (PHY5a PHY5b)	-28nt	-4bp	-37bp	-10bp	0	0	-5bp
phy6- (PHY3 phy5a phy5b*)*	-14bp	-8bp	0	-13bp	-3bp	-6bp	-5bp

4.3.2 Sensitivity of phototropism in red light

Mittmann *et al.* reported that phototropism in Physcomitrella showed a complex fluence rate dependency (Mittmann et al. 2004). In order further to investigate the processes involved, phototropic sensitivity in the WT and mutants (4.3.1) was measured quantitatively (Fig. 12). Dark-adapted filaments were grown negatively gravitropically and then irradiated with unilateral collimated R at different fluence rates.

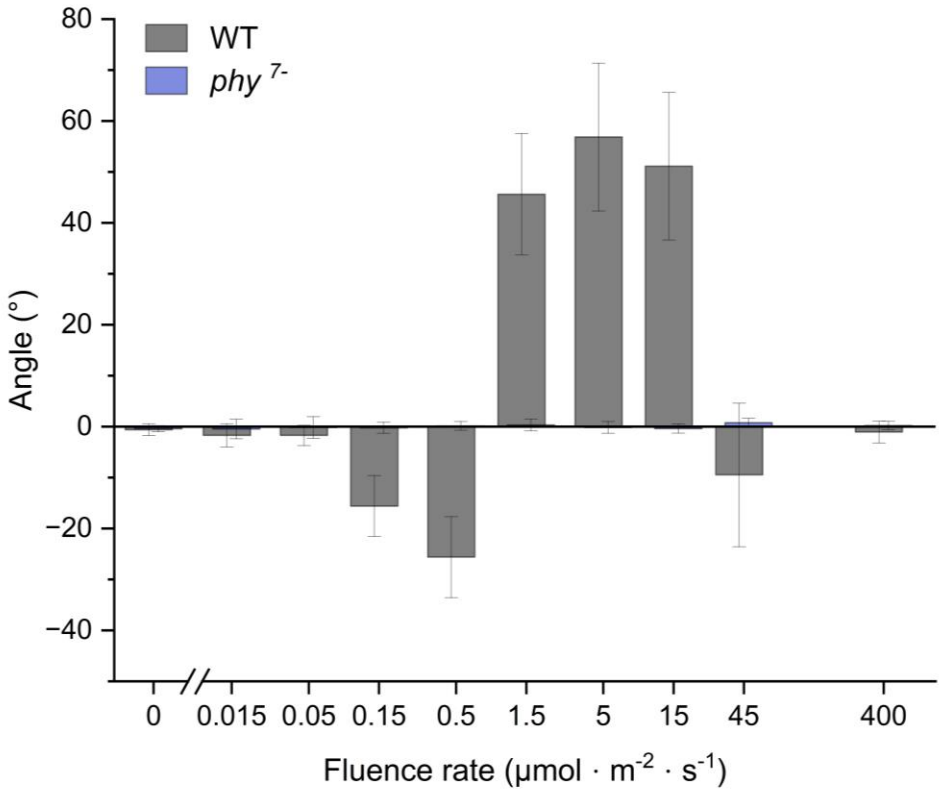

Fig. 12 Quantitative assay of phototropism in the WT and *phy*$^{7-}$ mutant. Error bars (±SD) are included for each mean.

In WT filaments negative and positive phototropism was seen at 0.05 to 0.5 and 1.5 to 15 µmol m^{-2} s^{-1} with maxima of about -25° and +60°, respectively. Phototropism was lost above 45 µmol m^{-2} s^{-1} (Fig. 12). Confirming the previous result (Fig. 9a), the *phy*$^{7-}$ mutant showed the strongest phenotype with no phototropic response at any fluence rate tested (Fig. 12).

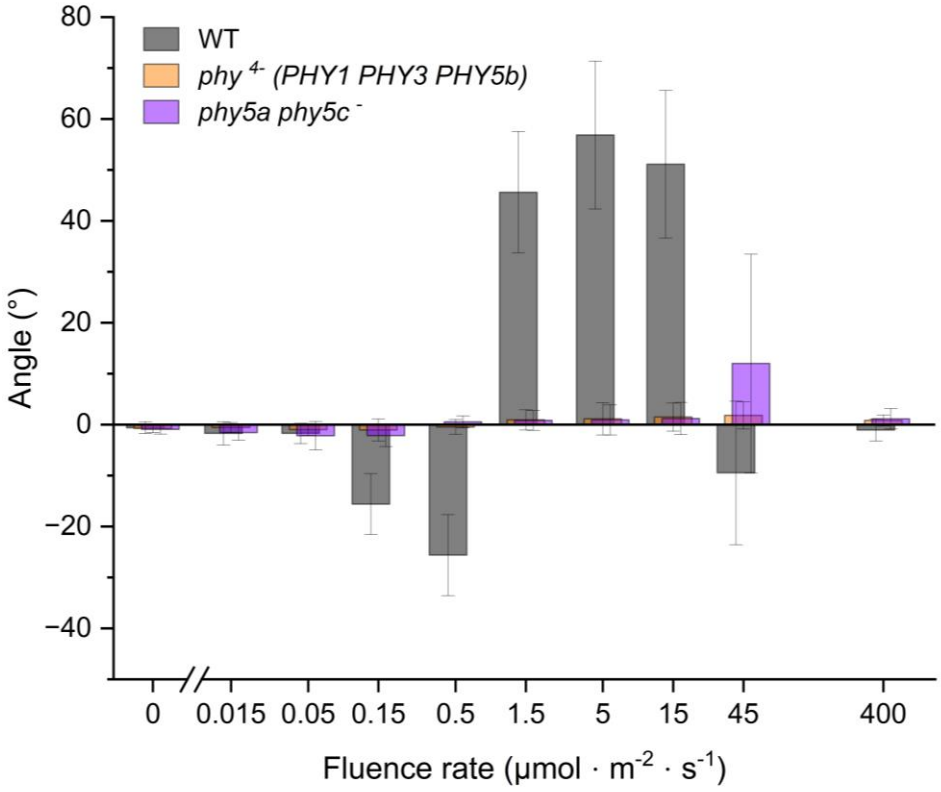

Fig. 13 Quantitative assay of phototropism in the *phy5a phy5c* and the *phy^{4-} (PHY1 PHY3 PHY5b)* lines. Fluence-rate response curves (mean bending angle) for the two mutated lines compared to the WT. Error bars (±SD) are included for each mean.

Similarly, in the *phy5a phy5c* line, phototropism was lost below 15 µmol m^{-2} sec^{-1}. Many filaments showed positive bending at 45 µmol m^{-2} s^{-1} but the data showed considerable variability. No phototropic response at 400 µmol m^{-2} s^{-1} was observed in this mutant as with the WT. Responses of *phy5a phy5c^{-}* were confirmed by a complete fluence-rate response analysis for two additional knock-out lines. In the *phy^{4-} (PHY1 PHY3 PHY5b)* mutant, phototropism was lost similarly to the *phy^{7-}* line (Fig. 13). It is therefore apparent that under high light conditions, phy2 and/or phy4 are able to induce a weak phototropic response.

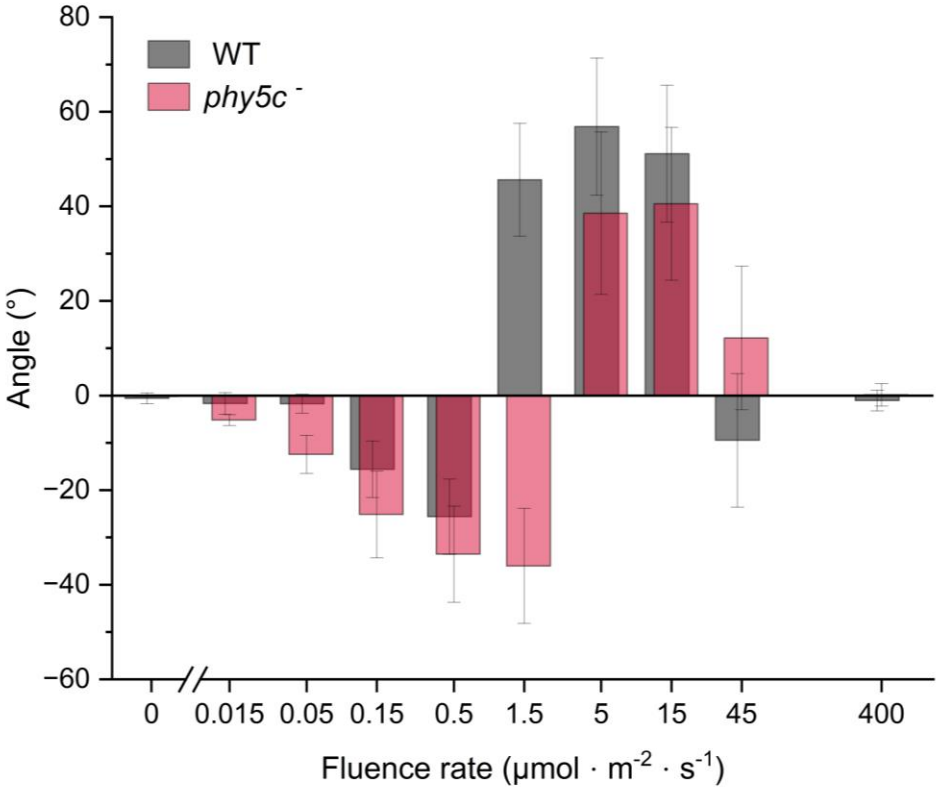

Fig. 14 Quantitative assay of phototropism in the *phy5c*⁻ mutant. Fluence-rate response curves (mean bending angle) for the *phy5c* line compared to the WT. Error bars (±SD) are included for each mean.

The fluence-rate response analysis for the *phy5c*⁻ (Fig. 14) was intriguing. Negative phototropism was stronger than in the WT and seen even at 1.5 µmol m^{-2} s^{-1}, a fluence rate at which the WT already showed a strong positive response. At higher fluence rates 5 to 45 µmol m^{-2} s^{-1}, positive phototropism was observed, albeit rather weaker than in the WT. This implies enhanced negative phototropic sensitivity in *phy5c*⁻. As in the WT phototropism was lost at high fluence rates.

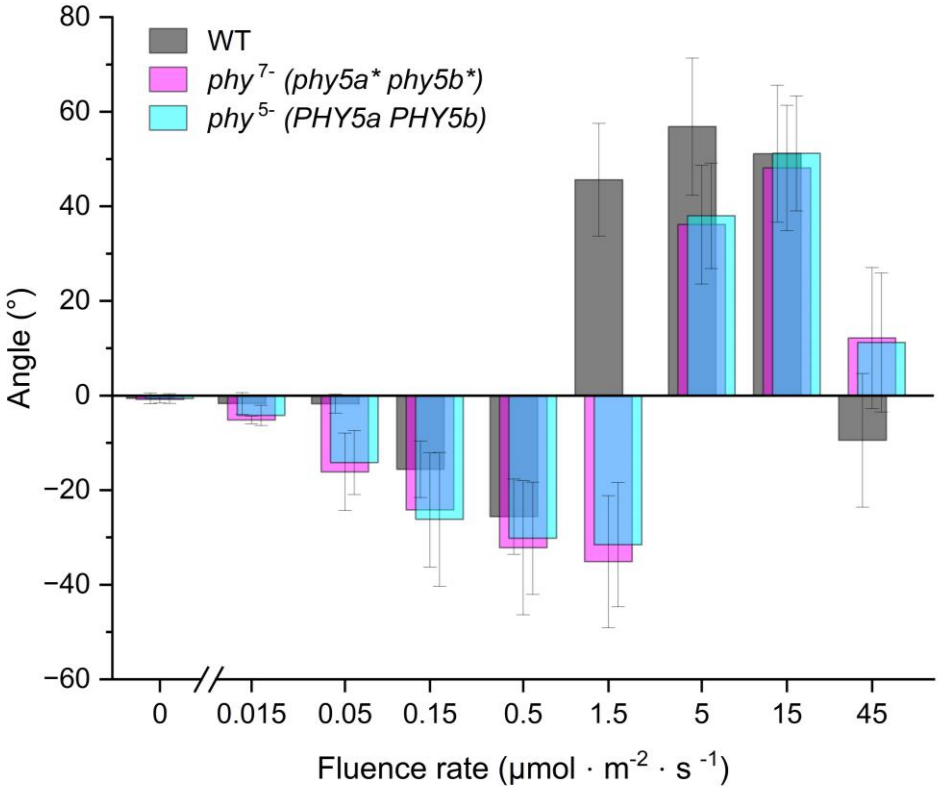

Fig. 15 Quantitative assay of phototropism in the *phy^{7-} (phy5a* phy5b*)* and *phy^{5-} (PHY5a PHY5b)* mutants. Fluence-rate response curves (mean bending angle) for the two mutated lines compared to the WT. Error bars (±SD) are included for each mean.

The *phy^{5-} (PHY5a PHY5b)* and the *phy^{7-} (phy5a* phy5b*)* lines showed changes in their fluence-response curves similar to the those observed for the *phy5c* line: negative bending still present at 1.5 µmol m^{-2} sec^{-1} and positive bending observed at higher fluence rates (Fig. 15).

4.3.3 Polarotropism in red light

As paralleled in many other non-seed plants, the direction of Physcomitrella protonemal filament growth can be steered by the polarisation plane of incident light. Like phototropism, polarotropism is a phytochrome-mediated vectorial response to light that cannot be transmitted via gene regulation. This response too is likely mediated by phytochrome cytoplasmic action, perhaps via phy-phot interaction (Jaedicke et al. 2012). To assay this response quantitatively, negative gravitropically grown filaments were exposed to 30 nmol m^{-2} sec^{-1} of R_{pol} (see 3.4.7.3 and Fig. 4).

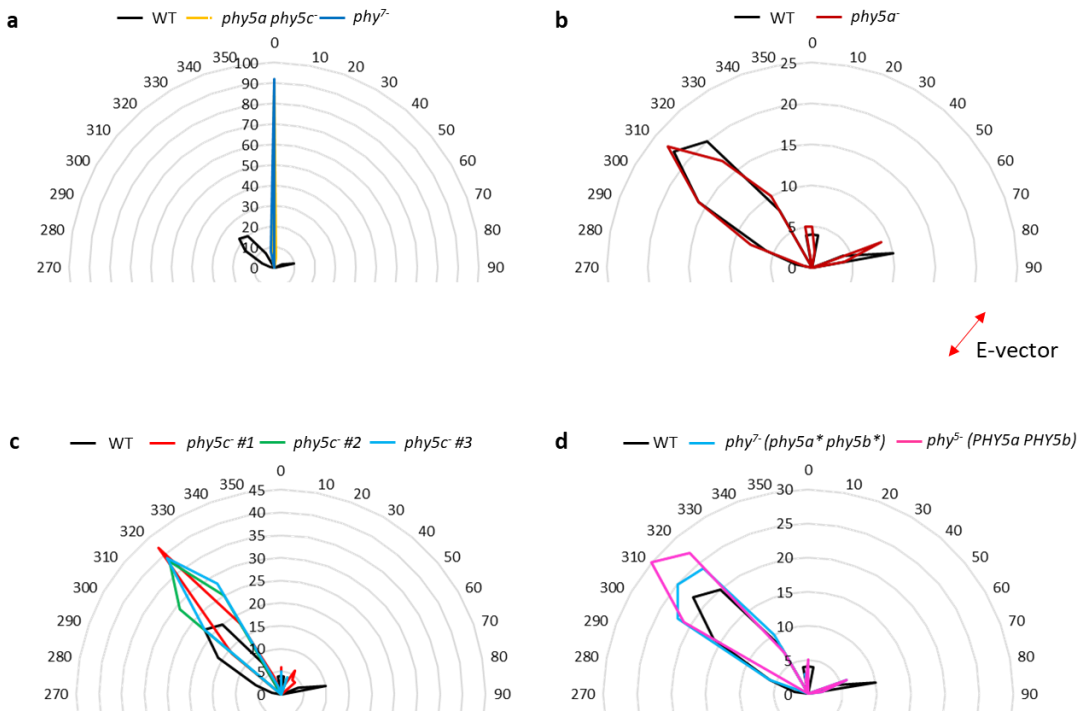

Fig. 16 R polarotropic bending of the WT and *phy* mutated lines. a-d Radar charts showing the percentage distribution of bending directions of caulonemata filaments in WT and mutated lines irradiated from above with continuous linearly polarised R light. The vibration plane of the E-vector was 45° relative to the cell axis after vertical growth.

Polarotropic responses of the different phytochrome mutants were in line with the phenotypes observed for phototropism in unilateral R. WT tip cells grew perpendicular to the E-vector, whereas this response was completely absent in both the *phy*$^{7-}$ and *phy5a phy5c*$^{-}$ lines (Fig. 16a). *phy5a*$^{-}$ showed a similar polarotropic response to the wild-type (Fig. 16b). Interestingly, filaments from *phy5c*$^{-}$, *phy*$^{5-}$ *(PHY5a PHY5b)* and *phy*$^{7-}$*(phy5a* phy5b*)* mutants all responded similarly to the WT (Fig. 16c-d).

Table 7. Polarotropic responses of WT and *phy* mutants

Line	SE	*n*
WT	2.1	300
phy^{7-}	0.2	220
phy5a phy5c^{-}	0.3	220
phy5a^{-}	2	250
phy5c^{-} *#1*	1.3	250
phy5c^{-} *#2*	1.2	250
phy5c^{-} *#3*	1.1	250
phy^{7-}*(phy5a* phy5b*)*	1.5	220
phy^{5-} *(PHY5a PHY5b)*	1.6	220

4.4 Response analysis of phytochrome mutants in continuous and pulsed light at different wavelengths

4.4.1 Phototropism at different wavelengths

The phenotypes of the *phy5c*$^{-}$, *phy5a phy5c*$^{-}$ and *phy*$^{7-}$ lines under continuous unilateral R light raised intriguing questions regarding the role of phytochrome in mediating this response. Consequently, these lines were compared with the WT at different wavelengths. In particular, phototropic responses were tested under FR light, under simultaneous illumination with R and FR light, and under B light. Dark-adapted caulonemata were grown negatively gravitropically and then irradiated with unilateral collimated light as in the previous experiments (4.3.1).

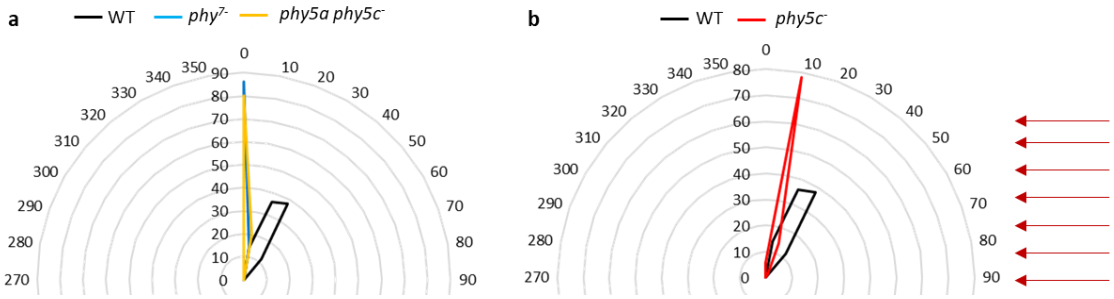

Fig. 17 Phototropic responses of *phy* mutants under continuous FR. Radar charts showing the percentage distribution of bending directions of caulonemata filaments in WT and mutated lines irradiated with unidirectional collimated FR light; **a** WT (SE 0.5, *n* 450*)*, *phy*$^{7-}$ (SE 0.3, *n* 205) and *phy5a phy5c*$^{-}$ (SE 0.4, *n* 225); **b** *phy5c*$^{-}$ line (SE 0.9, *n* 293).

Irradiation with continuous FR light is expected to maintain a constant low level of Pfr. It was previously shown that filaments from primary chloronemata were positively phototropic over a wide range of fluence rates of unilateral FR (Jenkins et al. 1983). Here, phototropism in caulonemata was evaluated under FR light at 1.5 µmol m^{-2} s^{-1}, here too revealing positive phototropism. WT filaments showed about +25° bending, whereas the *phy*$^{7-}$ and the *phy5a phy5c*$^{-}$ remained aphototropic (Fig. 17a). Interestingly, the *phy5c*$^{-}$ mutant, which was negatively phototropic in R light at the same fluence rate, showed weak positive phototropism of about +10° (Fig. 17b).

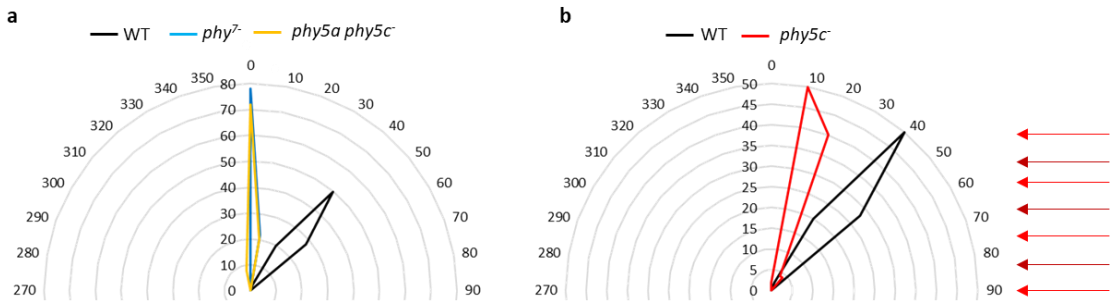

Fig. 18 Phototropic responses of *phy* mutants under simultaneous irradiation with R and FR. Radar charts showing the percentage distribution of bending directions of caulonemata filaments in WT and mutated lines irradiated with unidirectional collimated R supplemented with FR; **a** WT (SE 0.9, *n* 249), *phy*$^{7-}$ (SE 0.3, *n* 200) and *phy5a phy5c*$^{-}$ (SE 0.4, *n* 212); **b** *phy5c*$^{-}$ (SE 1, *n* 225).

Whereas continuous R light is expected to induce a high proportion of Pfr, simultaneous irradiation with FR would reduce the proportion of Pfr at photoequilibrium. In order to investigate the effect of this in direction sensing, the phototropic responses of the WT and *phy* mutants previously tested under continuous FR, were assayed under simultaneous irradiation with R at 1.5 µmol m^{-2} s^{-1} and FR at 0.8 µmol m^{-2} s^{-1}. The phenotypes observed were similar to those obtained under continuous FR. Whereas WT filaments showed strong positive bending of about +40°, *phy*$^{7-}$ and the *phy5a phy5c*$^{-}$ mutants were aphototropic, whereas the *phy5c*$^{-}$ showed a weak positive response of about +15° (Fig. 18).

Next, phototropic responses of the WT and *phy* mutants were tested under continuous B light. B-induced tropic responses were previously reported in chloronemata. In particular, weak positive phototropism was observed at lower fluence rates and negative phototropism at higher fluence rates (Jenkins et al. 1983). With dark-adapted caulonemata, however, B at 1 µmol m^{-2} s^{-1} did not induce significant phototropism (Jaedicke et al. 2012). Although phototropism in seed plants is clearly a B light response mediated by phototropins, in Physcomitrella R acting through phytochrome predominates. However, since phytochrome weakly absorbs in the B region too, a directional response to B might be expected, perhaps at higher fluence. Thus, phototropism in the WT and *phy* mutants was tested at 5 and 10 µmol m^{-2} s^{-1}.

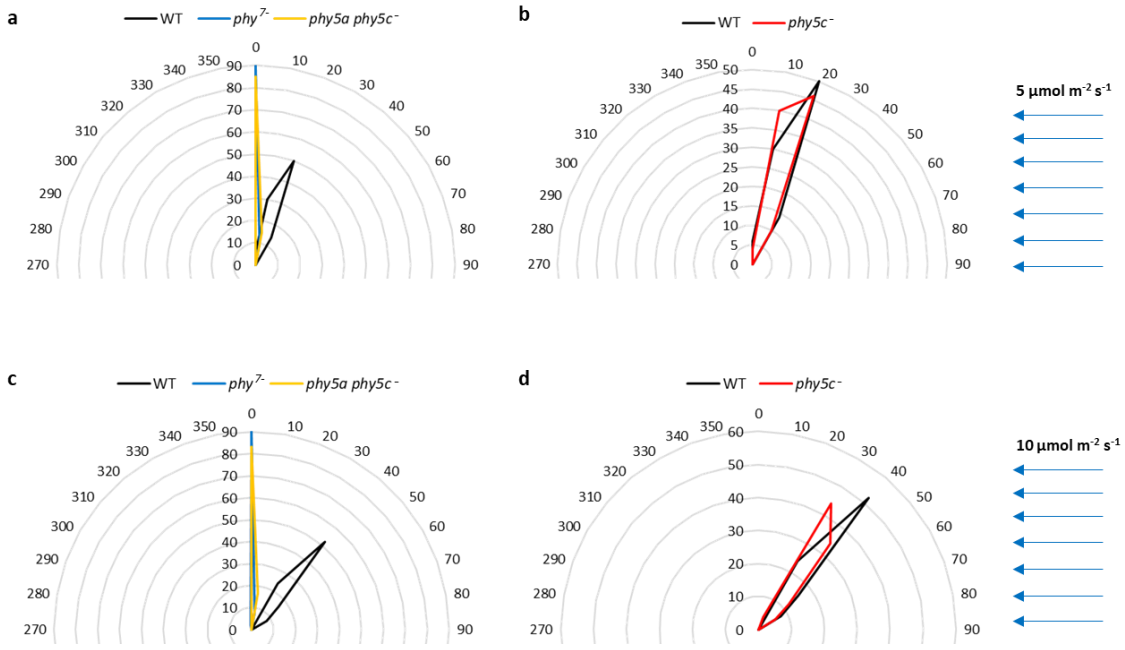

Fig. 19 Phototropic responses of *phy* mutants under B irradiation. Radar charts showing the percentage distribution of bending directions of caulonemata filaments in WT and mutated lines irradiated with unidirectional B light at 5 µmol m^{-2} s^{-1} (**a**-**b**) and 10 µmol m^{-2} s^{-1} (**c**-**d**).

Table 8. Responses of WT and *phy* mutants under B irradiation

Line	SE	*n*
At 5 µmol m^{-2} s^{-1}		
WT	1	457
phy7^{-}	0.2	245
phy5a phy5c^{-}	0.4	250

phy5c^{-}	0.6	420
At 10 µmol m^{-2} s^{-1}		
WT	1.1	450
phy7^{-}	0.3	200
phy5a phy5c^{-}	0.4	200
phy5c^{-}	0.9	250

The WT showed positive phototropism of +17°and +40° at 5 and 10 µmol m^{-2} s^{-1}, respectively, whereas, interestingly, both the *phy7*$^{-}$ null mutant and the *phy5a phy5c*$^{-}$ mutant showed no reaction, implying their requirement for phototropism in B light (Fig.17a-c). The *phy5c*$^{-}$ mutant, instead, showed positive bending at both fluence rates with a response comparable to the WT (Fig. 19b-d).

Overall, these results indicate that phytochrome plays an important role in the induction of B light phototropic response in caulonemata. Moreover, phy5a and phy5c are necessary for the induction of both R and B phototropism.

4.4.2 Phototropism in pulsed light

After characterizing the phototropic responses of the WT and mutant lines under continuous irradiation, pulsed light conditions were assessed. These experimental conditions were chosen to test the idea of phytochrome molecules being restricted in their movements (see 1.4.3.1) and thus being capable to produce a Pfr gradient in the cell that would remain in darkness to induce a phototropic response.

WT responses were compared to *phy5a phy5c*$^{-}$ and *phy5c*$^{-}$ mutants. Dark-adapted caulonemata were grown negatively gravitropically and then given 5 min R (1.5 µmol m^{-2}s^{-1}) pulses (Rp) followed by 30 min of darkness (Rp-D), or 10 min FR (1.5 µmol m^{-2}s^{-1}) pulses (FRp) followed by 30 min of darkness (FRp-D) over a period of 24h until assayed. In order to test R/FR reversibility, the same lines were irradiated with 5 min of Rp followed by 5 min of FRp (Rp-FRp) and subsequently 30 min of darkness. This irradiation program was repeated for 24 hours.

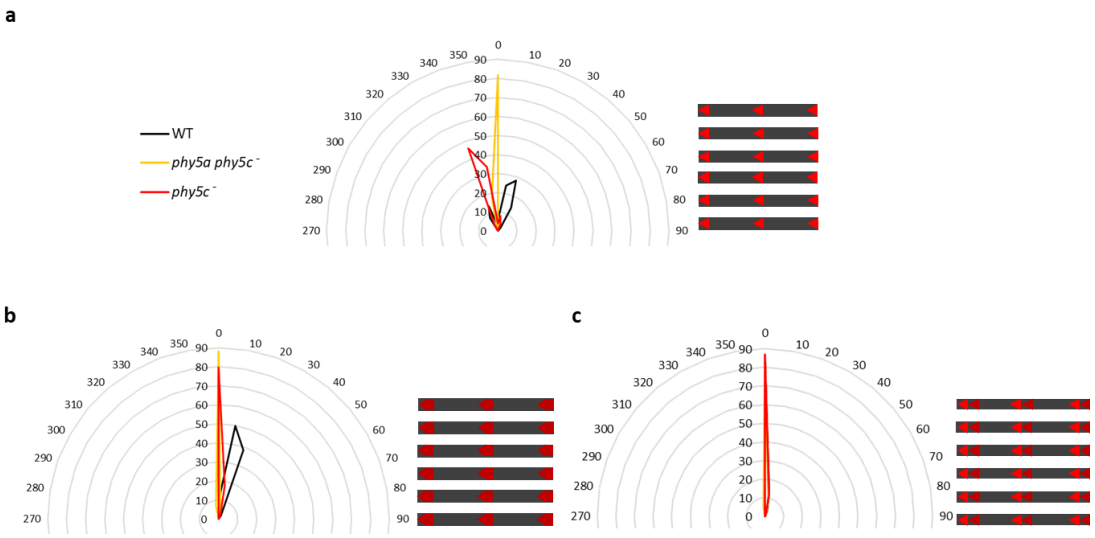

Fig. 20 Phototropic responses of WT and *phy* mutants under pulsed light. Radar charts showing the percentage distribution of bending directions of filaments in WT, *phy5a phy5c⁻ and phy5c⁻* mutants irradiated with unilateral collimated pulsed R (**a**), FR (**b**) and R-FR (**c**).

Table 9. Phototropic responses of WT and *phy* mutants under pulsed light conditions

Line	SE	*n*
In Rp-D		
WT	2.8	303
phy5a phy5c⁻	0.4	251
phy5c⁻	1.5	287
In FRp-D		
WT	0.4	250
phy5a phy5c⁻	0.4	220
phy5c⁻	0.5	268
In Rp-FRp		
WT	0.5	252
phy5a phy5c⁻	1.2	220
phy5c⁻	0.9	250

In the Rp-D treatment, WT filaments showed predominantly positive but also negative phototropism. Bending was weaker than seen under continuous R. This may be related to the different number of photons received in pulsed light compared to continuous light, that is $8 \cdot 10^{21}$ and $5 \cdot 10^{22}$ respectively. *phy5c⁻* on the other hand was predominantly negatively phototropic. Here too the response was reduced compared to that in continuous R. The *phy5a phy5c⁻* mutant, which showed no reaction to continuous R, remained aphototropic also under pulsed light conditions (Fig. 20a).

Under FRp-D irradiation, the WT showed a weak positive phototropic response, whereas in both *phy5c⁻* and *phy5a phy5c⁻* there was no measurable reaction (Fig. 20b).

Treatment with Rp-FRp irradiation allows phytochrome-typical photoreversibility of the phototropic response to be tested. Indeed, phototropic reaction induced by the Rp in the WT

and *phy5c*$^{-}$ line was inhibited by the subsequent FRp, resulting in an aphototropic phenotype. The *phy5a phy5c*$^{-}$ mutant remained aphototropic (Fig. 20c).

4.5 Phototropic response of phototropin mutants

4.5.1 Phototropism in continuous light

To better understand the nature of the phy-phot interaction at the plasma membrane (Jaedicke et al. 2012) and in particular the role of phototropins in directional sensing, quintuple *phot*$^{5-}$ mutants generated in 4.2 were analysed regarding their phototropic responses under unilateral collimated R, FR and B.

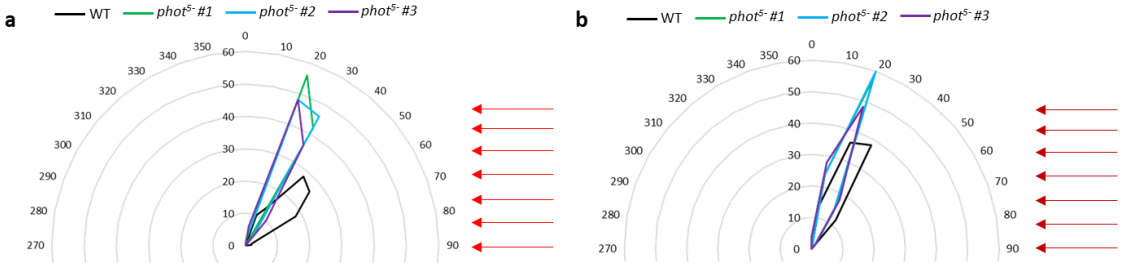

Fig. 21 Phototropic responses of *phot*$^{5-}$ mutants under R and FR irradiation. Radar charts showing the percentage distribution of bending directions of caulonemata filaments in *phot*$^{5-}$ lines irradiated with unidirectional collimated R (**a**) and FR (**b**).

Table 10. Phototropic responses of *phot*$^{5-}$ mutants under R and FR

Line	SE	*n*
In R		
phot^{5-} *#1*	0.5	400
phot^{5-} *#2*	0.8	400
phot^{5-} *#3*	0.9	400
In FR		
phot^{5-} *#1*	0.7	300
phot^{5-} *#2*	0.9	300
phot^{5-} *#3*	1	300

Phototropic responses of three *phot*$^{5-}$ lines (*phot*$^{5-}$ *#1*, *phot*$^{5-}$ *#2, phot*$^{5-}$ *#3*) were analysed under R at 1.5 µmol $m^{-2}s^{-1}$ and compared to the WT. Unexpectedly, the mutants still showed positive phototropism (*ca.* +25°), albeit rather weaker than the +45° seen in the WT (Fig. 21a).
Next, phototropic responses of the same set of *phot5-* mutants were analysed under FR at 1.5 µmol $m^{-2}s^{-1}$. They all showed positive phototropism (*ca*. +18°), only a little weaker than the +25° seen for the WT (Fig. 21b). The significance of this result regarding the phy-phot complex at the plasma membrane is discussed in 5.2.3.

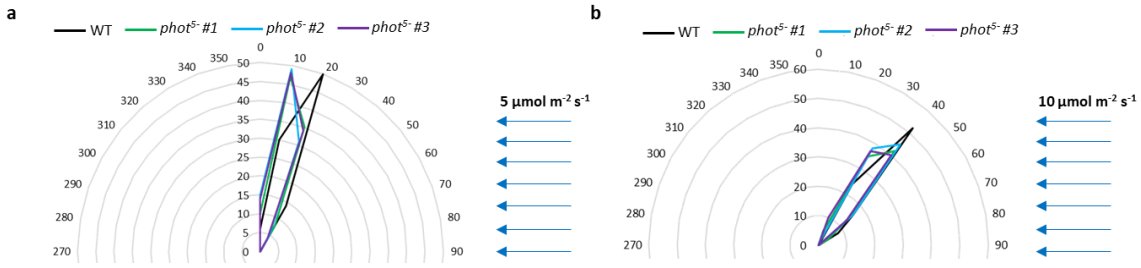

Fig. 22 Phototropic responses of *phot*$^{5-}$ under B irradiation. Radar charts showing the percentage distribution of bending directions of caulonemata filaments in *phot*$^{5-}$ irradiated with unidirectional B light at 5 µmol m^{-2} s^{-1} (**a**) and 10 µmol m^{-2} s^{-1} (**b**).

Table 11. *phot*$^{5-}$ responses under B irradiation

Line	SE	*n*
At 5 µmol m^{-2} s^{-1}		
phot^{5-} #1	0.8	225
phot^{5-} #2	0.8	225
phot^{5-} #3	0.7	225
At 10 µmol m^{-2} s^{-1}		
phot^{5-} #1	0.9	225
phot^{5-} #2	0.7	225
phot^{5-} #3	0.8	225

It had been shown earlier (Fig. 19) that B-induced phototropism was lost in both the *phy*$^{7-}$ and *phy5a phy5c*$^{-}$ lines, indicating that phytochrome is necessary for this response but not proving that the B-vector is perceived by phytochrome: that function might still be fulfilled by phototropin. Therefore, phototropic responses of the *phot*$^{5-}$ mutants were analysed under B at 5 and at 10 µmol $m^{-2}s^{-1}$. Under both fluence rates tested, the positive bending of the three *phot*$^{5-}$ mutants was similar to that of the WT (Fig. 22). This result, together with the aphototropic phenotype of the *phy*$^{7-}$, confirmed that phytochrome is the photoreceptor mediating directional sensing in phototropism.

Table 12. Mutations profile of the *phot* mutants

Line	***PHOTA1***	***PH*OTA2**	***PH*OTA3**	***PH*OTB1**	***PH*OTB2**
phot^{5-}*#1*	-4bp	-13bp	+2bp, +2bp	-2bp	+10bp
phot^{5-}*#2*	-4bp	+4bp	-10bp	-2bp	+10bp
phot^{5-}*#3*	-4bp	-44bp	-10bp	-2bp	+10bp

4.5.2 Phototropism in pulsed light

Phototropic responses of the *phot*$^{5-}$ mutants under different pulsed light treatments (Rp-D, FRp-D, and Rp-FRp) were assessed as before (see 4.2.2). In the Rp-D treatment, the WT and the *phot*$^{5-}$ lines showed similar, weak positive phototropism although a small proportion bent away from the light (Fig. 23a). No phototropic response was apparent in *phot*$^{5-}$ mutants under

FRp-D although a weak positive response was seen in the WT (Fig. 23b). The weak positive bending observed under Rp was abrogated by subsequent FRp, even in the WT (Fig. 23c).

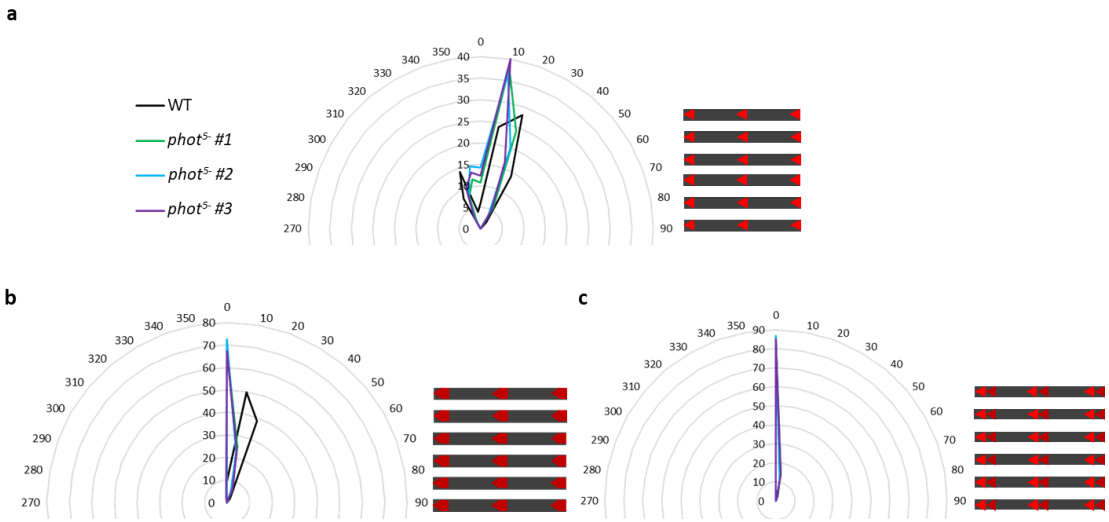

Fig. 23 Phototropic responses of *phot*$^{5-}$ mutants under pulsed light. Radar charts showing the percentage distribution of bending directions of caulonemata irradiated with unilateral collimated pulsed R (**a**), FR (**b**) and R-FR (**c**).

Table 13. *phot*$^{5-}$ responses under pulsed light conditions

Line	SE	*n*
In Rp-D		
phot^{5-} #1	1.8	220
phot^{5-} #2	1.4	289
phot^{5-} #3	1.5	250
In FRp-D		
phot^{5-} #1	0.7	320
phot^{5-} #2	0.6	249
phot^{5-} #3	0.6	250
In Rp-FRp		
phot^{5-} #1	0.4	226
phot^{5-} #2	0.3	230
phot^{5-} #3	0.4	310

4.6 Phototropism in *phy5c photA2*$^{-}$ double mutants

The four Physcomitrella phototropins originally identified by Kasahara et al., were shown by Jaedicke et al. to interact directly with phy4 in both Y2H, pull-down and sYFP-assays, the strongest Y2H interaction being with photA2 (Kasahara et al. 2004, Jaedicke et al. 2012). This interaction was corroborated by the weaker phototropic responses shown by the double and triple *phot* mutants (Jaedicke et al. 2012). Physiological analysis here showed, however, that phy5c rather than phy4 is predominant in mediating directional responses (see 5.3.1), possibly via an interaction with phot at the plasma membrane as observed with phy4. The contribution of photA2 and phy5c in the phototropic response were therefore analysed further. Two

transfections were performed to produce new sets of mutants with the improved CRISPR/Cas9 system. In the first, *PHY5c* and *PHOTA2* were targeted simultaneously in the WT background, while in the second only *PHY5c* was targeted in the *photA2* background generated by Kasahara *et al.* (Kasahara et al. 2004). *phy5c photA2*$^{-}$ double mutants were successfully obtained in both. These lines were grown negatively gravitropically and their phototropic responses were analysed relative to the WT under different light conditions.

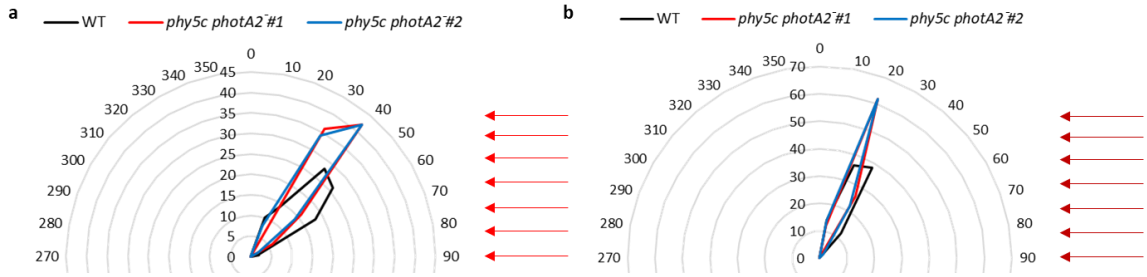

Fig. 24 Phototropic responses of *phy5c photA2*$^{-}$ lines under R and FR irradiation. Radar charts showing the percentage distribution of bending directions of caulonemata in the two mutants irradiated with unidirectional collimated R (**a**) and FR (**b**).

Table 14. Phototropic responses of *phy5c photA2*$^{-}$ mutants under R and FR

Line	SE	*n*
In R		
phy5c photA2^{-} *#1*	0.9	402
phy5c photA2^{-} *#2*	0.9	400
In FR		
phy5c photA2^{-}*#1*	0.6	380
phy5c photA2^{-}*#2*	0.7	320

Both *phy5c photA2*$^{-}$ double mutants irradiated with continuous R at 1.5 µmol $m^{-2}s^{-1}$ showed positive phototropic responses comparable to the WT (*ca*. +39° and +36°, respectively; Fig. 24a). Interestingly, negative phototropism observed in the *phy5c* mutant (Fig. 10a), was lost in the double *phy5c photA2*$^{-}$ mutant, clearly indicating a key role for photA2 in the negative phototropic responses. A similar response (*ca*. +20°) was observed for the WT and both mutated lines in continuous FR at 1.5 µmol $m^{-2}s^{-1}$ (Fig. 24b).

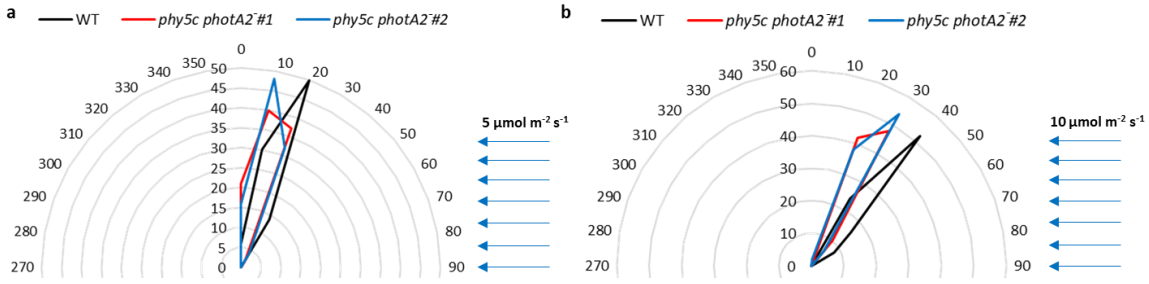

Fig. 25 Phototropic responses of *phy5c photA2*$^{-}$ mutants under B irradiation. Radar charts showing the percentage distribution of bending directions of filaments in *phy5c photA2*$^{-}$ mutants irradiated with unidirectional B light at 5 µmol m^{-2} s^{-1} (**a**) and 10 µmol m^{-2} s^{-1} (**b**).

Table 15. *phy5c photA2*⁻ responses under B irradiation

Line	SE	*n*
At 5 µmol m^{-2} s^{-1}		
phy5c photA2 #1	0.8	250
phy5c photA2 #2	0.8	250
At 10 µmol m^{-2} s^{-1}		
phy5c photA2 #1	0.7	400
phy5c photA2 #2	0.6	400

Irradiation with continuous B at 5 µmol $m^{-2}s^{-1}$ induced weak positive phototropism comparable to that of the WT (*ca*. +12°; Fig. 25a). The responses were stronger in 10 µmol $m^{-2}s^{-1}$ B (+26° and +40° in the mutants and the WT, respectively; Fig. 25b).

Next, phototropic reactions under pulsed light conditions were analysed for the *phy5c photA2*⁻ lines.

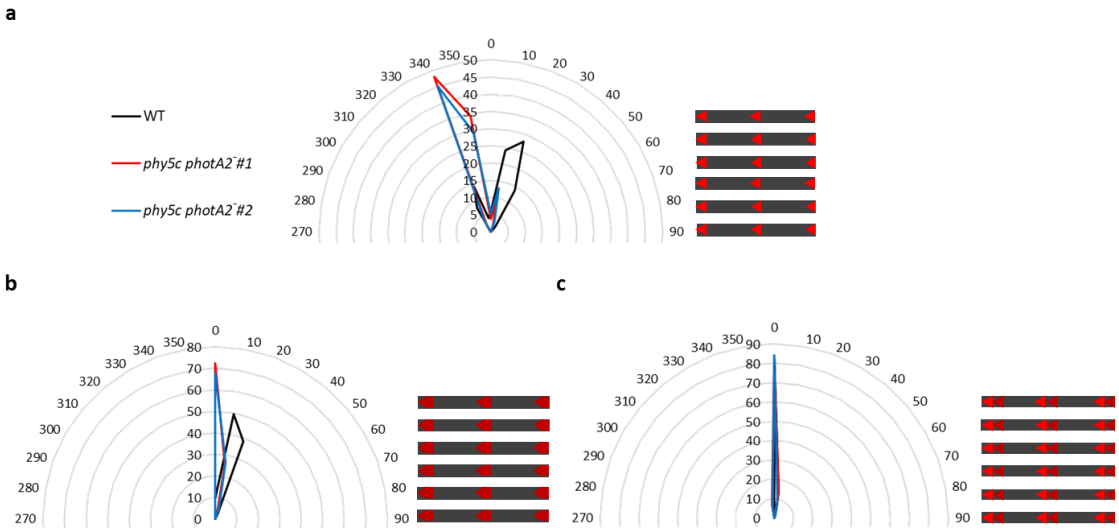

Fig. 26 Phototropic responses of *phy5c photA2*⁻ lines under pulsed light. Radar charts showing the percentage distribution of bending directions of caulonemata in *phy5c photA2*⁻ mutants irradiated with unilateral collimated pulsed R (**a**), FR (**b**) and R-FR (**c**).

Table 16. *phy5c photA2*⁻ responses under pulsed light conditions

Line	SE	*n*
In Rp-D		
phy5c photA2⁻ #1	1	340
phy5c photA2⁻ #2	1.2	350
In FRp-D		
phy5c photA2⁻ #1	0.7	400
phy5c photA2⁻ #2	0.6	408
In Rp-FRp		
phy5c photA2⁻ #1	0.5	287
phy5c photA2⁻ #2	0.4	280

In contrast to continuous R (Fig. 24a), under Rp-D, *phy5c photA2*$^{-}$ mutants showed negative phototropism (Fig. 26a) comparable to that of the *phy5c*$^{-}$ single mutant (Fig 20a). Both mutants were aphototropic under FRp-D although the WT showed a weakly positive response (Fig. 26b). The Rp-FRp assay showed negligible phototropism in both WT and *phy5c photA2*$^{-}$ mutants (Fig. 26c).

Table 17. Mutations profile of the *phy5c photA2*$^{-}$ mutants

Line	*PHY5c*	*PHOTA2*
phy5c photA2^{-} *#1*	-5bp	-16bp
phy5c photA2^{-} *#2*	-5bp	*Kasahara et al.* (Kasahara et al. 2004)

4.7 Optics in perception of light direction

In order to address the fundamental question of how an individual cell perceives the direction of illumination, experiments aiming toward a better understanding of the cell as an optical system were conducted. At the highest fluence rate tested, both the WT and all mutant lines were aphototropic (see 4.3.2). Early work (see 1.4.3.1) led to the hypothesis that perception of light direction in protonemata tip cells may depend on an effect whereby the tip cell would act as a lens, focusing light on the opposite side to the irradiated one. In order to test this idea, phototropic responses of the WT were investigated with filaments immersed in media of different refractive indices.

Phototropic experiments described earlier (see 4.3.1) were carried out with cultures growing on cellophane. In these conditions, the surface of the approximately cylindrical filaments is exposed to the air, a refractive index difference that would allow light to be focused on the distal side of the cell. In water, the effect would be much weaker, whereas in solutions with a refractive index similar to that of the cell, no focusing would be expected. Therefore, phototropic responses induced by unilateral collimated R at 1.5 µmol m^{-2} s^{-1} were analysed in dark-adapted caulonemata immersed in water and in a PEG solution of near zero osmotic potential to avoid turgor-related artefacts.

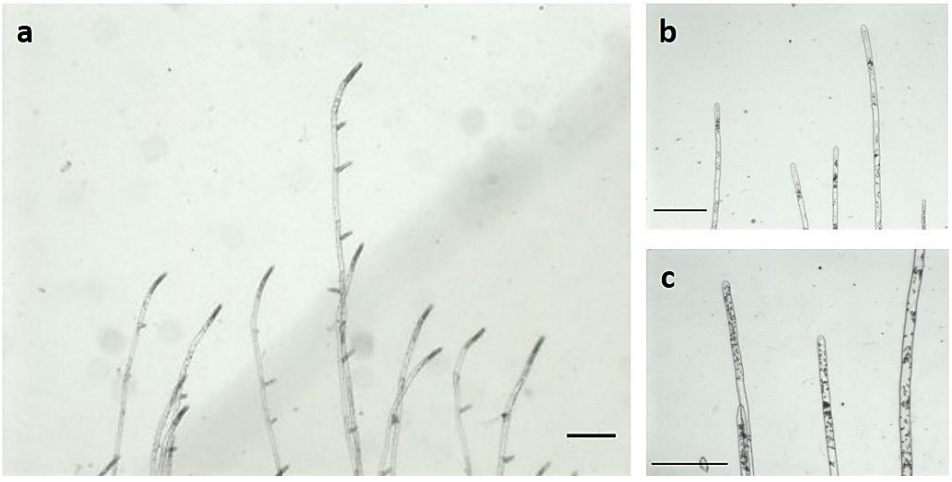

Fig. 27 Phototropic response of wild-type filaments immersed in water and 30% PEG 40000. a WT caulonemata immersed in water showed positive phototropism after unilateral collimated R irradiation at 1.5µmol $m^{-2}s^{-1}$ coming from the right; **b-c** under the same light conditions, filaments immersed in 30% PEG 40000 were instead aphototropic. Both experiments, in water and PEG solution, were repeated four times. Scale bars: 300µm.

In water (*n* = 1.33), filaments predominantly showed positive phototropism (Fig. 27a), suggesting that the focusing effect is still be present, although probably weakened. A 30% PEG (polyethylene glycol) 40000 solution in water was used due to its biocompatibility and high molecular weight to maintain cell turgor while increasing the refractive index slightly (to *n* = 1.38, similar to that expected for the cytoplasm). After R irradiation, filaments immersed in the PEG solution were aphototropic (Fig. 27b-c), suggesting that the focussing effect had been lost.

5. Discussion

5.1 Multiplex CRISPR/Cas9 mutagenesis in *P. patens*

(See also Appendix 12.1 (Trogu et al. 2021))

Multiplex CRISPR/Cas9 mutagenesis of the 7 members of the phytochrome gene family was carried out aiming to generate single and multiple mutants for functional genetics studies. In this study, the creation of an improved transient selection/Cas9 plasmid (pAL114), along with an efficient screening procedure with high-resolution PAGE gels, not only expanded Physcomitrella CRISPR-toolkit available, but was instrumental in the successful generation of a septuple mutant along with lower-order mutated lines. Using the pAL114 plasmid, which comprises both Cas9 and the *HPT1* hygromycin resistance gene, offered several advantages. Firstly, it reduced the number of plasmids in the mixture, allowing the concentration of sgRNA constructs to be increased, a factor that was consistently found to be important (Table 4 & Fig. 5). Secondly, pAL114 provided better security that *Cas9* had not inserted into the genome. After transfection, antibiotic selection was applied only transiently to eliminate cells that have not taken up DNA. Afterwards, selection was removed usually accompanied by loss of resistance -and thus of Cas9 too- over the following weeks. The benefits of this improved system were particularly evident when targeting all 7 genes simultaneously. Indeed, more efficient high-order multiplex targeting was achieved using pAL114 than with Cas9 and the antibiotic resistance gene on separate plasmids (Fig. 5a).
Interestingly, it was observed that *PHY* gene mutations occurred much more frequently than expected from the incidence of individual mutations. For example, in the six-fold targeting experiment (Table 4d), the projected probability of any quintuple mutant was about 10^{-5}, whereas one such mutant was found in only 74 lines investigated. This was even more apparent in the seven-fold targeting experiment using pAL114 (Table 4e), the projected probabilities of sextuple and septuple mutants were about 0.41% and 0.16%, respectively, whereas 5 and 1, respectively, were obtained in only 85 lines. A similar effect was observed in previous work (Lopez-Obando et al. 2016). The high incidence of multiple mutations might arise from physiological differences between individual protoplasts regarding the effectiveness either of Cas9 in inducing DSB's or of the NHEJ machinery in repairing them, irrespective of the number of sgRNA plasmids present.
The improved CRISPR-system was implemented in subsequent multiplex experiments aimed to edit *PHY5a-c* and the 5 members of the phototropin gene family.

The efficiency of DNA cleavage by Cas9 depends not only on the intrinsic nuclease activity, but also on target site accessibility and affinity of the sgRNA to the target sequence. Therefore, designing efficient sgRNAs is critical in gene editing with CRISPR/Cas9. Computational prediction tools can analyse and extract knowledge from large-scale CRISPR screens together with whole genome sequences to identify appropriate sgRNA targets that are likely to be efficient which avoiding off-target mutations.
In this study, Cas9-mediated multiplex editing of the phytochrome and phototropin gene family in Physcomitrella was performed using sgRNAs designed with the help of CRISPOR (Concordet et al. 2018).

In the *PHY* multiplex editing, *PHY5b* and *PHY3* sgRNA constructs were least efficient, whereas *PHY5a* and *PHY5c* sgRNA constructs were most efficient in both transfections targeting 6 and 7 *PHY* genes (Fig. 5d-e). Certain sgRNA sequence motifs have been shown to be correlated with significantly reduced editing efficiency, one being the low CG content (< 25%) within the first 10 bp of the sgRNA (distal to the PAM) (Graf et al. 2019). However, the PAM-distal CG content for all the sgRNA constructs used in the *PHY* editing was > 30% (indeed, the *PHY3*-sgRNA was one of the highest at 60%), thus this character cannot explain the lower efficiency observed. The constructs also bear none of the sequence motifs such as TT or GCC that commonly reduce CRISPR editing efficiency. On the contrary, the PHY5c-sgRNA carried the low efficiency TT-motif near its PAM sequence yet was particularly effective in this work.

In the *PHOT* multiplex editing, all 5 phototropin genes were targeted in a single transfection. Subsequent PCR-screening revealed, however, that targeting efficiency of the *PHOTA2* and *PHOTA3* sgRNA constructs was very low (see Fig. 8a) even though both sgRNAs were ranked amongst the most efficient by CRISPOR. Indeed, the low efficiency TT or GCC motifs were not present. Moreover, PAM-distal CG content within the first 10 bp of the sgRNA was higher than 25% in both cases (Graf et al. 2019). Analysing the *PHOTA2* and *PHOTA3* sgRNA constructs with CRISPR-P 2.0 (Liu et al. 2017), another popular bioinformatic tool for sgRNA design in plants, on-target efficiency values reported were instead quite low. CRISPR-P 2.0 derives these values from previous research that analysed sgRNA editing efficiency by a high-throughput analysis in mammalian cells (Doench et al. 2014, Doench et al. 2016, Liu et al. 2017) (similarly to CRISPOR). According to this tool, the best sgRNAs have an on-target score higher than 0.5, whereas the intermediate ones have a score between 0.2 and 0.5. CRISPR-P 2.0 scores for the *PHOTA2* and *PHOTA3* sgRNAs recommended by CRISPOR were 0.02 and 0.12, respectively, on which basis it is hardly surprising that the sgRNAs were ineffective.

Secondary structure of sgRNA has been shown to be associated with targeting efficiency. Conserved structural motifs within the sgRNA allow proper Cas9 loading as well as endonuclease activation (Jiang et al. 2017). Changes in the programmable part of the sgRNA can, therefore, alter its secondary structure, potentially reducing Cas9 activity. The crRNA sequence consists of guide (20nt) (the spacer sequence) and repeat (12nt) region, whereas the tracrRNA sequence consists of anti-repeat (14nt) and three stem loops. The repeat and anti-repeat regions form the stem loop RAR, which is important for pre-crRNA processing by the enzyme RNase III and the subsequent activation of crRNA-guided DNA cleavage by Cas9 (Jinek et al. 2012). Analysis of sgRNA secondary structures revealed that all sgRNAs validated in plants have intact stem loop RAR, as well as intact stem loop 2 and 3, implying that these three hairpin structures are crucial for genome editing (Liang et al. 2016). CRISPR-P 2.0 provides a secondary structure analysis of sgRNAs to help the user design efficient sgRNAs. According to the secondary structural analysis performed by CRISPR-P 2.0, both *PHOTA2* and *PHOTA3* sgRNA constructs showed some features that may lead to a reduced editing efficiency. On the other hand, the alternative *PHOTA2 #2* and *PHOTA3 #2* sgRNAs designed subsequently according to CRISPOR gave intermediate efficiency scores of 0.4 and 0.38 according to CRISPR-P 2.0. Indeed, the actual efficiencies in these cases was rather high (76% for *PHOTA2 #2 and* 90% for *PHOTA3 #2)*, allowing several *phot*$^{5-}$ mutants to be generated (see Fig. 8b).

PHY5a and *PHY5c* sgRNA constructs, used in multiplex editing of the phytochrome gene family, were consistently the most efficient sgRNAs among the seven used following CRISPOR

recommendation. CRISPR-P 2.0, however, reported low scores for these sequences (0.10 and 0.07, respectively) and also the values related to the secondary structure analysis predicted a reduced efficiency.
Clearly, although *in silico* tools provide essential information for selecting sgRNA sequences, their recommendations are inconsistent and sometimes unreliable. Although many features modulating sgRNAs efficiency have been identified, the mechanisms driving many of these features remain unclear, making it difficult to predict the activity profile of a sgRNA confidently. In particular, target-specific features not captured in data used for training the algorithm can also influence sgRNAs activity. Moreover, the factors influencing CRISPR efficiency might be different in Physcomitrella from those in human and mouse upon which the usual parameters are based (Graf et al. 2019). Using more than one bioinformatic tool to choose the best-scoring sgRNAs, might help minimize the risk of designing the most inefficient ones. However, experimental validation of sgRNA activity still appears to be the best way to maximize gene editing success.

The other important information provided by sgRNA design tools relates to avoiding off-target mutagenesis. Off-target activity is a perennial problem in gene targeting and unwanted mutations need to be carefully analysed. In phytochrome six- and seven-fold mutants, all eight of the off-target sites predicted by CRISPOR were analysed via PCR/PAGE and Sanger sequencing (Appendix 12.1 & Table S3 in Appendix 12.1.1). None was found. Of course, other off-target mutations might have arisen, in which case the only reliable and comprehensive way to detect them would be through whole genome sequencing. Nevertheless, as no off-target mutations were found in other Physcomitrella studies using methods similar to what was used in this work (Lopez-Obando et al. 2016, Nomura et al. 2016), it can be concluded that targeting fidelity is very high in this system.

CRISPR-induced DSBs are prevalently repaired by the error-prone NHEJ pathway. However, the involvement of the microhomology-mediated end joining (MMEJ), an alternative highly mutagenic pathway, has been observed in a variety of human cell types (Bae et al. 2014). MMEJ relies on the annealing of short micro-homologous sequences located on both sides of the DSB, usually uncovered by a limited trimming of DNA flaps (Seol et al. 2018). The data presented in this work is in line with that (Table 1 in Appendix 12.1.1), as seen in previous studies (Seol et al. 2018, Mara et al. 2019). Efficient MMEJ-mediated repair in Physcomitrella might be connected to its potentially particular handling of the DSBs linked also to its unique HR-proficiency, when compared to the CRISPR-induced mutation pattern in *Arabidopsis*. Indeed, indels of 1 or 2 bp (which are not repaired with the help of microhomologies) appeared much less frequently compared to *Arabidopsis* (Pauwels et al. 2018).

CRISPR/Cas9 system has proven to be a highly valuable technology for genome editing in plants. The high efficiency observed in Physcomitrella allowed the creation of mutant collections able to provide unique functional insights into plant biology through efficient genome editing. The combination of high efficiency with the rapidity in successful mutations assessment that Physcomitrella offers, makes this model system particularly suitable not only for studying CRISPR technology but also to evaluate new strategies that may be implemented in other less efficient systems.

5.2 Directional sensing of light by phytochrome

Phototropism in Physcomitrella protonemata is fundamentally different from that in seed plant stems. In the latter, the response is exclusively to blue light and is mediated by phototropin (Fankhauser et al. 2015), whereas in Physcomitrella the response is primarily to red light and is mediated by phytochrome (Mittmann et al. 2004, Jaedicke et al. 2012, Hughes 2013) - immediately raising a particularly intriguing and perhaps important question: Undoubtedly, the primary function of phytochrome in biology is transcriptional regulation of nuclear genes, so how can it transmit directional information?

The remarkable discovery of a phy-phot interaction at the plasma membrane described by Jaedicke et al. offered a possible solution to the paradox and at the same time represented a possible link to the machinery controlling cytoskeleton (Meske et al. 1995, Meske et al. 1996) and therefore light-directed tip growth (Jaedicke et al. 2012). A physical interaction between the two photoreceptors is also reflected by the occurrence of neochrome, a phytochrome-phototropin chimera, that seems to have evolved twice in evolution (Suetsugu et al. 2005). Given that phototropin steers directional growth in higher plants, it might provide the link to the signal transduction mechanism involved in Physcomitrella and presumably other lower plants. Moreover, Jaedicke et al. provided evidence that phy-phot interaction might occur in higher plants too – for some unknown but perhaps interesting reason (Jaedicke et al. 2012).

However, the nature of the phy-phot interaction is still poorly understood, while the signalling mechanism involved, rather like that of phototropin itself, remains unknown. Whereas at the cellular level the reorganisation of the microfilament cytoskeleton seen in *Ceratodon* filament tips (Meske et al. 1995, Meske et al. 1996) provides an attractive explanation of how tip growth itself might be redirected by influencing cell wall construction, how actin nucleation might connect to the directional stimulation of the phy-phot complex remains unknown. With this aim, the present study generated and investigated different CRISPR/Cas9-generated mutants regarding their phototropic and polarotropic reactions.

5.2.1 phy5a and phy5c in directional light sensing

Phototropic responses were initially assayed in unilateral, collimated R at 1.5 µmol m^{-2} s^{-1}. The aphototropic phenotype of the *phy7-* line confirmed that phytochrome is essential for R phototropism in Physcomitrella (see Fig. 9a & 11b). This conclusion was corroborated by the R/FR- reversibility seen with light pulses (see Fig. 20c), showing also that the phytochrome molecules responsible are relatively immobile in the cell. Physiological analysis of lower-order mutants revealed three different phenotypes: aphototropic, positively phototropic and, surprisingly, negatively phototropic. Comparison of lines carrying phytochrome mutations in different combinations suggested a certain degree of functional redundancy for all phytochromes except for phy1 and phy3 which appear to not be involved in phototropism (see Fig. 9c). Surprisingly, the strongest phenotype observed was not in *phy4-* (Mittmann et al. 2004) but in the *phy5a phy5c-* double mutants. This difference might be related to the fact that the WT line used by Mittmann subsequently lost phototropic sensitivity entirely (see 2.1.1). In the genetic background used here, the absence of functional phy5a and phy5c abolished phototropism as effectively as in *phy7-*, whereas the absence of phy5a alone led to

a positively phototropic phenotype similar to that of the WT. These results clearly indicate a dominant role of phy5a and phy5c in the phototropic response. Notably, *Cp*.PHY4 (AAM94956), the main phytochrome responsible for photo- and polarotropic responses at moderate fluence rates in *Ceratodon*, belongs to the same clade as PHY5 (Mittmann et al. 2009). Remarkably, however, *phy5c*$^{-}$ mutants showed negative phototropism. This interesting phenotype was also observed in all multiplex phototropic lines (except *phy*$^{7-}$) that carry knock-out mutations in *PHY5c*, suggesting a very specific role of this phytochrome in mediating the response, as well as providing a crucial information to further elucidate the mechanism of directional light sensing. The function of a specific gene can often be inferred if that locus is mutated, so that the resulting loss of function manifests itself in the mutant phenotype. However, the loss of phy5c did not cancel the positive phototropic response, but gave rise to a new response. In light of the fact that the phototropic response is mediated by more than one phytochrome, this result may be interpreted on the basis of a competition between different phytochrome molecules. This could relate to interaction with phototropins at the plasma membrane to ultimately induce the phototropic bending. Positive phototropic bending at 1.5 µmol m^{-2} s^{-1} would therefore be ensured by the participation of phy5c in the interaction at the plasma membrane, thus regulating the response. Its loss in the *phy5c*$^{-}$ mutants would let mainly phy5a steer the directional response, resulting in negative phototropism.

While phototropism is steered by the directionality of the light stimulus, polarotropic responses are steered by the orientation of the *E*-vector. In particular, the *phy5a phy5c*$^{-}$ double mutant showed no reaction to polarized light, providing the robust genetic evidence that photo- and polarotropic responses to R involve the same photoreceptors, namely phy5a and phy5c. Separating the two actors revealed a different pattern in polarotropism from that in phototropism, however. Loss of either phy5a or phy5c had no effect on polarotropism relative to the WT (see Fig. 16). This remarkable result too might help us to understand the underlying mechanism of phytochrome-mediated direction sensing.

5.2.2 Possible mechanisms underlying light direction sensing

Given the encouraging results obtained in the first phototropism assay, phototropic reactions of the WT and mutated lines were therefore measured quantitatively. The fluence-rate response analysis of the WT showed negative phototropism between 0.05 and 0.15 µmol m^{-2} s^{-1} and positive phototropism between 5 and 15 µmol m^{-2} s^{-1}. Positive phototropism was lost above 45 µmol m^{-2} s^{-1}. According to expectations and consistent with the previous observation, the *phy*$^{7-}$ remained aphototropic at each of the fluence rates tested (see Fig. 12). The *phy5a phy5c*$^{-}$ line, on the other hand, remained aphototropic at each fluence rate except perhaps 45 µmol m^{-2} s^{-1} at which both positively and negatively responding filaments were observed. Comparison with the fluence-rate response obtained for the *phy*$^{4-}$ *(PHY1 PHY3 PHY5b)* mutant suggests that phy2 and/ or phy4 are responsible for the weak positive bending shown at 45 µmol m^{-2} s^{-1} (see Fig. 13).
Phototropic analysis of *phy5c*$^{-}$ showed an interesting fluence-rate dependent behaviour. Negative phototropism was already detectable at 0.015 µmol m^{-2} s^{-1} – a fluence rate below the threshold for phototropism of the WT – and remained so at 1.5 µmol m^{-2} s^{-1}, a fluence rate

inducing positive bending in the WT. At higher fluence rates, between 5 and 45 µmol m^{-2} s^{-1}, positive phototropism was observed. Similar to the WT, no phototropic response was observed at the highest fluence rate tested (see Fig. 14). The fluence-response curves of the *phy^{7-} (phy5a* phy5b*) and phy^{5-} (PHY5a PHY5b)* mutants showed similar changes to those seen in the *phy5c^{-}* lines (see Fig. 15).

Together these results provide interesting insights into the optical nature of the phototropic response in Physcomitrella filaments. This occurs in a single cell, in particular at the apex of the tip cell. In a single cell, light direction might be perceived either via attenuation or via a lens effect (refraction) (Hughes 2013) (Fig. 1). In the case of perception of light direction by attenuation, when the light passes through the cell, the internal photon fluence rate decreases from the front (where the light enters) to the rear, due to absorption from pigments and/or scattering. In the case of perception of light direction by a lens effect, the unilateral light beam is focused across the cell to the distal side, at which point the photon fluence rate is therefore higher than that at the front of the cell – and in the peripheral region on the distal side.

In Physcomitrella, both refractive index experiments and the fluence-rate response analysis of the WT and phototropic mutants suggest that a lens effect is the predominant effect in detecting light direction. Assuming that phototropism is mediated by Pfr, the lensing effect occurring at the tip cell would explain the presence of negative phototropism at low fluence rates, positive phototropism at medium fluence rates, and in particular, aphototropism observed at the highest fluence rate tested. Upon light irradiation, a dynamic photoequilibrium between Pfr and Pr is established depending on the light conditions and due to the different light-absorption properties of both states. At fluence rates lower than the saturation level at the distal side of the cell, lens effect would cause a greater stimulation of the photoreceptors in the focal area at the distal side, resulting in negative phototropism (see Fig. 10 & 11c). At higher fluence rates, however, the proportion of Pfr saturates at photoequilibrium. Then the number of photoreceptor molecules stimulated over the entire proximal side would increase and exceed those in the distal focal region (surrounded by a dark area). A positive phototropic effect would then emerge, as was observed. Importantly however, when the fluence rate becomes sufficiently high to saturate photoconversion throughout on account of scattering effects, no Pfr gradients would exist, abolishing phototropism. This effect was indeed seen clearly (Fig. 12, 13 and 14). The data presented here are thus consistent with a plausible model.

Two conditions are necessary for a good lens effect. Firstly, the cell should be transparent with a fairly homogeneous and colourless cytoplasm and vacuole, so that attenuation by absorption is minimal. Indeed, the apical part of caulonemata tip cell, free of chloroplasts, satisfies this condition. Minimal attenuation might still be present due to some light scattering and absorption, and may play a role in softening the lens effect. Secondly, the difference in refractive index between the cell and the surrounding medium has to be great enough to cause appreciable focusing. This is the case in caulonemata because the cytoplasm has a higher refractive index than air (or even water). Unquestionably, a lens effect requires different refractive indices and would thus be lost if the cell and the surrounding medium had similar refractive properties. Indeed, the aphototropic phenotype observed when the wild-type filaments were immersed in a solution of highly polymeric PEG (avoiding osmotic effects yet providing a refractive index similar to that of the cell), supports this notion (see Fig. 25).

Similarly, a lensing effect is considered to underlie phototropism in the *Phycomyces* sporangiophore (Banbury 1952, Shropshire 1962, Bergman et al. 1969).

In order to clarify the nature of Physcomitrella phototropism, however, the particular properties of phytochrome must be taken into account.
Firstly, we assume that in this case as in all others in plants, Pr is inactive and Pfr is the signalling state and that Pfr rapidly accumulating to reach photoequilibrium with Pr even at low fluence rates. In that respect, phytochrome is a singularly inappropriate photoreceptor for a fluence-rate dependent response like phototropism. In natural daylight, photoequilibrium is probably reached within seconds or even milliseconds, so how can the often-proposed Pfr gradient across the cell (see 1.4.3.1) occur under continuous irradiation? There exist several *a posteriori* explanations invoking action dichroism of how a gradient might nevertheless occur, none of which have received direct experimental support (see below). The optical model above explains much of the data too, however.
The present study reveals an additional level of complexity, however, namely that two specific phytochromes are involved that act antagonistically, one generating positive, the other generating negative phototropic responses. There is no option other than to include this in models of phytochrome action in direction sensing.
Secondly, if a gradient is to be established somehow, photoactivated phytochrome molecules must be relatively immobile. Moreover, if actin nucleation at the plasma membrane is to control cell wall construction (see 1.4.3.2)(Meske et al. 1995, Meske et al. 1996), that is where the photoreceptors must be. While this view conflicts with the idea of phytochrome as a freely-soluble protein, it was thought for many years that phytochrome indeed acts as though it is fixed at the plasma membrane (Hughes 2013). This is the classical Jaffe/Etzold/Haupt model primarily based on experiments involving chloroplast movement in the zygnemal alga *Mougeotia scalaris* (Haupt 1959, Haupt 1960). Phytochrome fixed dichroically at the plasma membrane might also explain polarotropism in moss filaments (see 1.4.3.1 and (Hughes 2013). In the meantime, however, it has been shown that these effects on chloroplast movement in *Mougeotia*, *Mesotaenium* and *Adiantum* derive from neochrome photoreceptors that do not exist in mosses (or seed plants). Remarkably, however, it seems likely that phytochrome in Physcomitrella mimics the neochrome molecular structure by binding to phototropin at the plasma membrane, so that possibly some of the observations associated with neochromes might apply to the situation in moss protonemata too (Suetsugu et al. 2005, Jaedicke et al. 2012). In particular, phototropic responses under pulsed light conditions (see Fig. 20) are in line with the idea of phytochrome molecules being immobile: this is a necessary condition if the presumptive Pfr gradient is to remain in darkness. The present study provides a new and perhaps decisive clue as to the functional mechanism used by phytochrome to sense light direction. In both continuous R and R pulses, the WT showed positive phototropism, whereas *phy5c*$^{-}$ was negatively phototropic (see Fig. 9 & Fig. 20). Negative bending observed in the *phy5c*$^{-}$ mutant is the result of phy5a action in mediating the phototropic response. This indicates that the molecular properties of phy5a must be different from those of phy5c. A possibility might be that phy5a has different rates of dark reversion than phy5c. Indeed, dark reversion has a more prominent role at low fluence rates, and although it is an intrinsic property of phytochrome molecules, it can be modulated by intermolecular interactions. In this regard, phy5a interaction with phot at the plasma

membrane might be responsible for its different dark reversion rates. An altered dark reversion might have an effect on accumulation of intermediates. During both Pr → Pfr and Pfr → Pr photoconversion, intermediate states with different lifetimes are generated. Faster rates of dark reversion in phy5a might facilitate accumulation of intermediates, thereby decreasing the amount of Pfr available to induce the response. Therefore, higher fluence rates would be needed to induce positive bending (Fig. 14). Under FR irradiation, instead, a more complete conversion of Pfr → Pr might explain the positive phototropism observed (see Fig. 17).
Under FR pulses, a weak positive bending was still present in the WT, implying R/FR reversibility, whereas the *phy5c* mutant was instead aphototropic (see Fig. 20) This result may be also explained by phy5a faster dark reversion rates leading to insufficient Pfr to maintain a stable gradient to sustain a phototropic response. In the WT, instead, the presence of phy5c ensures the presence of enough Pfr to induce a weak positive response.

Assuming the establishment of a fluence rate gradient across the cell and the prerequisite of anisotropic phytochrome, a photoequilibrium would be established in the relevant pool of phytochrome molecules. Photocycling between Pr and Pfr could account for the formation of the Pfr gradient that reflects the light gradient established within the cell, ultimately inducing the phototropic response. This is suggested by the positive bending observed in the WT under simultaneous irradiation with R and FR and the weak positive phototropism observed in the *phy5c*$^{-}$ mutant (see Fig. 18), this weak positive bending being possibly related to the different dark reversion properties of phy5a compared to phy5c. Correct light direction sensing in Physcomitrella may therefore be ensured by antagonistic effects of phy5a and phy5c, possibly based on their distinct properties and different capacity to interact with phototropins at the plasma membrane, both of which are currently unknown. Balance between phy5a and phy5c opposing actions ultimately allows for fine modulation of light sensitivity, particularly at low fluence rates.

5.2.3 Phy-phot interaction in mediating phototropic responses

In order to achieve a better understanding of the phy-phot interaction at the plasma membrane, phototropism was investigated in *phot*$^{5-}$ mutants generated via CRISPR/Cas9. Three separate *phot*$^{5-}$ lines irradiated with unilateral collimated R at 1.5 µmol m^{-2} s^{-1} (see Fig. 21). In particular because phototropism was weakened in the triple *photA2*$^{-}$*B1*$^{-}$*B2*$^{-}$ mutant (Jaedicke et al. 2012), it was considered that the phy-phot complex at the plasma membrane mediates light direction sensing (Jaedicke et al. 2012). Consequently, deletion of all five phototropin genes was expected to abrogate phototropism entirely. However, this was not the case, the *phot*$^{5-}$ lines all showed weak but nevertheless clear phototropism (see Fig. 21a). Positive phototropism was also seen in FR, similarly to the WT (see Fig. 21b). Under pulsed light conditions, while *phot*$^{5-}$ mutants showed weak positive bending in Rp-D, they were aphototropic after FRp-D (see Fig. 23). Although these results suggest that phototropin is involved in mediating phytochrome-induced phototropism, they contradict the idea of phototropin as an essential component of the signalling complex.

A possible explanation is that the phytochrome might also bind to an additional protein associated with the phy-phot complex. Indeed, an additional component must exist in all cells in which phototropin is associated with the plasma membrane because phototropins are otherwise soluble and freely cytosolic (Jaedicke et al. 2012, Christie et al. 2018). This membrane anchor protein has yet to be identified, however, so whether a direct interaction with phytochrome occurs remains to be seen. In Physcomitrella at least, the complex would be able to signal to the cell without phototropin (Fig. 28). In *Arabidopsis*, phot1 has been shown to interact via its C-terminal region with NPH3, an essential signalling factor in phototropism (Christie et al. 2018). Indeed, this NPH3-phot complex too is localized at the plasma membrane (Motchoulski et al. 1999). Otherwise, like phot1 and phytochromes, NPH3 is soluble and freely cytosolic. In *Arabidopsis*, phyB induces dissociation of NPH3 from phot1. Although some NPH3 proteins are released from the plasma membrane into the cytoplasm, others remain at the plasma membrane, perhaps implying a role as an anchor. RPT2, a member of the NPH3/RPT2-like (NRL) family, might also be involved. Members of the NLR family are also present in Physcomitrella, however their role has not yet been elucidated. The anchor protein/s might or might not be involved in signalling. From the recent cryo-EM model of the *Arabidopsis* phyB dimer there appears to be extensive opportunity for interactions with other proteins (Li et al. 2022). Recently, *Pp*.phots (*photA1*, *photA2*, *photB1*, *photB2*) were shown to be able to mediate B-dependent phototropism in a phototropin-deficient mutant of *Arabidopsis*, together with the existence of NPH3 homologs in Physcomitrella, implying that at least some of the physiological properties of phototropin are common to higher and lower plants. Indeed, in the context of the phy-phot complex, neochrome (phy3/NEO1) from *Adiantum* conferred R-dependent phototropism in *Arabidopsis phot1phot2* seedlings (Kanegae et al. 2015).

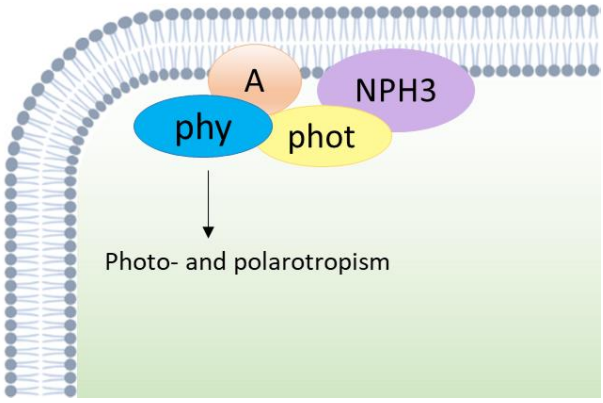

Fig. 28 Schematic representation of the phy-phot complex associated with a membrane anchor protein (A).

The importance of phy-phot interaction complex in directional sensing can also be observed in the phototropic responses of the *phy5c photA2*$^{-}$ double mutants. Interestingly, although the *phy5c*$^{-}$ single mutant was negatively phototropic under R at 1.5 µmol $m^{-2}s^{-1}$, under the same conditions the additional loss of PHOTA2 in *phy5c photA2*$^{-}$ resulted in positive phototropism (see Fig. 24). The presence of a competition between different phytochrome molecules to interact with phototropins at the plasma membrane could explain the positive phototropism observed in the *phy5c photA2*$^{-}$ mutants. Under pulsed light conditions, *phy5c photA2*$^{-}$ mutants

showed similar responses to of *phy5c*$^{-}$, with negative bending under Rp-D and an aphototropic phenotype under FRp-D (see Fig. 26).

5.2.4 Phytochromes mediate phototropism in B light

Although phototropism in seed plants is clearly a B-dependent response mediated by phototropins, in Physcomitrella B-induced tropic responses were previously observed only in chloronemal filaments (Jenkins et al. 1983). In caulonemata, instead, unilateral irradiation with B at 1 µmol m^{-2} s^{-1} failed to induce a phototropic response (Jaedicke et al. 2012). However, the higher B fluence rates used here were effective in the WT. This response was lost in both *phy*$^{7-}$ and *phy5a phy5c*$^{-}$ mutants (see Fig. 19). On the other hand, *phot*$^{5-}$ lines and *phy5c photA2*$^{-}$ mutants also showed positive phototropism (see Fig. 22 & Fig. 25). Thus, although the response is rather insensitive, B-induced phototropism occurs in caulonemata and is mediated predominantly by phy5a and phy5c as in R. Indeed, the reduced sensitivity is readily explained by the much weaker absorption cross-section of phytochromes in the B region (the so-called Soret band). Although, it is surprising that a B response is mediated by phytochrome in a phy-phot complex, neochrome from *Adiantum* seems not to require a LOV domain in the phototropin-like portion to induce B-dependent phototropism. Moreover, the response is inhibited by subsequent irradiation with FR, implying phytochrome-typical R/FR reversibility and thus phytochrome rather than phototropin involvement. These observations strengthen the connection between the phytochrome mediated phototropism, the phy-phot complex and the phy-phot chimeric neochromes (Kanegae et al. 2015).

On the basis of earlier work and the present study, a model emerges that could explain phytochrome-mediated directional sensing in Physcomitrella filament tip cells. Light direction is mainly perceived via lens effect. This creates a fluence rate gradient across the cell that can be perceived by anisotropic phytochrome molecules associated with both phototropins and an additional protein(s) providing anchoring function to the plasma membrane. phy5a and phy5c mediate directional responses by acting antagonistically, generating negative and positive phototropic responses respectively. Balance between phy5a and phy5c opposing actions at photoequilibrium allows the formation of a Pfr gradient that reflects the light gradient established within the cell, ultimately inducing the phototropic response. Therefore, negative phototropism at fluence rates lower than the saturation level at the distal side of the cell is caused by a greater stimulation of the photoreceptors in the focal area at the rear side. At medium fluence rates, the number of photoreceptor molecules stimulated over the proximal side increases until a positive phototropic effect emerges. When the fluence rate is high enough to saturate photoconversion due to the blurring effect of scattering on Pfr gradients, phototropism is lost (see Fig. 29).

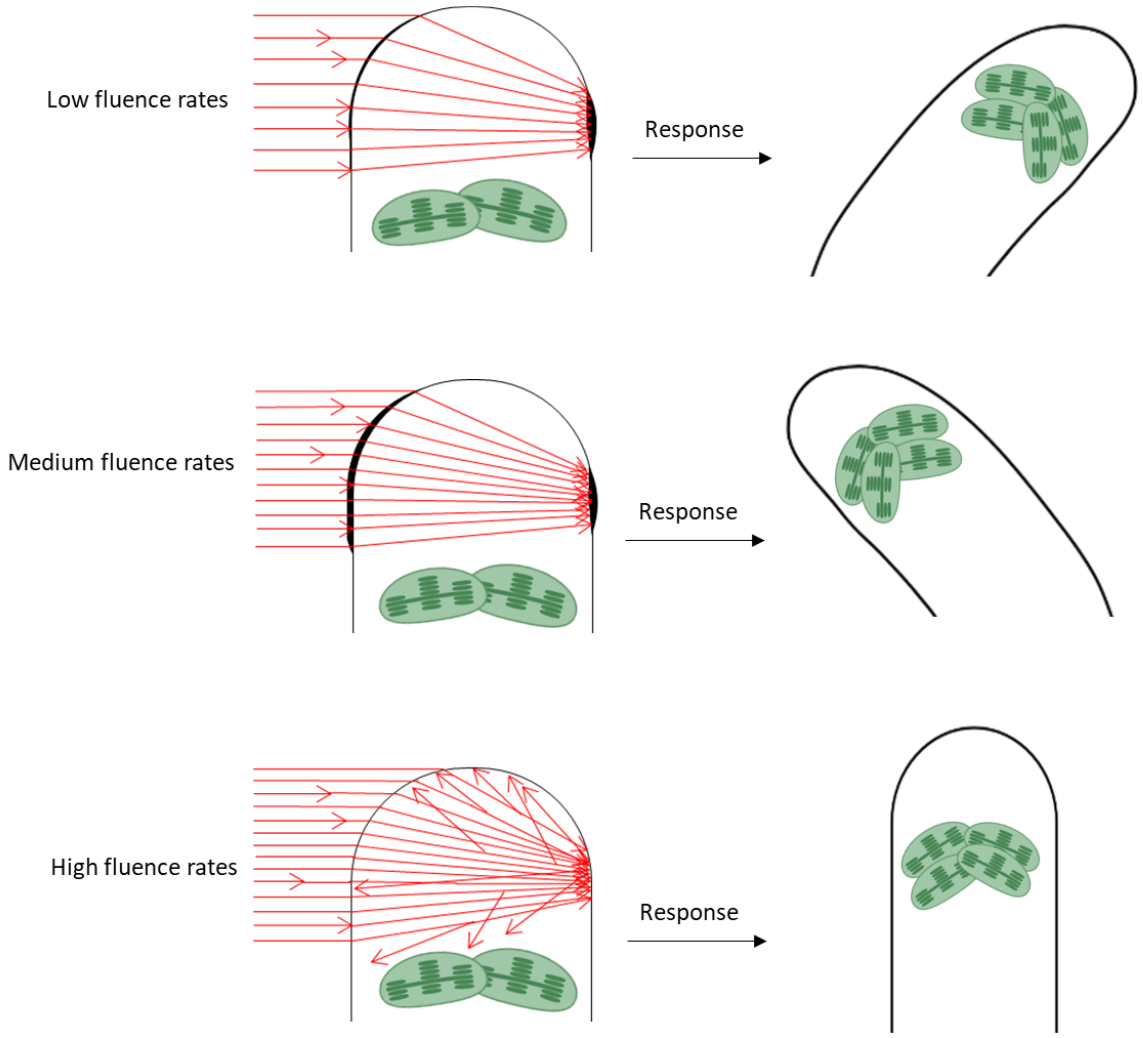

Fig. 29 Schematic representation of how light direction sensing is brought about in Physcomitrella caulonemata tip cell. At low fluence rates phytochrome molecules at the distal side of the cell are more stimulated (thicker line) than the ones at the proximal side due to lens effect. At the focal area, a Pfr gradient allows the induction of a negative phototropic response. At medium fluence rates, the number of phytochrome molecules stimulated over the proximal side increases (thicker line) and a positive phototropic effect emerges. At fluence rates high enough to saturate photoconversion throughout, on account of scattering effects no Pfr gradients exists, thus phototropism is lost.

6. Summary

The main objective of this thesis was to generate libraries of mutants of the phytochrome and phototropin gene family and to analyse them physiologically in order to gain a better insight into the steering processes involved in phytochrome-mediated light directional sensing in *Physcomitrium patens*. Since Physcomitrella has no less than seven phytochrome genes, with both specific and overlapping functions, and five phototropin genes, the CRISPR/Cas9 technology was used to overcome this obstacle. A highly-efficient multiplex CRISPR/Cas9 based on the co-delivery of an improved Cas9 plasmid with multiple sgRNA plasmids was established and used to target multiple phytochrome genes simultaneously in different combinations. This improved multiplexing approach, together with an efficient screening procedure based on high-resolution PAGE gels to identify high-order multiple mutants prior to sequencing, allowed the isolation of phy^{7-} lines along with lower-order mutants and $phot^{5-}$ mutants. Phototropic responses, initially assayed in unilateral, collimated R, confirmed that phytochrome is essential for R phototropism in Physcomitrella as observed in the aphototropic phenotype of the phy^{7-} mutant. This conclusion was corroborated by the R/FR-reversibility observed with light pulses, which also showed that the phytochrome molecules responsible are relatively immobile in the cell. Physiological analysis of lower-order mutants revealed a certain degree of functional redundancy for all phytochromes except for phy1 and phy3 which appear to not be involved in phototropism. Interestingly, the strongest phenotype was observed in the *phy5a* $phy5c^{-}$ double mutants where the absence of both phy5a and phy5c abolished the phototropic response as effectively as in the phy^{7-} line. This result clearly indicated a dominant role of both phy5a and phy5c in the phototropic response. Furthermore, $phy5c^{-}$ mutants showed negative phototropism, suggesting a very specific role of this phytochrome in mediating the response, as well as providing a crucial information to further elucidate the mechanism of directional light sensing. These results showed that phy5a and phy5c act antagonistically, one generating positive and the other negative phototropic responses, revealing an additional level of complexity in the mechanism previously hypothesised in the Jaffe/Etzold/Haupt model of phytochrome action in direction sensing. WT and *phy* mutants were also analysed in their polarotropic responses. *phy5a* $phy5c^{-}$ double mutant showed no reaction to polarized light, providing the robust genetic evidence that photo- and polarotropic responses to R involve the same photoreceptors, namely phy5a and phy5c.

Given the encouraging results obtained in the first phototropism assay, phototropic reactions of the WT and mutated lines were therefore measured quantitatively. The fluence-rate response analysis provided interesting insights into the optical nature of the phototropic response in Physcomitrella filaments, suggesting that a lens effect is the predominant effect in detecting light direction. Lens effect would explain the presence of negative phototropism at low fluence rates, positive phototropism at medium fluence rates, and in particular, aphototropism observed at the highest fluence rate tested. This notion was also supported by the refractive index experiments carried out in WT caulonemata. The positive curvature observed in the WT under simultaneous irradiation with R and FR and the weak positive phototropism observed in the $phy5c^{-}$ mutant suggested the formation of a Pfr gradient, possibly due to photocycling between Pr and Pfr, reflecting the light gradient established within the cell and ultimately inducing the phototropic response. Correct sensing of light direction in Physcomitrella would be ensured by antagonistic effects of phy5a and phy5c, allowing fine modulation of light sensitivity, especially at low fluence rates. In order to achieve a better understanding of the phy-phot interaction at the plasma membrane, phototropism

was investigated in *phot*$^{5-}$ mutants. The results revealed an unexpected phototropic phenotype, although with a weakened bending curvature compared to WT. The generation of *phy5c photA2*$^{-}$ double mutants via CRISPR/Cas9 and their physiological analysis further confirmed the importance phy-phot interaction complex in directional sensing. Although these results suggest that phototropin is involved in mediating phytochrome-induced phototropism, they contradict the idea of phototropin as an essential component of the signalling complex. One possibility is that phytochrome may also bind to an unknown additional protein that is associated with the phy-phot complex and provides an anchoring function at the plasma membrane.

Phototropic responses were also assessed under unilateral, collimated B light. Previously, a low fluence rate had failed to induce a phototropic response. Higher B fluence rates used in this work were effective in the WT. This response was lost in both *phy*$^{7-}$ and *phy5a phy5c*$^{-}$ mutants. On the other hand, *phot*$^{5-}$ lines and *phy5c photA2*$^{-}$ mutants also showed positive phototropism. Thus, although the response is rather insensitive, B-induced phototropism occurs in caulonemata and is mediated predominantly by phy5a and phy5c as in R.

The data generated from the CRISPR/Cas9 experiments, together with the optimisation of the mutant screening procedure, have increased our understanding of the CRISPR/Cas9 system in plants and in Physcomitrella in particular. The multiplex mutants and light experiments provided deep insights into the photoperception system and allowed the creation of a model that, combining previous work and the present results, could explain phytochrome-mediated directional sensing in Physcomitrella filament tip cells.

7. *Zusammenfassung*

Das Hauptziel dieser Arbeit war es, Bibliotheken von Mutanten der Phytochrom- und Phototropin-Genfamilie zu erstellen und diese physiologisch zu analysieren, um ein besseres Verständnis der Kontrollprozesse bei der Phytochrom-vermittelten Lichtrichtungserkennung in *Physcomitrium patens* zu erhalten. Da Physcomitrella nicht weniger als sieben Phytochrom-Gene mit spezifischen und überlappenden Funktionen sowie fünf Phototropin-Gene besitzt, wurde die CRISPR/Cas9-Technologie eingesetzt, um dieses Hindernis zu überwinden. Ein hocheffizientes CRISPR/Cas9-Multiplexing-Verfahren, das auf der Kombination eines verbesserten Cas9-Plasmids mit mehreren sgRNA-Plasmiden basiert, wurde entwickelt und eingesetzt, um mehrere Phytochrom-Gene gleichzeitig in verschiedenen Kombinationen zu adressieren. Dieser verbesserte Multiplexing-Ansatz ermöglichte zusammen mit einem effizienten Screening-Verfahren auf der Basis von hochauflösenden PAGE-Gelen zur Identifizierung von Mehrfachmutanten höherer Ordnung vor der Sequenzierung die Isolierung von *phy*$^{7-}$ Linien sowie von Mutanten niedriger Ordnung und *phot*$^{5-}$ Mutanten. Phototrope Reaktionen, die zunächst in einseitig kollimiertem R getestet wurden, bestätigten, dass Phytochrom für den R-Phototropismus in Physcomitrella essentiell ist, wie der aphotrope Phänotyp der *phy*$^{7-}$ Mutante zeigt. Diese Schlussfolgerung wurde durch die mit Lichtimpulsen beobachtete R/FR-Reversibilität bestätigt, die auch zeigte, dass die verantwortlichen Phytochrom-Moleküle in der Zelle relativ unbeweglich sind. Die physiologische Analyse von Mutanten niedrigerer Ordnung ergab ein gewisses Maß an funktioneller Redundanz für alle Phytochrome mit Ausnahme von phy1 und phy3, die anscheinend nicht am Phototropismus beteiligt sind. Interessanterweise wurde der stärkste Phänotyp in den *phy5a phy5c*$^{-}$ Doppelmutanten beobachtet, in denen das Fehlen von phy5a und phy5c die phototrope Reaktion ebenso effektiv unterdrückte wie in der *phy*$^{7-}$ Linie. Dieses Ergebnis weist eindeutig auf eine dominante Rolle von phy5a und phy5c in der phototropen Reaktion hin. Darüber hinaus zeigten die *phy5c*$^{-}$ Mutanten einen negativen Phototropismus, was auf eine sehr spezifische Rolle dieses Phytochroms bei der Vermittlung der Reaktion hindeutet und wichtige Informationen für die weitere Aufklärung des Mechanismus der gerichteten Lichtsensorik liefert. Die Ergebnisse zeigten, dass phy5a und phy5c antagonistisch wirken, wobei phy5a positive und phy5c negative phototrope Reaktionen hervorruft, was auf eine zusätzliche Ebene der Komplexität des Mechanismus hinweist, der zuvor im Jaffe/Etzold/Haupt-Modell der Phytochromeffekte bei der Richtungserkennung vermutet wurde. WT und *phy* Mutanten wurden auch auf polarotrope Reaktionen untersucht. Die *phy5a phy5c*$^{-}$ Doppelmutante zeigte keine Reaktion auf polarisiertes Licht und lieferte damit einen robusten genetischen Beweis, dass dieselben Photorezeptoren, nämlich phy5a und phy5c, an den phototropen und polarotropen Reaktionen auf R beteiligt sind. Aufgrund der ermutigenden Ergebnisse des ersten Phototropie-Tests wurden die phototropen Reaktionen der WT und mutierten Linien quantitativ gemessen. Die Analyse der Fluenzratenreaktion lieferte interessante Einblicke in die optische Natur der phototropen Reaktion in Physcomitrella-Filamenten und deutet darauf hin, dass ein Linseneffekt der vorherrschende Effekt bei der Erkennung der Lichtrichtung ist. Der Linseneffekt würde das Vorhandensein von negativem Phototropismus bei niedrigen Fluenzen, von positivem Phototropismus bei mittleren Fluenzen und insbesondere von Aphotropismus bei der höchsten getesteten Fluenz erklären. Diese Idee wurde auch durch Experimente zum Brechungsindex in WT Caulonemata unterstützt. Die in der WT-Pflanze beobachtete positive Krümmung bei gleichzeitiger Bestrahlung mit R und FR und der in der *phy5c*$^{-}$ Mutante beobachtete schwache positive Phototropismus deuten auf die Bildung eines Pfr-Gradienten hin, der

möglicherweise auf das Photocycling zwischen Pr und Pfr zurückzuführen ist, das den in der Zelle etablierten Lichtgradienten widerspiegelt und schließlich die phototrope Reaktion auslöst. Die korrekte Erkennung der Lichtrichtung in Physcomitrella könnte durch antagonistische Effekte von phy5a und phy5c gewährleistet werden, die eine feine Modulation der Lichtempfindlichkeit ermöglichen, insbesondere bei niedrigen Fluenzen. Um die Phy-Phot-Interaktion an der Plasmamembran besser zu verstehen, wurde der Phototropismus in *phot*$^{5-}$ Mutanten untersucht. Die Ergebnisse zeigten einen unerwartet phototropen Phänotyp, jedoch mit einer abgeschwächten Biegekrümmung im Vergleich zu WT. Die Erzeugung von *phy5c photA2*$^{-}$ Doppelmutanten mittels CRISPR/Cas9 und deren physiologische Analyse bestätigte die Bedeutung des phy-phot-Interaktionskomplexes für die Richtungserkennung. Obwohl diese Ergebnisse darauf hindeuten, dass Phototropin an der Vermittlung des Phytochrom-induzierten Phototropismus beteiligt ist, widersprechen sie der Vorstellung, dass Phototropin ein wesentlicher Bestandteil des Signalkomplexes ist. Eine Möglichkeit ist, dass Phytochrom auch an ein unbekanntes zusätzliches Protein bindet, das mit dem Phy-Phot-Komplex assoziiert ist und eine Verankerungsfunktion an der Plasmamembran übernimmt. Die phototropen Reaktionen wurden auch unter einseitig kollimiertem B-Licht untersucht. Zuvor hatte eine niedrige Fluenzrate keine phototrope Reaktion hervorgerufen. Höhere B-Fluenzraten, wie sie in dieser Arbeit verwendet wurden, waren bei WT wirksam. Diese Reaktion ging sowohl bei *phy*$^{7-}$ als auch bei *phy5a*$^{-}$ und *phy5c*$^{-}$ Mutanten verloren. Andererseits zeigten *phot*$^{5-}$ Linien und *phy5c photA2*$^{-}$ Mutanten auch positiven Phototropismus. Obwohl die Reaktion eher unempfindlich ist, tritt B-induzierter Phototropismus also in Caulonemata auf und wird wie in R. hauptsächlich durch phy5a und phy5c vermittelt.

Die aus den CRISPR/Cas9-Experimenten gewonnenen Daten haben zusammen mit der Optimierung des Mutanten-Screening-Verfahrens unser Verständnis des CRISPR/Cas9-Systems in Pflanzen und insbesondere in Physcomitrella verbessert. Die Multiplex-Mutanten und die Lichtexperimente lieferten tiefe Einblicke in das Lichtsinnes-System und ermöglichten die Erstellung eines Modells, das durch die Kombination früherer Arbeiten und der vorliegenden Ergebnisse die Phytochrom-vermittelte Richtungserkennung in den Filamentspitzenzellen von Physcomitrella erklären könnte.

8. References

Abdelrahman, M., Z. Wei, J. S. Rohila and K. Zhao (2021). "Multiplex Genome-Editing Technologies for Revolutionizing Plant Biology and Crop Improvement." Front Plant Sci **12**: 721203.

Ahmad, M. and A. R. Cashmore (1993). "HY4 gene of *A. thaliana* encodes a protein with characteristics of a blue-light photoreceptor." Nature **366**: 162-166.

Algarra, P., S. Linder and F. Thümmler (1993). "Biochemical evidence that phytochrome of the moss Ceratodon purpureus is a light-regulated protein kinase." FEBS **315**: 69-73.

Alok, A., D. Sandhya, P. Jogam, V. Rodrigues, K. K. Bhati, H. Sharma and J. Kumar (2020). "The Rise of the CRISPR/Cpf1 System for Efficient Genome Editing in Plants." Front Plant Sci **11**: 264.

Anzalone, A. V., P. B. Randolph, J. R. Davis, A. A. Sousa, L. W. Koblan, J. M. Levy, P. J. Chen, C. Wilson, G. A. Newby, A. Raguram and D. R. Liu (2019). "Search-and-replace genome editing without double-strand breaks or donor DNA." Nature **576**(7785): 149-157.

Bae, S., J. Kweon, H. S. Kim and J.-S. Kim (2014). "Microhomology-based choice of Cas9 nuclease target sites." Nature Methods **11**(7): 705-706.

Banbury, G. H. (1952). "Physiological Studies in the Mucorales: PART I THE PHOTOTROPISM OF SPORANGIOPHORES OF PHYCOMYCES BLAKESLEEANUS." Journal of Experimental Botany **3**(1): 77-85.

Banbury, G. H. (1952). "Physiological Studies in the Mucorales: PART II SOME OBSERVATIONS ON GROWTH REGULATION IN THE SPORANGIOPHORE OF PHYCOMYCES." Journal of Experimental Botany **3**(7): 86-94.

Bao, L., N. Inoue, M. Ishikawa, E. Gotoh, O. K. Teh, T. Higa, T. Morimoto, E. F. Ginanjar, H. Harashima, N. Noda, M. Watahiki, Y. Hiwatashi, M. Sekine, M. Hasebe, M. Wada and T. Fujita (2022). "A PSTAIRE-type cyclin-dependent kinase controls light responses in land plants." Sci Adv **8**(4): eabk2116.

Bergman, K., P. V. Burke, E. Cerdá-Olmedo, C. N. David, M. Delbrück, K. W. Foster, E. W. Goodell, M. Heisenberg, G. Meissner, M. Zalokar, D. S. Dennison and W. Shropshire (1969). "Phycomyces." Bacteriological Reviews **33**(1): 99-157.

Blumenstein, A., K. Vienken, R. Tasler, J. Purschwitz, D. Veith, N. Frankenberg-Dinkel and R. Fischer (2005). "The Aspergillus nidulans phytochrome FphA represses sexual development in red light." Curr Biol **15**(20): 1833-1838.

Borthwick, H. A., S. B. Hendricks, M. W. Parker, E. H. Toole and V. K. Toole (1952). "A Reversible photoreaction controlling seed germination." Proc. Natl. Acad. Sci. U.S.A. **38**(8): 662-666.

Briggs, W. R. (2006). Blue/UV-A Receptors: Historical Overview. Photomorphogenesis in Plants and Bacteria. E. Schäfer and F. Nagy. Dordrecht, Springer**:** 171-197.

Briggs, W. R., C. F. Beck, A. R. Cashmore, J. M. Christie, J. Hughes, J. A. Jarillo, T. Kagawa, H. Kanegae, E. Liscum, A. Nagatani, K. Okada, M. Salomon, W. Rüdiger, T. Sakai, M. Takano, M. Wada and J. C. Watson (2001). "The phototropin family of photoreceptors." Plant Cell **13**(5): 993-997.

Briggs, W. R. and J. M. Christie (2002). "Phototropins 1 and 2: versatile plant blue-light receptors." Trends Plant Sci **7**(5): 204-210.

Burgess, J. and P. J. Linstead (1981). "Studies on the Growth and Development of Protoplasts of the Moss, *Physcomitrella patens*, and its Control by light." Planta(151): 331-338.

Butler, W. L., K. H. Norris, H. W. Siegelman and S. B. Hendricks (1959). "Detection, assay, and preliminary purification of the pigment controlling photoresponsive development of plants." Proc. Natl. Acad. Sci. U.S.A. **45**: 1703-1708.

Butt, H., G. S. Rao, K. Sedeek, R. Aman, R. Kamel and M. Mahfouz (2020). "Engineering herbicide resistance via prime editing in rice." Plant Biotechnol J **18**(12): 2370-2372.

Chen, D., M. Lyu, X. Kou, J. Li, Z. Yang, L. Gao, Y. Li, L. M. Fan, H. Shi and S. Zhong (2022). "Integration of light and temperature sensing by liquid-liquid phase separation of phytochrome B." Mol Cell.

Chen, G. H., M. J. Liu, Y. Xiong, J. Sheen and S. H. Wu (2018). "TOR and RPS6 transmit light signals to enhance protein translation in deetiolating Arabidopsis seedlings." Proc Natl Acad Sci U S A **115**(50): 12823-12828.

Chen, J., S. Li, Y. He, J. Li and L. Xia (2022). "An update on precision genome editing by homology-directed repair in plants." Plant Physiol **188**(4): 1780-1794.

Chen, Z., A. Taflove and V. Backman (2004). "Photonic nanojet enhancement of backscattering of light by nanoparticles: a potential novel visible-light ultramicroscopy technique." Opt Express **12**(7): 1214-1220.

Cheng, M. C., P. K. Kathare, I. Paik and E. Huq (2021). "Phytochrome Signaling Networks." Annu Rev Plant Biol **72**: 217-244.

Christie, J. M., L. Blackwood, J. Petersen and S. Sullivan (2015). "Plant flavoprotein photoreceptors." Plant Cell Physiol **56**(3): 401-413.

Christie, J. M., N. Suetsugu, S. Sullivan and M. Wada (2018). "Shining Light on the Function of NPH3/RPT2-Like Proteins in Phototropin Signaling." Plant Physiol **176**(2): 1015-1024.

Coleman, R. A. and L. H. Pratt (1974). "Electron microscopic localization of phytochrome in plants using an indirect antibody-labeling method." J.Histochem.Cytochem. **22**: 1039-1047.

Collonnier, C., A. Epert, K. Mara, F. Maclot, A. Guyon-Debast, F. Charlot, C. White, D. G. Schaefer and F. Nogue (2017). "CRISPR-Cas9-mediated efficient directed mutagenesis and RAD51-dependent and RAD51-independent gene targeting in the moss Physcomitrella patens." Plant Biotechnol J **15**(1): 122-131.

Concordet, J.-P. and M. Haeussler (2018). "CRISPOR: intuitive guide selection for CRISPR/Cas9 genome editing experiments and screens." Nucleic Acids Research **46**(W1): W242-W245.

Cove, D. J., P. F. Perroud, A. J. Charron, S. F. McDaniel, A. Khandelwal and R. S. Quatrano (2009). "Isolation and regeneration of protoplasts of the moss Physcomitrella patens." Cold Spring Harb.Protoc. **2009**(2): db.

Cove, D. J., P. F. Perroud, A. J. Charron, S. F. McDaniel, A. Khandelwal and R. S. Quatrano (2009). "Transformation of the moss Physcomitrella patens using direct DNA uptake by protoplasts." Cold Spring Harb.Protoc. **2009**(2): db.

Cove, D. J., R. S. Quatrano and E. Hartmann (1996). "The alignment of the axis of asymmetry in regenerating protoplasts of the moss *Ceratodon purpureus* is determined independently of axis polarity." Development **122**: 371-379.

Davis, S. J., A. V. Vener and R. D. Vierstra (1999). "Bacteriophytochromes: phytochrome-like photoreceptors from nonphotosynthetic eubacteria." Science **286**(5449): 2517-2520.

Deng, X. W., T. Caspar and P. H. Quail (1991). "cop1: a regulatory locus involved in light-controlled development and gene expression in *Arabidopsis*." Genes & Development **5**(7): 1172-1182.

Doench, J. G., N. Fusi, M. Sullender, M. Hegde, E. W. Vaimberg, K. F. Donovan, I. Smith, Z. Tothova, C. Wilen and R. Orchard (2016). "Optimized sgRNA design to maximize activity and minimize off-target effects of CRISPR-Cas9." Nature biotechnology **34**(2): 184-191.

Doench, J. G., E. Hartenian, D. B. Graham, Z. Tothova, M. Hegde, I. Smith, M. Sullender, B. L. Ebert, R. J. Xavier and D. E. Root (2014). "Rational design of highly active sgRNAs for CRISPR-Cas9–mediated gene inactivation." Nature biotechnology **32**(12): 1262-1267.

Dong, J., H. Chen, X. W. Deng, V. F. Irish and N. Wei (2020). "Phytochrome B Induces Intron Retention and Translational Inhibition of PHYTOCHROME-INTERACTING FACTOR3." Plant Physiol **182**(1): 159-166.

Eilfeld, P. and W. Rüdiger (1985). "Absoprtion spectra of phytochrome intermediates." Z.Naturforsch. **40c**: 109-114.

Ermert, A. L., K. Mailliet and J. Hughes (2016). "Holophytochrome-interacting proteins in *Physcomitrella*: Putative actors in phytochrome cytoplasmic signaling." Front Plant Sci **7**: 613.

Ermert, A. L., F. Nogue, F. Stahl, T. Gans and J. Hughes (2019). "CRISPR/Cas9-mediated knockout of *Physcomitrella patens* phytochromes." Methods Mol Biol **2026**: 237-263.

Ermert, A. L., F. Stahl, T. Gans and J. Hughes (2019). "Analysis of *Physcomitrella* phytochrome mutants via phototropism and polarotropism." Methods Mol Biol **2026**: 225-236.

Etzold, H. (1965). "Der Polarotropismus und Phototropismus der Chloronemen von *Dryopteris filix-mas* (L.) Schott." Planta **64**(3): 254-280.

Fankhauser, C. and J. M. Christie (2015). "Plant phototropic growth." Curr Biol **25**(9): R384-389.

Flint, L. H. and E. D. McAlister (1937). "Wavelengths of radiation in the visible spectrum promoting the germination of light-sensitive lettuce seed." Smiths.Misc.Coll. **96**: 1-8.

Fondeville, J. C., H. A. Borthwick and S. B. Hendricks (1966). "Leaflet movement of *Mimosa pudica* L. indicative of phytochrome action." Planta **69**(4): 357-364.

Froehlich, A. C., B. Noh, R. D. Vierstra, J. Loros and J. C. Dunlap (2005). "Genetic and molecular analysis of phytochromes from the filamentous fungus Neurospora crassa." Eukaryot Cell **4**(12): 2140-2152.

Furuya, M. and P. S. Song (1994). Assembly and properties of holophytochrome. Photomorphogenesis in Plants. R. E. Kendrick and G. H. M. Kronenberg. Dortrecht, Kluwer**:** 105-140.

Ge, Z., L. Zheng, Y. Zhao, J. Jiang, E. J. Zhang, T. Liu, H. Gu and L. J. Qu (2019). "Engineered xCas9 and SpCas9-NG variants broaden PAM recognition sites to generate mutations in Arabidopsis plants." Plant Biotechnol J **17**(10): 1865-1867.

Gong, S., H. H. Yu, K. A. Johnson and D. W. Taylor (2018). "DNA Unwinding Is the Primary Determinant of CRISPR-Cas9 Activity." Cell Rep **22**(2): 359-371.

Graf, R., X. Li, V. T. Chu and K. Rajewsky (2019). "sgRNA Sequence Motifs Blocking Efficient CRISPR/Cas9-Mediated Gene Editing." Cell Rep **26**(5): 1098-1103.e1093.

Guyon-Debast, A., A. Alboresi, Z. Terret, F. Charlot, F. Berthier, P. Vendrell-Mir, J. M. Casacuberta, F. Veillet, T. Morosinotto, J. L. Gallois and F. Nogue (2021). "A blueprint for gene function analysis through Base Editing in the model plant Physcomitrium (Physcomitrella) patens." New Phytol **230**(3): 1258-1272.

Hart, J. E. and K. H. Gardner (2021). "Lighting the way: Recent insights into the structure and regulation of phototropin blue light receptors." J Biol Chem **296**: 100594.

Haupt, W. (1959). "Die Chloroplastendrehung bei *Mougeotia*. I: Über den quantitativen und qualitativen Lichtbedarf der Schwachlichtbewegung." Planta **53**: 484-501.

Haupt, W. (1960). "Die Chloroplastendrehung bei *Mougeotia*. II: Die Induktion der Schwachlichtbewegung durch linear polarisiertes Licht." Planta **55**: 465-479.

Haupt, W. (1970). "Über den Dichroismus von Phytochrom-660 und Phytochrom-730 bei *Mougeotia*." Z.Pflanzenphysiol. **62**: 287-298.

Haupt, W. and G. Bock (1962). "Die Chloroplastendrehung bei *Mougeotia*: IV. Die Orientierung der Phytochrom-Moleküle im Cytoplasma." Planta **59**: 38-48.

Haupt, W. and R. Thiele (1961). "Chloroplastenbewegung bei *Mesotaenium*." Planta **56**: 388-401.

Heifetz, A., S. C. Kong, A. V. Sahakian, A. Taflove and V. Backman (2009). "Photonic Nanojets." JComput Theor Nanosci **6**(9): 1979-1992.

Helizon, H., J. Rosler-Dalton, P. Gasch, S. von Horsten, L. O. Essen and M. Zeidler (2018). "Arabidopsis phytochrome A nuclear translocation is mediated by a far-red elongated hypocotyl 1-importin complex." Plant J **96**(6): 1255-1268.

Hillman, W. S. and W. L. Koukkari (1967). "Phytochrome effects in the nyctinastic leaf movements of *Albizzia julibrissin* and some other legumes." Plant Physiol **42**(10): 1413-1418.

Hiltbrunner, A., A. Tscheuschler, A. Viczian, T. Kunkel, S. Kircher and E. Schäfer (2006). "FHY1 and FHL act together to mediate nuclear accumulation of the phytochrome A photoreceptor." Plant Cell Physiol **47**(8): 1023-1034.

Hiltbrunner, A., A. Viczian, E. Bury, A. Tscheuschler, S. Kircher, R. Toth, A. Honsberger, F. Nagy, C. Fankhauser and E. Schäfer (2005). "Nuclear accumulation of the phytochrome A photoreceptor requires FHY1." Curr Biol **15**(23): 2125-2130.

Hisada, A., H. Hanzawa, J. L. Weller, A. Nagatani, J. B. Reid and M. Furuya (2000). "Light-induced nuclear translocation of endogenous pea phytochrome A visualized by immunocytochemical procedures." Plant Cell **12**: 1063-1078.

Horiuchi, N. (2012). "Photonic nanojets." Nature Photonics **6**(3): 138-139.

Hsiao, A. I. and W. I. L. L. Vidaver (1984). "Effects of Temperature and Various Red or Far-red Irradiations on Phytochrome- and Gibberellin A3-mediated Germination Control in Partially Hydrated Lettuce Seeds." J.Exp.Bot. **35**: 1771-1781.

Hu, J. H., S. M. Miller, M. H. Geurts, W. Tang, L. Chen, N. Sun, C. M. Zeina, X. Gao, H. A. Rees, Z. Lin and D. R. Liu (2018). "Evolved Cas9 variants with broad PAM compatibility and high DNA specificity." Nature **556**(7699): 57-63.

Hua, K., P. Han and J. K. Zhu (2022). "Improvement of base editors and prime editors advances precision genome engineering in plants." Plant Physiol **188**(4): 1795-1810.

Hua, K., Y. Jiang, X. Tao and J. K. Zhu (2020). "Precision genome engineering in rice using prime editing system." Plant Biotechnol J **18**(11): 2167-2169.

Huang, T. K. and H. Puchta (2019). "CRISPR/Cas-mediated gene targeting in plants: finally a turn for the better for homologous recombination." Plant Cell Rep **38**(4): 443-453.

Hughes, J. (2010). "Phytochrome three-dimensional structures and functions." Biochem Soc Trans **38**(2): 710-716.

Hughes, J. (2013). "Phytochrome cytoplasmic signaling." Annu Rev Plant Biol **64**: 377-402.

Hughes, J., T. Lamparter and F. Mittmann (1996). "Cerpu;PHY0;2, a "normal" phytochrome in *Ceratodon* (Accession No. U56698) (PGR 96-067)." Pl.Physiol. **112**: 446-446.

Hughes, J., T. Lamparter, F. Mittmann, E. Hartmann, W. Gärtner, A. Wilde and T. Börner (1997). "A prokaryotic phytochrome." Nature **386**: 663-663.

Imaizumi, T., T. Kiyosue, T. Kanegae and M. Wada (1999). "Cloning of the cDNA encoding the blue-light photoreceptor cryptochrome from the moss *Physcomitrella patens* (Accession No. AB027528)." Plant Physiol. **120**: 1205-1205.

Inoue, K., R. Nishihama, H. Kataoka, M. Hosaka, R. Manabe, M. Nomoto, Y. Tada, K. Ishizaki and T. Kohchi (2016). "Phytochrome Signaling Is Mediated by PHYTOCHROME INTERACTING FACTOR in the Liverwort Marchantia polymorpha." Plant Cell **28**(6): 1406-1421.

Inoue, S. I. and T. Kinoshita (2017). "Blue Light Regulation of Stomatal Opening and the Plasma Membrane H(+)-ATPase." Plant Physiol **174**(2): 531-538.

Ishino, Y., M. Krupovic and P. Forterre (2018). "History of CRISPR-Cas from Encounter with a Mysterious Repeated Sequence to Genome Editing Technology." J Bacteriol **200**(7).

Jaedicke, K., A. L. Lichtenthaler, R. Meyberg, M. Zeidler and J. Hughes (2012). "A phytochrome-phototropin light signaling complex at the plasma membrane." Proc Natl Acad Sci U S A **109**(30): 12231-12236.

Jaganathan, D., K. Ramasamy, G. Sellamuthu, S. Jayabalan and G. Venkataraman (2018). "CRISPR for Crop Improvement: An Update Review." Front Plant Sci **9**: 985.

Jenkins, G. I. and D. J. Cove (1983). "Phototropism and polarotropism of primary chloronemata of the moss #Physcomitrella patens#: responses of the wild-type." Planta **158**: 357-364.

Jiang, F. and J. A. Doudna (2017). "CRISPR–Cas9 Structures and Mechanisms." Annual Review of Biophysics **46**(1): 505-529.

Jiang, Y. Y., Y. P. Chai, M. H. Lu, X. L. Han, Q. Lin, Y. Zhang, Q. Zhang, Y. Zhou, X. C. Wang, C. Gao and Q. J. Chen (2020). "Prime editing efficiently generates W542L and S621I double mutations in two ALS genes in maize." Genome Biol **21**(1): 257.

Jiang, Z., L. R. Swem, B. G. Rushing, S. Devanathan, G. Tollin and C. E. Bauer (1999). "Bacterial photoreceptor with similarity to photoactive yellow protein and plant phytochromes." Science **285**: 406-409.

Jinek, M., K. Chylinski, I. Fonfara, M. Hauer, J. A. Doudna and E. Charpentier (2012). "A programmable dual-RNA-guided DNA endonuclease in adaptive bacterial immunity." Science **337**(6096): 816-821.

Jones, D. L., P. Leroy, C. Unoson, D. Fange, V. Curic, M. J. Lawson and J. Elf (2017). "Kinetics of dCas9 target search in Escherichia coli." Science **357**(6358): 1420-1424.

Kadota, A., M. Wada and M. Furuya (1982). "Phytochrome-mediated phototropism and different dichroic orientation of Pr and Pfr in protonemata of the fern *Adiantum capillus-veneris*." Photochem.Photobiol. **35**: 533-536.

Kami, C., M. Hersch, M. Trevisan, T. Genoud, A. Hiltbrunner, S. Bergmann and C. Fankhauser (2012). "Nuclear phytochrome A signaling promotes phototropism in Arabidopsis." Plant Cell **24**(2): 566-576.
Kanegae, T. and I. Kimura (2015). "A phytochrome/phototropin chimeric photoreceptor of fern functions as a blue/far-red light-dependent photoreceptor for phototropism in Arabidopsis." Plant J **83**(3): 480-488.

Kasahara, M., T. Kagawa, Y. Sato, T. Kiyosue and M. Wada (2004). "Phototropins mediate blue and red light-induced chloroplast movements in *Physcomitrella patens*." Plant Physiol. **135**(3): 1388-1397.

Kim, L., S. Kircher, R. Toth, E. Adam, E. Schäfer and F. Nagy (2000). "Light-induced nuclear import of phytochrome-A:GFP fusion proteins is differentially regulated in transgenic tobacco and Arabidopsis." Plant J **22**(2): 125-133.

Kimura, Y., I. Kimura and T. Kanegae (2018). "Phototropins of the moss Physcomitrella patens function as blue-light receptors for phototropism in Arabidopsis." Plant Signal Behav **13**(10): e1525995.

Kinoshita, T., M. Doi, N. Suetsugu, T. Kagawa, M. Wada and K. Shimazaki (2001). "Phot1 and phot2 mediate blue light regulation of stomatal opening." Nature **414**(6864): 656-660.

Kircher, S., L. Kozma-Bognar, L. Kim, E. Adam, K. Harter, E. Schafer and F. Nagy (1999). "Light quality dependent nuclear import of the plant photoreceptors phytochrome A and B." Plant Cell **11**(8): 1445-1456.

Kircher, S., L. Kozma-Bognar, L. Kim, E. Adam, K. Harter, E. Schäfer and F. Nagy (1999). "Light quality-dependent nuclear import of the plant photoreceptors phytochrome A and B." Plant Cell **11**: 1445-1456.

Knight, S. C., L. Xie, W. Deng, B. Guglielmi, L. B. Witkowsky, L. Bosanac, E. T. Zhang, M. El Beheiry, J. B. Masson, M. Dahan, Z. Liu, J. A. Doudna and R. Tjian (2015). "Dynamics of CRISPR-Cas9 genome interrogation in living cells." Science **350**(6262): 823-826.

Knott, G. J. and J. A. Doudna (2018). "CRISPR-Cas guides the future of genetic engineering." Science **361**(6405): 866-869.

Kolukisaoglu, H. Ü., B. Braun, W. F. Martin and H. A. Schneider-Poetsch (1993). "Mosses do express conventional, distantly B-type-related phytochromes. Phytochrome of *Physcomitrella patens*." FEBS **334**: 95-100.

Kong, S. G., T. Suzuki, K. Tamura, N. Mochizuki, I. Hara-Nishimura and A. Nagatani (2006). "Blue light-induced association of phototropin 2 with the Golgi apparatus." Plant J **45**(6): 994-1005.

Koukkari, W. L. and W. S. Hillman (1968). "Pulvini as the photoreceptors in the phytochrome effect on nyctinasty in *Albizzia julibrissin*." Plant Physiol **43**(5): 698-704.

Kraml, M. (1994). Light direction and polarisation. Photomorphogenesis in plants. R. E. Kendrick and G. H. M. Kronenberg. Dortrecht, Kluwer**:** 417-446.

Kutschera, U. and W. R. Briggs (2012). "Root phototropism: from dogma to the mechanism of blue light perception." Planta **235**(3): 443-452.

Łabuz, J., O. Sztatelman and P. Hermanowicz (2022). "Molecular insights into the phototropin control of chloroplast movements." Journal of Experimental Botany **73**(18): 6034-6051.

Laforest, L. C. and S. S. Nadakuduti (2022). "Advances in Delivery Mechanisms of CRISPR Gene-Editing Reagents in Plants." Front Genome Ed **4**: 830178.

Lamparter, T., H. Esch, D. Cove, J. Hughes and E. Hartmann (1996). "Aphototropic mutants of the moss *Ceratodon purpureus* with spectrally normal and with spectrally dysfunctional phytochrome." Pl.Cell &.Environ. **19**: 560-568.

Lang, D., K. K. Ullrich, F. Murat, J. Fuchs, J. Jenkins, F. B. Haas, M. Piednoel, H. Gundlach, M. Van Bel, R. Meyberg, C. Vives, J. Morata, A. Symeonidi, M. Hiss, W. Muchero, Y. Kamisugi, O. Saleh, G. Blanc,

E. L. Decker, N. van Gessel, J. Grimwood, R. D. Hayes, S. W. Graham, L. E. Gunter, S. F. McDaniel, S. N. W. Hoernstein, A. Larsson, F. W. Li, P. F. Perroud, J. Phillips, P. Ranjan, D. S. Rokshar, C. J. Rothfels, L. Schneider, S. Shu, D. W. Stevenson, F. Thummler, M. Tillich, J. C. Villarreal Aguilar, T. Widiez, G. K. Wong, A. Wymore, Y. Zhang, A. D. Zimmer, R. S. Quatrano, K. F. X. Mayer, D. Goodstein, J. M. Casacuberta, K. Vandepoele, R. Reski, A. C. Cuming, G. A. Tuskan, F. Maumus, J. Salse, J. Schmutz and S. A. Rensing (2018). "The Physcomitrella patens chromosome-scale assembly reveals moss genome structure and evolution." Plant J **93**(3): 515-533.

Ledford, H. and E. Callaway (2020). "Pioneers of revolutionary CRISPR gene editing win chemistry Nobel." Nature **586**(7829): 346-347.

Lee, S. and E. Huq (2022). "Phase separation at the heart of "heat" sensing." Mol Cell **82**(16): 2916-2918.

Legris, M., Y. C. Ince and C. Fankhauser (2019). "Molecular mechanisms underlying phytochrome-controlled morphogenesis in plants." Nat Commun **10**(1): 5219.

Li, F. W., M. Melkonian, C. J. Rothfels, J. C. Villarreal, D. W. Stevenson, S. W. Graham, G. K. Wong, K. M. Pryer and S. Mathews (2015). "Phytochrome diversity in green plants and the origin of canonical plant phytochromes." Nat Commun **6**: 7852.

Li, H., E. S. Burgie, Z. T. K. Gannam, H. L. Li and R. D. Vierstra (2022). "Plant phytochrome B is an asymmetric dimer with unique signalling potential." Nature.

Liang, G., H. Zhang, D. Lou and D. Yu (2016). "Selection of highly efficient sgRNAs for CRISPR/Cas9-based plant genome editing." Scientific Reports **6**(1): 21451.

Lin, B. Y., C. J. Shih, H. Y. Hsieh, H. C. Chen and S. L. Tu (2020). "Phytochrome Coordinates with a hnRNP to Regulate Alternative Splicing via an Exonic Splicing Silencer." Plant Physiol **182**(1): 243-254.

Lin, Q., Y. Zong, C. Xue, S. Wang, S. Jin, Z. Zhu, Y. Wang, A. V. Anzalone, A. Raguram, J. L. Doman, D. R. Liu and C. Gao (2020). "Prime genome editing in rice and wheat." Nat Biotechnol **38**(5): 582-585.

Liscum, E. and W. R. Briggs (1995). "Mutations in the NPH1 locus of *Arabidopsis* disrupt the perception of phototropic stimuli." Plant Cell **7**: 473-485.

Liu, H., Y. Ding, Y. Zhou, W. Jin, K. Xie and L.-L. Chen (2017). "CRISPR-P 2.0: An Improved CRISPR-Cas9 Tool for Genome Editing in Plants." Molecular Plant **10**(3): 530-532.

Liu, M. J., S. H. Wu, H. M. Chen and S. H. Wu (2012). "Widespread translational control contributes to the regulation of Arabidopsis photomorphogenesis." Mol Syst Biol **8**: 566.

Lopez-Obando, M., B. Hoffmann, C. Gery, A. Guyon-Debast, E. Teoule, C. Rameau, S. Bonhomme and F. Nogue (2016). "Simple and Efficient Targeting of Multiple Genes Through CRISPR-Cas9 in Physcomitrella patens." G3 (Bethesda) **6**(11): 3647-3653.

Ma, H., L. C. Tu, A. Naseri, M. Huisman, S. Zhang, D. Grunwald and T. Pederson (2016). "CRISPR-Cas9 nuclear dynamics and target recognition in living cells." J Cell Biol **214**(5): 529-537.

Mallett, D. R., M. Chang, X. Cheng and M. Bezanilla (2019). "Efficient and modular CRISPR-Cas9 vector system for Physcomitrella patens." Plant Direct **3**(9): e00168.

Mancinelli, A. (1994). The physiology of phytochrome action. Photomorphogenesis in plants. R. E. Kendrick and G. H. M. Kronenberg. Dordrecht, Kluwer Academic Publishers**:** 211-269.

Mara, K., F. Charlot, A. Guyon-Debast, D. G. Schaefer, C. Collonnier, M. Grelon and F. Nogué (2019). "POLQ plays a key role in the repair of CRISPR/Cas9-induced double-stranded breaks in the moss Physcomitrella patens." New Phytologist **222**(3): 1380-1391.

Matsushita, T., N. Mochizuki and A. Nagatani (2003). "Dimers of the N-terminal domain of phytochrome B are functional in the nucleus." Nature **424**(6948): 571-574.

Meske, V. and E. Hartmann (1995). "Reorganisation of microfilaments in protonemal tip cells of the moss *Ceratodon purpureus* during the phototropic response." Protoplasma **188**: 59-69.

Meske, V., V. Rupert and E. Hartmann (1996). "Structural basis for the red light induced repolarisation of tip growth in caulonemal cells of *Ceratodon purpureus*." Protoplasma **192**: 189-198.

Mittmann, F., G. Brucker, M. Zeidler, A. Repp, T. Abts, E. Hartmann and J. Hughes (2004). "Targeted knockout in Physcomitrella reveals direct actions of phytochrome in the cytoplasm." Proc Natl Acad Sci U S A **101**(38): 13939-13944.

Mittmann, F., S. Dienstbach, A. Weisert and C. Forreiter (2009). "Analysis of the phytochrome gene family in Ceratodon purpureus by gene targeting reveals the primary phytochrome responsible for photo- and polarotropism." Planta **230**(1): 27-37.

Möglich, A., X. Yang, R. A. Ayers and K. Moffat (2010). "Structure and function of plant photoreceptors." Annu Rev Plant Biol **61**: 21-47.

Motchoulski, A. and E. Liscum (1999). "*Arabidopsis* NPH3: A NPH1 photoreceptor-interacting protein essential for phototropism." Science **286**: 961-964.

Nagano, S., K. Guan, S. M. Shenkutie, C. Feiler, M. Weiss, A. Kraskov, D. Buhrke, P. Hildebrandt and J. Hughes (2020). "Structural insights into photoactivation and signalling in plant phytochromes." Nat Plants **6**(5): 581-588.

Naramoto, S., Y. Hata, T. Fujita and J. Kyozuka (2022). "The bryophytes Physcomitrium patens and Marchantia polymorpha as model systems for studying evolutionary cell and developmental biology in plants." Plant Cell **34**(1): 228-246.

Nomura, T., T. Sakurai, Y. Osakabe, K. Osakabe and H. Sakakibara (2016). "Efficient and Heritable Targeted Mutagenesis in Mosses Using the CRISPR/Cas9 System." Plant Cell Physiol **57**(12): 2600-2610.

Nozue, K., T. Kanegae, T. Imaizumi, S. Fukuda, H. Okamoto, K. C. Yeh, J. C. Lagarias and M. Wada (1998). "A phytochrome from the fern *Adiantum* with features of the putative photoreceptor NPH1." Proc. Natl. Acad. Sci. U.S.A. **95**(26): 15826-15830.

Oelmuller, R. and H. Mohr (1985). "Mode of coaction between blue/UV light and light absorbed by phytochrome in light-mediated anthocyanin formation in the milo (Sorghum vulgare Pers.) seedling." Proc. Natl. Acad. Sci. U.S.A. **82**(18): 6124-6128.

Oide, M., K. Okajima, S. Kashojiya, Y. Takayama, T. Oroguchi, T. Hikima, M. Yamamoto and M. Nakasako (2016). "Blue Light-excited Light-Oxygen-Voltage-sensing Domain 2 (LOV2) Triggers a Rearrangement of the Kinase Domain to Induce Phosphorylation Activity in Arabidopsis Phototropin1." J Biol Chem **291**(38): 19975-19984.

Oide, M., K. Okajima, H. Nakagami, T. Kato, Y. Sekiguchi, T. Oroguchi, T. Hikima, M. Yamamoto and M. Nakasako (2018). "Blue light-excited LOV1 and LOV2 domains cooperatively regulate the kinase activity of full-length phototropin2 from Arabidopsis." J Biol Chem **293**(3): 963-972.

Paik, I. and E. Huq (2019). "Plant photoreceptors: Multi-functional sensory proteins and their signaling networks." Semin Cell Dev Biol **92**: 114-121.

Paik, I., P. K. Kathare, J. I. Kim and E. Huq (2017). "Expanding Roles of PIFs in Signal Integration from Multiple Processes." Mol Plant **10**(8): 1035-1046.

Pattanayak, V., S. Lin, J. P. Guilinger, E. Ma, J. A. Doudna and D. R. Liu (2013). "High-throughput profiling of off-target DNA cleavage reveals RNA-programmed Cas9 nuclease specificity." Nat Biotechnol **31**(9): 839-843.

Pauwels, L., R. De Clercq, J. Goossens, S. Iñigo, C. Williams, M. Ron, A. Britt and A. Goossens (2018). "A Dual sgRNA Approach for Functional Genomics in Arabidopsis thaliana." G3 Genes|Genomes|Genetics **8**(8): 2603-2615.

Pawelczak, K. S., N. S. Gavande, P. S. VanderVere-Carozza and J. J. Turchi (2018). "Modulating DNA Repair Pathways to Improve Precision Genome Engineering." ACS Chem Biol **13**(2): 389-396.

Perroud, P. F., A. Guyon-Debast, F. Veillet, M. P. Kermarrec, L. Chauvin, J. E. Chauvin, J. L. Gallois and F. Nogue (2022). "Prime Editing in the model plant Physcomitrium patens and its potential in the tetraploid potato." Plant Sci **316**: 111162.

Perroud, P. F. and R. S. Quatrano (2006). "The role of ARPC4 in tip growth and alignment of the polar axis in filaments of Physcomitrella patens." Cell Motil Cytoskeleton **63**(3): 162-171.

Pfeiffer, A., M. K. Nagel, C. Popp, F. Wust, J. Bindics, A. Viczian, A. Hiltbrunner, F. Nagy, T. Kunkel and E. Schäfer (2012). "Interaction with plant transcription factors can mediate nuclear import of phytochrome B." Proc. Natl. Acad. Sci. U.S.A. **109**(15): 5892-5897.

Pham, V. N., P. K. Kathare and E. Huq (2018). "Phytochromes and Phytochrome Interacting Factors." Plant Physiol **176**(2): 1025-1038.

Possart, A. and A. Hiltbrunner (2013). "An evolutionarily conserved signaling mechanism mediates far-red light responses in land plants." Plant Cell **25**(1): 102-114.

Possart, A., T. Xu, I. Paik, S. Hanke, S. Keim, H. M. Hermann, L. Wolf, M. Hiss, C. Becker, E. Huq, S. A. Rensing and A. Hiltbrunner (2017). "Characterization of Phytochrome Interacting Factors from the Moss Physcomitrella patens Illustrates Conservation of Phytochrome Signaling Modules in Land Plants." Plant Cell **29**(2): 310-330.

Pratt, L. H. and R. A. Coleman (1971). "Immunocytochemical Localization of Phytochrome." Proc. Natl. Acad. Sci. U.S.A. **68**(10): 2431-2435.

Pu, X., L. Liu, P. Li, H. Huo, X. Dong, K. Xie, H. Yang and L. Liu (2019). "A CRISPR/LbCas12a-based method for highly efficient multiplex gene editing in Physcomitrella patens." Plant J **100**(4): 863-872.
Puchta, H., B. Dujon and B. Hohn (1993). "Homologous recombination in plant cells is enhanced by in vivo induction of double strand breaks into DNA by a site-specific endonuclease20." Nucleic Acids Res. **21**(22): 5034-5040.

Quail, P. H. (2002). "Phytochrome photosensory signalling networks." Nat Rev Mol Cell Biol **3**(2): 85-93.

Quail, P. H. (2010). "Phytochromes." Curr Biol **20**(12): R504-507.

Rees, H. A. and D. R. Liu (2018). "Base editing: precision chemistry on the genome and transcriptome of living cells." Nat Rev Genet **19**(12): 770-788.

Rensing, S. A., B. Goffinet, R. Meyberg, S. Z. Wu and M. Bezanilla (2020). "The Moss Physcomitrium (Physcomitrella) patens: A Model Organism for Non-Seed Plants." Plant Cell **32**(5): 1361-1376.

Rensing, S. A., D. Lang, A. D. Zimmer, A. Terry, A. Salamov, H. Shapiro, T. Nishiyama, P. F. Perroud, E. A. Lindquist, Y. Kamisugi, T. Tanahashi, K. Sakakibara, T. Fujita, K. Oishi, I. T. Shin, Y. Kuroki, A. Toyoda, Y. Suzuki, S. Hashimoto, K. Yamaguchi, S. Sugano, Y. Kohara, A. Fujiyama, A. Anterola, S. Aoki, N. Ashton, W. B. Barbazuk, E. Barker, J. L. Bennetzen, R. Blankenship, S. H. Cho, S. K. Dutcher, M. Estelle, J. A. Fawcett, H. Gundlach, K. Hanada, A. Heyl, K. A. Hicks, J. Hughes, M. Lohr, K. Mayer, A. Melkozernov, T. Murata, D. R. Nelson, B. Pils, M. Prigge, B. Reiss, T. Renner, S. Rombauts, P. J. Rushton, A. Sanderfoot, G. Schween, S. H. Shiu, K. Stueber, F. L. Theodoulou, H. Tu, Y. Van de Peer, P. J. Verrier, E. Waters, A. Wood, L. Yang, D. Cove, A. C. Cuming, M. Hasebe, S. Lucas, B. D. Mishler, R. Reski, I. V. Grigoriev, R. S. Quatrano and J. L. Boore (2008). "The *Physcomitrella* genome reveals evolutionary insights into the conquest of land by plants." Science **319**(5859): 64-69.

Rizzini, L., J. J. Favory, C. Cloix, D. Faggionato, A. O'Hara, E. Kaiserli, R. Baumeister, E. Schäfer, F. Nagy, G. I. Jenkins and R. Ulm (2011). "Perception of UV-B by the Arabidopsis UVR8 protein." Science **332**(6025): 103-106.

Rockwell, N. C. and J. C. Lagarias (2020). "Phytochrome evolution in 3D: deletion, duplication, and diversification." New Phytol **225**(6): 2283-2300.

Ronald, J. and S. J. Davis (2019). "Focusing on the nuclear and subnuclear dynamics of light and circadian signalling." Plant Cell Environ **42**(10): 2871-2884.

Rosler, J., I. Klein and M. Zeidler (2007). "Arabidopsis fhl/fhy1 double mutant reveals a distinct cytoplasmic action of phytochrome A." Proc Natl Acad Sci U S A **104**(25): 10737-10742.

Sakai, T., T. Kagawa, M. Kasahara, T. E. Swartz, J. M. Christie, W. R. Briggs, M. Wada and K. Okada (2001). "Arabidopsis nph1 and npl1: blue light receptors that mediate both phototropism and chloroplast relocation." Proc. Natl. Acad. Sci. U.S.A. **98**(12): 6969-6974.

Sakamoto, K. (2002). "Cellular and Subcellular Localization of Phototropin 1." The Plant Cell Online **14**(8): 1723-1735.

Sakamoto, K. and A. Nagatani (1996). "Nuclear localization activity of phytochrome B." Plant J. **10**: 859-868.

Sambrook, J. and D. Russel (2001). Molecular cloning: A laboratory manual. Cold Spring Harbor, NY, Cold Spring Harbor Laboratory Press.

Satter, R. L., P. B. Applewhite, J. Chaudhri and A. W. Galston (1976). "Pfr phytochrome and sucrose requirement for rhythmic leaflet movement in *Albizzia*." Photochem.Photobiol. **23**: 107-112.
Schaefer, D. G. and J.-P. Zrÿd (1997). "Efficient gene targeting in the moss *Physcomitrella patens*." Plant J. **11**: 1195-1206.

Schuergers, N., T. Lenn, R. Kampmann, M. V. Meissner, T. Esteves, M. Temerinac-Ott, J. G. Korvink, A. R. Lowe, C. W. Mullineaux and A. Wilde (2016). "Cyanobacteria use micro-optics to sense light direction." eLife **5**: e12620.

Schwenk, P. and A. Hiltbrunner (2022). "Phytochrome A Mediates the Disassembly of Processing Bodies in Far-Red Light." Front Plant Sci **13**: 828529.

Searle, I. and G. Coupland (2004). "Induction of flowering by seasonal changes in photoperiod." EMBO J. **23**(6): 1217-1222.

Seo, H. S., E. Watanabe, S. Tokutomi, A. Nagatani and N. H. Chua (2004). "Photoreceptor ubiquitination by COP1 E3 ligase desensitizes phytochrome A signaling." Genes Dev. **18**(6): 617-622.

Seol, J.-H., E. Y. Shim and S. E. Lee (2018). "Microhomology-mediated end joining: Good, bad and ugly." Mutation Research/Fundamental and Molecular Mechanisms of Mutagenesis **809**: 81-87.
Sharrock, R. A. and T. Clack (2002). "Patterns of expression and normalized levels of the five Arabidopsis phytochromes." Plant Physiol **130**(1): 442-456.

Sharrock, R. A. and P. H. Quail (1989). "Novel phytochrome sequences in *Arabidopsis thaliana*: structure, evolution, and differential expression of a plant regulatory photoreceptor family." Genes Dev. **3**: 1745-1757.

Shih, C. J., H. W. Chen, H. Y. Hsieh, Y. H. Lai, F. Y. Chiu, Y. R. Chen and S. L. Tu (2019). "Heterogeneous Nuclear Ribonucleoprotein H1 Coordinates with Phytochrome and the U1 snRNP Complex to Regulate Alternative Splicing in Physcomitrella patens." Plant Cell **31**(10): 2510-2524.

Shikata, H., K. Hanada, T. Ushijima, M. Nakashima, Y. Suzuki and T. Matsushita (2014). "Phytochrome controls alternative splicing to mediate light responses in Arabidopsis." Proc Natl Acad Sci U S A **111**(52): 18781-18786.

Shinomura, T., A. Nagatani, H. Hanzawa, M. Kubota, M. Watanabe and M. Furuya (1996). "Action spectra for phytochrome A- and B-specific photoinduction of seed germination in Arabidopsis thaliana." Proc. Natl. Acad. Sci. U.S.A. **93**: 8129-8133.

Shropshire, W. (1962). "The Lens Effect and Phototropism of Phycomyces." J Gen Physiol **45**(5): 949-958.

Smith H (2000) "Phytochromes and light signal perception by plants--an emerging synthesis." *Nature* 407:585-591.

Smith, H. and G. C. Whitelam (1997). "The shade avoidance syndrome: multiple responses mediated by multiple phytochromes." Plant Cell Environ. **20**: 840-844.

Somers, D. E., P. F. Devlin and S. A. Kay (1998). "Phytochromes and cryptochromes in the entrainment of the Arabidopsis circadian clock." Science **282**: 1488-1490.

Somers, D. E., T. F. Schultz, M. Milnamow and S. A. Kay (2000). "ZEITLUPE Encodes a Novel Clock-Associated PAS Protein from Arabidopsis." Cell **101**(3): 319-329.

Stadler, L. J. (1928). "Genetic Effects of X-Rays in Maize." Proc Natl Acad Sci U S A **14**(1): 69-75.

Stadler, L. J. (1928). "Mutations in Barley Induced by X-Rays and Radium." Science **68**(1756): 186-187.

Sternberg, S. H., S. Redding, M. Jinek, E. C. Greene and J. A. Doudna (2014). "DNA interrogation by the CRISPR RNA-guided endonuclease Cas9." Nature **507**(7490): 62-67.

Suetsugu, N., F. Mittmann, G. Wagner, J. Hughes and M. Wada (2005). "A chimeric photoreceptor gene, NEOCHROME, has arisen twice during plant evolution." Proc. Natl. Acad. Sci. U.S.A. **102**(38): 13705-13709.

Suetsugu, N. and M. Wada (2020). "Signalling mechanism of phototropin-mediated chloroplast movement in Arabidopsis." Journal of Plant Biochemistry and Biotechnology **29**(4): 580-589.

Sundqvist, C. and L. O. Björn (1983). "Light-induced linear dichroism in photoreversibly phytochrome sensor pigements - II. Chromophore rotation in immobilized phytochrome." Photochem Photobiol **37**: 69-75.

Takagi, S., S. G. Kong, Y. Mineyuki and M. Furuya (2003). "Regulation of actin-dependent cytoplasmic motility by type II phytochrome occurs within seconds in *Vallisneria gigantea* epidermal cells." Plant Cell **15**(2): 331-345.

Tanada, T. (1968). "A rapid photoreversible response of barley root tips in the presence of 3-indoleacetic acid." Proc. Natl. Acad. Sci. U.S.A. **59**(2): 376-380.

Tang, X., S. Sretenovic, Q. Ren, X. Jia, M. Li, T. Fan, D. Yin, S. Xiang, Y. Guo, L. Liu, X. Zheng, Y. Qi and Y. Zhang (2020). "Plant Prime Editors Enable Precise Gene Editing in Rice Cells." Mol Plant **13**(5): 667-670.

Tepperman, J. M., M. E. Hudson, R. Khanna, T. Zhu, S. H. Chang, X. Wang and P. H. Quail (2004). "Expression profiling of phyB mutant demonstrates substantial contribution of other phytochromes to red-light-regulated gene expression during seedling de-etiolation." Plant J **38**(5): 725-734.

Tepperman, J. M., Y. S. Hwang and P. H. Quail (2006). "phyA dominates in transduction of red-light signals to rapidly responding genes at the initiation of Arabidopsis seedling de-etiolation." Plant J **48**(5): 728-742.

Terry, M. J. and R. E. Kendrick (1996). "The aurea and yellow-green-2 mutants of tomato are deficient in phytochrome chromophore synthesis." J.Biol.Chem. **271**: 21681-21686.

Thümmler, F., M. Dufner, P. Kreisl and P. Dittrich (1992). "Molecular cloning of a novel phytochrome gene of the moss *Ceratodon purpureus* which encodes a putative light-regulated protein kinase." Plant Mol.Biol. **20**: 1003-1017.

Trogu, S., A. L. Ermert, F. Stahl, F. Nogue, T. Gans and J. Hughes (2021). "Multiplex CRISPR-Cas9 mutagenesis of the phytochrome gene family in Physcomitrium (Physcomitrella) patens." Plant Mol Biol **107**(4-5): 327-336.

Valadon, L. R. G., M. Osman and R. S. Mummery (1979). "Phytochrome mediated carotenoid synthesis in the fungus *Verticillium agaricinum*." Photochemistry and Photobiology **29**(3): 605-607.

Veillet, F., L. Perrot, A. Guyon-Debast, M. P. Kermarrec, L. Chauvin, J. E. Chauvin, J. L. Gallois, M. Mazier and F. Nogue (2020). "Expanding the CRISPR Toolbox in P. patens Using SpCas9-NG Variant and Application for Gene and Base Editing in Solanaceae Crops." Int J Mol Sci **21**(3).

Vidali, L., G. M. Burkart, R. C. Augustine, E. Kerdavid, E. Tuzel and M. Bezanilla (2010). "Myosin XI is essential for tip growth in Physcomitrella patens." Plant Cell **22**(6): 1868-1882.

Vierstra, R. and P. H. Quail (1982). "Native phytochrome: inhibition of proteolysis yields a homogeneous monomer of 124 kilodaltons from #Avena#." Proc. Natl. Acad. Sci. U.S.A. **79**: 5272-5276.

von Wettstein, F. (1924). "Morphologie und Physiologie des Formvechsels der Moose auf genetischer Grundlage." Z.indukt.Abstamm.Vererb. **33**: 1-236.

Voytas, D. F. (2013). "Plant genome engineering with sequence-specific nucleases." Annu Rev Plant Biol **64**: 327-350.

Wada, N., K. Osakabe and Y. Osakabe (2022). "Expanding the plant genome editing toolbox with recently developed CRISPR-Cas systems." Plant Physiol **188**(4): 1825-1837.

Wahlgren, W. Y., D. Golonka, S. Westenhoff and A. Moglich (2021). "Cryo-Electron Microscopy of Arabidopsis thaliana Phytochrome A in Its Pr State Reveals Head-to-Head Homodimeric Architecture." Front Plant Sci **12**: 663751.

Wang, J., X. Meng, X. Hu, T. Sun, J. Li, K. Wang and H. Yu (2019). "xCas9 expands the scope of genome editing with reduced efficiency in rice." Plant Biotechnol J **17**(4): 709-711.

Wang, L., H. B. Kaya, N. Zhang, R. Rai, M. R. Willmann, S. C. D. Carpenter, A. C. Read, F. Martin, Z. Fei, J. E. Leach, G. B. Martin and A. J. Bogdanove (2021). "Spelling Changes and Fluorescent Tagging With Prime Editing Vectors for Plants." Front Genome Ed **3**: 617553.

Wang, W., B. Tian, Q. Pan, Y. Chen, F. He, G. Bai, A. Akhunova, H. N. Trick and E. Akhunov (2021). "Expanding the range of editable targets in the wheat genome using the variants of the Cas12a and Cas9 nucleases." Plant Biotechnol J **19**(12): 2428-2441.

Wolf, L., L. Rizzini, R. Stracke, R. Ulm and S. A. Rensing (2010). "The molecular and physiological responses of Physcomitrella patens to ultraviolet-B radiation." Plant Physiol **153**(3): 1123-1134.

Wu, H. P., Y. S. Su, H. C. Chen, Y. R. Chen, C. C. Wu, W. D. Lin and S. L. Tu (2014). "Genome-wide analysis of light-regulated alternative splicing mediated by photoreceptors in Physcomitrella patens." Genome Biol **15**(1): R10.

Wu, S. Z., M. Yamada, D. R. Mallett and M. Bezanilla (2018). "Cytoskeletal discoveries in the plant lineage using the moss Physcomitrella patens." Biophys Rev **10**(6): 1683-1693.

Xin, R., P. K. Kathare and E. Huq (2019). "Coordinated Regulation of Pre-mRNA Splicing by the SFPS-RRC1 Complex to Promote Photomorphogenesis." Plant Cell **31**(9): 2052-2069.

Xin, R., L. Zhu, P. A. Salome, E. Mancini, C. M. Marshall, F. G. Harmon, M. J. Yanovsky, D. Weigel and E. Huq (2017). "SPF45-related splicing factor for phytochrome signaling promotes photomorphogenesis by regulating pre-mRNA splicing in Arabidopsis." Proc Natl Acad Sci U S A **114**(33): E7018-E7027.

Xu, T. and A. Hiltbrunner (2017). "PHYTOCHROME INTERACTING FACTORs from Physcomitrella patens are active in Arabidopsis and complement the pif quadruple mutant." Plant Signal Behav **12**(11): e1388975.

Yan, T., Y. Heng, W. Wang, J. Li and X. W. Deng (2022). "SWELLMAP 2, a phyB-Interacting Splicing Factor, Negatively Regulates Seedling Photomorphogenesis in Arabidopsis." Front Plant Sci **13**: 836519.

Zheng, X., S. Wu, H. Zhai, P. Zhou, M. Song, L. Su, Y. Xi, Z. Li, Y. Cai, F. Meng, L. Yang, H. Wang and J. Yang (2013). "Arabidopsis phytochrome B promotes SPA1 nuclear accumulation to repress photomorphogenesis under far-red light." Plant Cell **25**(1): 115-133.

9. List of figures

10. List of tables

11. Abbreviations

bp	Base pairs
ca.	circa
D	Darkness
DNA	Deoxyribonucleic acid
dsDNA	Double strand DNA
EDTA	Ethylenediaminetetraacetic acid
EtBr	Ethidium bromide
E-vector	Electric vector of light
FMN	Flavin mononucleotide
GAF	cGMP phosphodiesterase/adenylate cyclase/FhlA
h	Hours
kDa	Kilodalton
LB	Lysogeny broth
min	Minutes
nPAS	n-terminal PAS domain
PAS	Period/ARNT/Singleminded
PCR	Polymerase chain reaction
PEG	Polyethylene glycol
Pfr	Phytochrome in its far-red light absorbing state
PHY	Phytochrome-specific
Pr	Phytochrome in its red-light absorbing state
sec	seconds
STE	Salt TE buffer
TBE	Tris-borate-EDTA buffer
TE	Tris EDTA buffer
YFP	Yellow fluorescent protein
λ_{max}	Wavelength of maximal absorbance

12. Appendix

12.1 Publication

Plant Molecular Biology
https://doi.org/10.1007/s11103-020-01103-x

Multiplex CRISPR-Cas9 mutagenesis of the phytochrome gene family in *Physcomitrium (Physcomitrella) patens*

Silvia Trogu[1] · Anna Lena Ermert[1] · Fabian Stahl[1] · Fabien Nogué[2] · Tanja Gans[1] · Jon Hughes[1]

Received: 14 July 2020 / Accepted: 6 December 2020

Key message **We mutated all seven *Physcomitrium (Physcomitrella) patens* phytochrome genes using highly-efficient CRISPR-Cas9 procedures. We thereby identified phy5a as the phytochrome primarily responsible for inhibiting gravitropism, proving the utility of the mutant library.**

Abstract The CRISPR-Cas9 system is a powerful tool for genome editing. Here we report highly-efficient multiplex CRISPR-Cas9 editing of the seven-member phytochrome gene family in the model bryophyte *Physcomitrium (Physcomitrella) patens*. Based on the co-delivery of an improved Cas9 plasmid with multiple sgRNA plasmids and an efficient screening procedure to identify high-order multiple mutants prior to sequencing, we demonstrate successful targeting of all seven *PHY* genes in a single transfection. We investigated further aspects of the CRISPR methodology in Physcomitrella, including the significance of spacing between paired sgRNA targets and the efficacy of NHEJ and HDR in repairing the chromosome when excising a complete locus. As proof-of-principle, we show that the septuple *phy*$^{-}$ mutant remains gravitropic in light, in line with expectations, and on the basis of data from lower order multiplex knockouts conclude that phy5a is the principal phytochrome responsible for inhibiting gravitropism in light. We expect, therefore, that this mutant collection will be valuable for further studies of phytochrome function and that the methods we describe will allow similar approaches to revealing specific functions in other gene families.

Keywords CRISPR-Cas9 · Lower plants · Phytochrome · Multiplex gene editing · Homologous recombination · Gravitropism

Introduction

Originally identified as part of the prokaryotic adaptive immunity providing resistance to phage, virus and plasmid infection, the CRISPR-Cas9 nuclease system has proved to be a powerful tool for genome manipulation even in eukaryotes, and has rapidly become the most widely used technology for genome editing (Jinek et al. 2012; Knott and Doudna 2018). This programmable restriction enzyme system comprises two components: a 20 bp single guide RNA (sgRNA) to target a specific locus, and the Cas9 endonuclease (Anders et al. 2014, 2015; Jinek et al. 2014) for the induction of a double strand break (DSB) at the target site. The only prerequisite for cleavage is the presence of a protospacer adjacent motif (PAM) downstream of the target. Cas9 then cleaves at a specific point usually located three or four nucleotides upstream of the PAM (Jinek et al. 2012).

CRISPR's mutagenic ability derives from the action of endogenous DNA repair pathways after the DSB has taken place. DSBs are usually repaired by the non-homologous end-joining (NHEJ) machinery that often creates random insertions or deletions (indels) at the target site. NHEJ is especially efficient when the sequence near the DSB shows microhomology (thus microhomology-mediated end joining (MMEJ)). If an indel occurs within a coding region, function is often lost on account of the shifted translational reading frame. Even complete loci can be excised if appropriately-spaced dual sgRNAs are employed. On the other hand, if an exogenous donor DNA flanked by sequences homologous

Supplementary information The online version of this article (https://doi.org/10.1007/s11103-020-01103-x) contains supplementary material, which is available to authorized users.

✉ Jon Hughes
jon.hughes@uni-giessen.de

[1] Institute for Plant Physiology, Justus Liebig University, Senckenbergstrasse 3, 35390 Giessen, Germany

[2] Institut Jean-Pierre Bourgin, INRAE, AgroParisTech, Université Paris-Saclay, 78000 Versailles, France

Published online: 21 December 2020

to the target site is provided, homology-dependent repair (HDR) may occur instead, in which case, a precisely customized gene can be generated with the help of an appropriate repair sequence.

In contrast to other prokaryotic and eukaryotic groups, seed plants (spermatophytes) show near-zero rates of homologous recombination (HR) (Horvath et al. 2016), NHEJ repair predominating in somatic cells (Puchta 2004). As gene targeting has huge benefits in breeding strategies, the development of HR-based methods in plants is of great importance. In this context, we have studied gene targeting in Physcomitrella, a bryophyte that naturally exhibits high frequencies of HR—the discovery of which enabled high-efficiency gene targeting in plants for the first time (Schaefer and Zrÿd 1997). Indeed, Physcomitrella represents a model system particularly suited for fundamental studies of plant biology, its utility being reinforced by its ease of genetic transformation and regeneration, small size and predominantly haploid life cycle. The complete genome sequence is publicly available (Rensing et al. 2008).

To date, CRISPR has been successfully applied in many plant species to edit single or multiple genes (Najera et al. 2019). The ability to create multiplex knockouts is especially useful in studying gene families or other cases of redundant function (Lopez-Obando et al. 2016). This is particularly significant in the case of Physcomitrella because it has undergone two rounds of whole-genome duplications during its evolution, which has contributed to the expansion of several gene families (Li et al. 2015). Moreover, the high rate of HR in Physcomitrella (Schaefer and Zrÿd 1997) might provide a particularly fertile field for CRISPR-induced gene modification in plants. Established transfection and regeneration protocols for Physcomitrella (Cove et al. 2009a, b, c) are appropriate for CRISPR applications, and indeed, both Cas9-mediated gene knock-out (KO) (with NHEJ or MMEJ) and knock-in (with HDR) have proven to be successful, including the capability to target multiple genes in a single transfection experiment (multiplexing) (Collonnier et al. 2017; Lopez-Obando et al. 2016; Nomura et al. 2016). More recently, a modular CRISPR-Cas9 vector system has been developed (Mallett et al. 2019) and multiplexing has also been demonstrated using the Cas12a (Cpf1) (Pu et al. 2019), thus expanding the Physcomitrella genetic toolkit.

A collection of multiplex KO lines allows gene functions to be identified even in the face of functional redundancy. An interesting and important case in this regard is the phytochrome (*PHY*) gene family. Phytochromes are red/far-red photochromic photoreceptors that act as master developmental switches, regulating the transcription of thousands of genes in all plants. Intriguingly, phytochrome is also able to steer the growth direction of the filaments in bryophytes, although that cannot be achieved via gene regulation as the directional information is lost in transcription/translation (Hughes 2013). Unfortunately for genetic analysis of these functions, however, the Physcomitrella genome (Lang et al. 2018; Rensing et al. 2008; Zimmer et al. 2013) encodes no less than seven phytochrome genes (*PHY1* to *PHY4* and *PHY5a* to *PHY5c*), more than known in any other species to-date, reflecting following whole genome duplication and perhaps also an evolutionary strategy to enhance acclimation in diverse light environments (Hughes 2013). As the different phytochromes have both specific and overlapping functions, the efficacy of using multiplex CRISPR in this context is rather clear. On the other hand, the 7 PHY genes show extensive sequence similarities reaching an identity of 80% higher than any of the seed-plant phytochromes (Li et al. 2015). CRISPR-based targeting of the phytochrome gene family in Physcomitrella is thus a challenging project.

In the present study, we describe CRISPR-based multiplex gene editing in Physcomitrella, focusing on the phytochrome gene family, successfully mutating all seven PHY genes in a single experiment. We have also developed a novel and efficient method for multiple indel screening and tested Cas9 efficiency in excising a complete gene or a small fragment either with or without HDR. In the process, we have generated a mutant collection for the community that will allow systematic analysis of phytochrome function in Physcomitrella. We demonstrate the efficacy of this by showing that suppression of gravitropism is lost completely in the septuple *phy*$^{-}$ mutant and that phytochrome 5a is the photoreceptor principally responsible.

Materials and methods

Design of sgRNAs and repair constructs

The coding sequences of the 7 *PHYTOCHROME* genes, including up- and downstream flanking sequences, were used to search for appropriate CRISPR RNA (crRNA) targets using the CRISPOR server (http://crispor.tefor.net/, Haeussler et al. 2016) with the Physcomitrella V11 genome sequence. crRNAs with high specificity scores and few potential off-target sequences were selected for cloning (Supplementary Information, Table S2). Each sgRNA and HR fragment was then cloned into the Gateway donor vector pDONR207, transferred to the pENTRsgRNA vector and the final constructs harvested from *E. coli* by alkaline lysis and purified by PEG/NaCl precipitation (Sambrook et al. 1989).

Dual-cut experiments exploiting NHEJ and HDR (Tables 2 and 3) (Ermert et al. 2019) are illustrated in Fig. 1.

Moss culture, protoplast isolation and transfection

Physcomitrium (Physcomitrella) patens patens (Gransden strain) was grown in 16 h white light (50–80 µmol/m^2 s

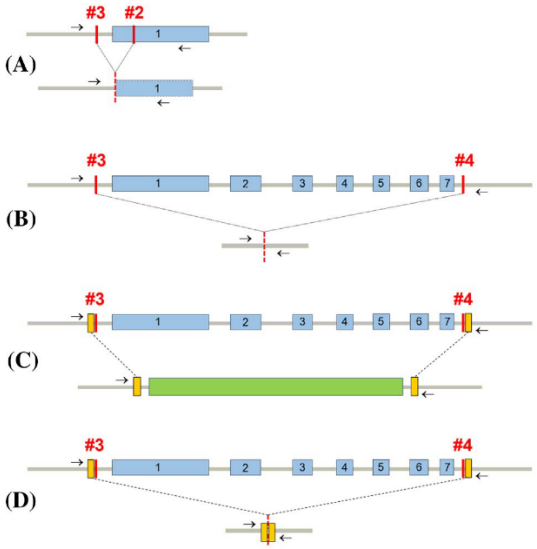

Fig. 1 The *PHY4* genomic locus with different Cas9-mediated genome editing approaches. **a** Excision of a ~ 480 bp fragment between the 5′UTR region and the first exon. **b** Excision of the entire ~ 6 kbp *PHY4* locus via NHEJ. **c**, **d** Replacement of the *PHY4* locus via HDR with and without the hygromycin resistance cassette, respectively. The exons are shown in blue and numbered. The sgRNAs are numbered #2–#4 and the PCR primers shown as small arrows. The hygromycin resistance cassette is shown in green. The homologous regions for HDR are shown in gold

Table 1 Multiplex *PHY* mutagenesis using single sgRNAs

Transfection	Targets	Total mutants identified
a	2-fold: *PHY2* + *PHY4*	26/75 (35%)
b	2-fold: *PHY5b* + *PHY5c*	38/48 (79%)
c	4-fold: *PHY1-4*	12/60 (20%)
d	6-fold: *PHY1-4* + *PHY5b-c*	28/74 (38%)
e	7-fold: *PHY1-5c*	80/85 (94%)
f	5 + 2-fold: *PHY5a* + *PHY5b* in a quintuple mutant background	47/53 (89%)

photosynthetically active radiation) and 8 h dark at 21 °C. Protonemata were cultured for 6 days on PpNH4 medium and harvested for protoplast isolation using Driselase (Sigma) and transfection as described (Cove et al. 2009a, c). Each transfection (except Tables 1e, f and 3a) included 8 µg of the pAct-Cas9 plasmid, the pBHRF plasmid containing a hygromycin resistance cassette for transient selection, and the appropriate sgRNA plasmids (Lopez-Obando et al. 2016). The pAL114 plasmid was constructed by cloning the blunted BanII-digested 35S::hygromycin resistance cassette from pBHRF into blunted ApaI-digested pActCas9

Table 2 NHEJ-mediated *PHY4* editing with dual sgRNAs

Transfection	Targets	Mutants identified
a	Excision of 480 bp fragment	2/39 (5.1%)
b	Excision of entire ~ 6 kbp locus	11/44 (25%)

Table 3 HDR-mediated ~ 6 kbp *PHY4* excision with dual sgRNAs

Transfection	HDR construct	Mutants identified
a	With hyg^R insertion	5/23 (22%)
b	Control (no insert)	1/63 (1.6%)

(Lopez-Obando et al. 2016). In transfections targeting all seven *PHY* genes (Table 1e), the mixture comprised the pAL114 plasmid and all sgRNA-plasmids, while in the retransfection experiment (Table 1f) the quintuple KO mutant (Table 1d) was transfected with the pSCOE-fcoCas9 plasmid (Nomura et al. 2016) and sgRNA-plasmids targeting *PHY5a* and *PHY5b*. In the dual-cut transfections (Tables 2 and 3, Fig. 1), two sgRNA plasmids, and in the case of HDR a plasmid carrying appropriate PHY4 sequences with or without a stably-selectable marker between the gene-flanking homologous regions, were included in the mixture. Protoplasts were transfected with a total of 20–25 µg of plasmid DNA. Protoplasts were allowed to regenerate on cellophane-overlaid PRMB plates for 1 week. Filaments were then transferred to antibiotic-supplemented medium without mannitol for selection of transfected cells. After another week, regenerants were placed on BCE225 plates without selection and grown further for 2 weeks. Finally, individual regenerants were transferred to wells in microtiter plates. After 4–6 months the loss of transient antibiotic resistance was verified through lethal reselection.

High throughput DNA extraction

In initial work, gDNA was extracted using a Mixer Mill (MM300; Retsch, Haan, Germany) followed by CTAB (cetyltrimethylammonium bromide) precipitation according to established methods. Later, a high-throughput procedure using 96-well microtitre plates exploiting cellulase rather than mechanical disruption of the cell wall was developed. Thereby, approximately 20 mg fresh weight of actively-growing filaments were treated enzymatically in 2% (w/v) Driselase in 8% mannitol for 45 min at 25–30 °C, then centrifuged at 3500×*g* for 10 min at 20 °C. After discarding the supernatants, 250 µl of extraction buffer (2% CTAB, 100 mM Tris/HCl pH 8.0, 20 mM EDTA pH 8.0, 1.4 M NaCl, 1% w/v PVP and freshly added 50 mM DTT) was added to each well, the plate then shaken briefly, incubated at 65 °C for 5 min and then centrifuged at 3500×*g* for 10 min

at 20 °C. 200 µl of each supernatant was transferred to a fresh plate and the gDNA precipitated by adding 1 volume of isopropanol and mixing. Following centrifugation at 3500×*g* for 25 min at 20 °C, the supernatants were discarded and the CTAB/DNA pellets washed in 70% ethanol then allowed to dry prior to uptake in 10 µl TE buffer.

Knockout and off-target screening

10 µl PCR reactions were performed using 1 µl of extracted DNA as template and Phusion High-Fidelity DNA Polymerase or Taq DNA Polymerase (New England Biolabs). ~ 100 bp fragments flanking each target site were amplified using appropriate gene-specific primers and separated on 15 cm 15% TBE/PAGE gels, allowing even 1 bp indels to be detected (Fig. 2). Appropriate products were then sequenced (Supplementary Information, Table S1). Sequences were aligned using Clustal and inspected for mutations around the PAM sequence.

Potential mutants produced in dual-cut transfections were tested by PCR using primers flanking the two target sites as previously described (Ermert et al. 2019).

Off-target mutants for each sgRNA used in the multiplex editing (Table 1a–f) were sought by PCR/PAGE directed to all 8 CRISPOR-predicted off-target sites in the six- and sevenfold mutants (Supplementary Information, Table S3). None was found. Coincidentally, the only predicted off-target site with less than four mismatches was that of *PHY5c*-sgRNA in the *PHY5b* gene, in a region that we had sequenced many times while screening putative *phy5b*$^{-}$ mutants.

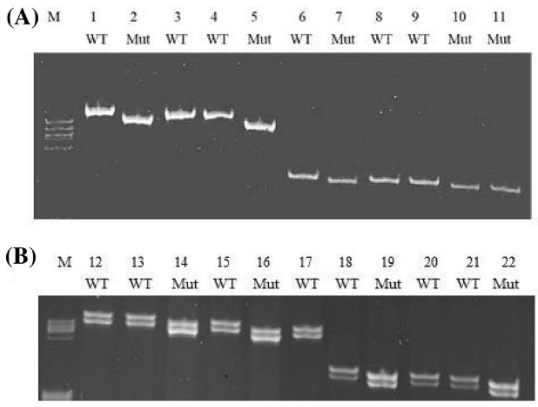

Fig. 2 Identification of Cas9-mediated indels in high-resolution PAGE Short DNA fragments (~ 100 bp) surrounding each target site were amplified and separated on 15% polyacrylamide gels. **a** Lanes 1–5 and 6–11 show *PHY5a* and *PHY2* products, respectively, from different lines amplified with Phusion High-Fidelity DNA Polymerase. Lanes 2 & 5 and 7, 10 & 11 show 2 and 1 bp deletions, respectively. **b** Lanes 12–17 and 18–22 show the same extracts amplified with Taq DNA Polymerase. Lanes 14 & 16 and 19 & 22 show 2 & 1 bp deletions, respectively

Phenotypic analysis

The effect of light on gravitropism was assayed as described (Lamparter et al. 1996) with at least two different mutant lines of each genotype in several independent experiments. Homogenized protonemata were plated on cellophane-covered agar medium and grown for 7–10 days. Approximately 2 mm slices were then placed on vertically-orientated square Perti dishes and grown for 6 days in darkness to generate uniform caulonemata. The plates were then rotated by 90° and either left in darkness or irradiated with 5 µmol/m^2 s of 660 nm red light from behind the plate for 3 days. The filaments were photographed using a zoom macroscope (Macro Z16 with DFX 500 CCD camera; Leica Microsystems, Wetzlar, Germany) and the tip orientations assayed using ImageJ (1.52d).

Results

Screening

Screening the indel complement of 7 loci in numerous lines is a daunting exercise. Although we routinely extracted gDNA from filaments using mixer-mill disruption followed by CTAB extraction/precipitation, methods offering higher through-put were clearly desirable. We thus developed a procedure appropriate for 96-well plates in which the filament cell walls were degraded enzymatically, allowing the nuclear material to be released into the medium without mechanical intervention. gDNA was subsequently extracted using CTAB. We also developed a pre-screening procedure in which indels in each locus could be identified prior to sequencing using PCR. By amplifying only a small ~ 100 bp region flanking the target site and analyzing the products on ~ 20 cm 15% polyacrylamide gels with appropriate resolution, we were able to detect even 1 bp indels confidently (Fig. 2). Whereas the expected single-band products were obtained using error-checking polymerases, we were surprised to find that Taq polymerase generated double-band products of almost equal strength with a mobility difference corresponding to 2 bp (Fig. 2b).

Multiplex phytochrome gene editing

In preliminary experiments, we targeted phytochrome genes with Cas9 by transfecting Physcomitrella protoplasts with separate pAct-Cas9 and pBHRF hygromycin-resistance plasmids together with appropriate sgRNA constructs designed with the help of CRISPOR (Haeussler

et al. 2016) according to established procedures (Ermert et al. 2019; Lopez-Obando et al. 2016) (Table 1a–d). After transient selection with hygromycin, we extracted gDNA using CTAB then amplified the targeted regions by PCR allowing indels down to ± 1 bp to be identified in high-resolution PAGE (see 'Materials and Methods') prior to sequencing. We thereby successfully targeted the sibling genes *PHY2* & *-4* (Table 1a) and *PHY5b* & *-c* (Table 1b), obtaining several double KOs in each case, whereas targeting *PHY1-4* (Table 1c) we identified two triple KOs (*phy1 phy2 phy4*) alongside double and single mutants but no quadruple mutant. We also targeted *PHY1-4* with *PHY5b & -c* (Table 1d) obtaining one quintuple KO mutant (*phy1 phy2 phy3 phy4 phy5c*) along with several lower-order mutants. Subsequently, we created the pAL114 plasmid carrying both Cas9 and the *35S*::hygromycin resistance cassette. This not only allowed us to increase the concentration of sgRNA plasmids in the mixtures, it linked the subsequent *loss* of transient hygromycin resistance with that of Cas9. With this improved system we targeted all 7 phytochrome genes in a single transfection (Table 1e), successfully generating a septuple along with several sextuple and numerous lower-order multiplex mutants. This was associated with a dramatically improved efficiency relative to the earlier sixfold targeting transfection and indeed most other experiments (Table 1; Fig. 3). We also generated a septuple mutant (Table 1f) by targeting the remaining wild-type *PHY5a* and *PHY5b* genes in a quintuple KO mutant generated earlier (Table 1d). For this we used the pSCOE-fcoCas9 plasmid containing a nptII cassette for kanamycin selection, avoiding the delay associated with waiting for the transient hygromycin resistance to be lost (see 'Materials and Methods'). We thereby obtained several sextuple and septuple KOs (Fig. 4).

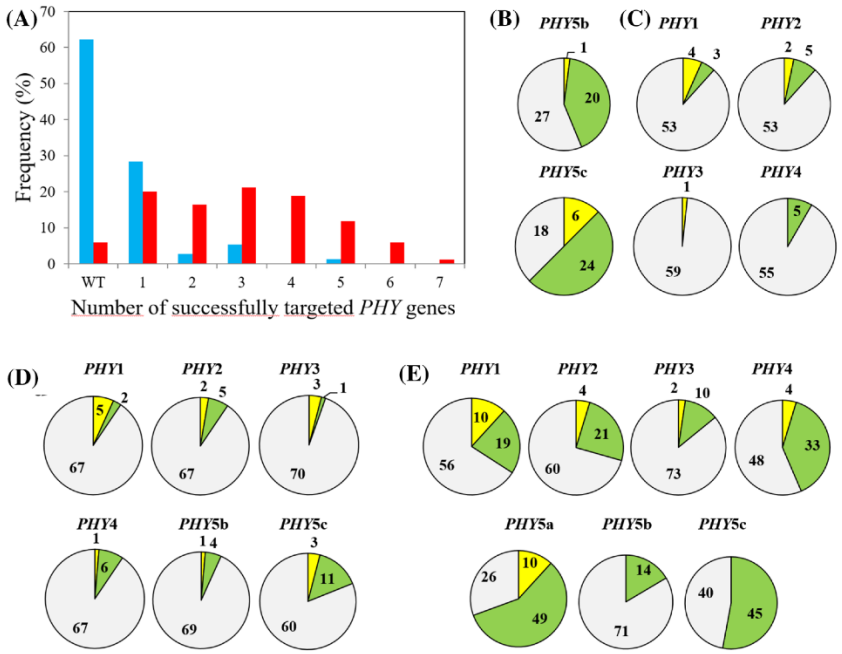

Fig. 3 Cas9-mediated multiplex gene targeting in Physcomitrella. **a** Frequency distribution of single and multiple mutants obtained in transfections targeting 6 (blue, Table 1d) and 7 (red, Table 1e) *PHY* genes, the latter exploiting the pAL114 plasmid carrying both *Cas9* and the hygromycin resistance cassette. **b**, **c** Distributions of indels identified for each target in the transfections targeting 2 and 4 *PHY* genes (Table 1b, c). **d**, **e** Distributions of indels identified for each target in the transfections targeting 6 and 7 *PHY* genes (Table 1d, e), respectively. Deletions (green), insertions (yellow), wild-type loci (grey)

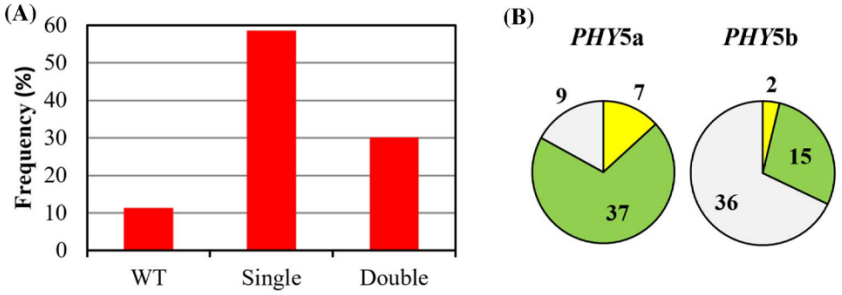

Fig. 4 Retransfection of a Physcomitrella quintuple mutant targeting the two remaining wild-type genes *PHY5a* and *PHY5b* (Table 1f). **a** Frequency distribution of single and double mutants. **b** Distribution of deletion and insertion events. Deletions (green), insertions (yellow), wild-type loci (grey)

sgRNAs targeting efficiency

Cas9-mediated gene editing efficiency critically depends on the characteristics of the sgRNAs used. The PCR screening allowed us to compare the efficiencies of the different sgRNA constructs in the multiplex transfections (Table 1b–e, Fig. 3b–e). Although the sgRNAs used induced both insertions and deletions, deletions were more abundant (Supplementary Information, Table S1), as seen in previous studies (Collonnier et al. 2017). The relative efficiency of each sgRNA was consistent throughout, differences between experiments arising from the different plasmid concentrations used in each case (Table 1b–d) and in particular from the improved pAL114-based transfection procedure (Table 1e, f).

Alternative approaches to Cas9-mediated knock-out

In order to investigate how CRISPR methods might be exploited most effectively in Physcomitrella, we evaluated the efficiency of different genome editing approaches targeting the *PHY4* locus. Thus, we investigated the significance of target spacing in dual-cut transfections by excising either a ~ 480 bp fragment between the 5′ UTR and the *PHY4* first exon or the entire ~ 6 kbp locus (Fig. 1a and b, respectively). In both cases the pAct-Cas9 and pBHRF plasmids together with two appropriate sgRNAs were employed to induce DSBs for repair through NHEJ. Surprisingly, the large deletion was consistently ~ fivefold more efficient than the smaller one (25% vs. 5.1%; Table 2).

We also tested the efficiency of HDR-enhanced gene excision of the *PHY4* locus with or without a stably selectable marker between the gene-homologous regions (Fig. 1c and d, respectively; Table 3). With marker insertion 22% of selected lines showed the desired mutation, and even without selection we found one excision event in 63 lines tested.

Abrogation of gravitropism in light is mediated by phytochrome 5a

In Physcomitrella, as in seed plants, the photoactivated phytochrome state, Pfr, suppresses gravitropism (Jenkins et al. 1986). We used the phytochrome mutant lines to identify the phytochrome/s responsible. Protonemata were initially grown on vertically-orientated Petri-dishes in darkness. Thereafter, the plates were rotated by 90° with respect to the gravity vector and irradiated with red light for 3 days (see 'Materials and Methods'). The strong negative gravitropism shown by the WT in darkness was inhibited by light, whereas the septuple null lines remained strongly gravitropic (Fig. 5). The responses of lower order multiplex KO lines indicated that gravitropic abrogation is primarily correlated with phy5a.

Discussion

We carried out multiplex CRISPR-Cas9 mutagenesis of the *PHYTOCHROME* gene family in Physcomitrella, aiming to generate single and multiple KOs for functional genetics studies. We expanded the CRISPR toolkit itself by creating an improved transient selection/Cas9 plasmid as well as developing efficient screening procedures prior to sequencing, both of which contributed significantly to the success of the work. We also assessed the efficiencies of various Cas9-based KO strategies in targeting *PHY4* to excise either a small fragment or the entire coding region with or without HDR.

We improved the protoplast-transfection-based CRISPR system by placing the *HPT1* hygromycin resistance gene on the same plasmid as *Cas9* (pAL114). This reduced the number of plasmids in the mixture, allowing the concentration of sgRNA constructs to be increased, a factor that we consistently found to be important (see Table 1b–d and Fig. 2b–d). An additional aspect is that pAL114 provides better security that *Cas9* has not inserted into the genome. In these procedures, antibiotic selection is applied only transiently to eliminate cells that have not taken up DNA. After that, selection is removed, usually accompanied by loss of resistance—and thus now of Cas9 too—over the following weeks. The benefits of this new tool were especially evident when targeting all 7 *PHY* genes simultaneously (Table 1e). Our results (Fig. 3a) clearly show more efficient high-order multiplex targeting using pAL114 than with Cas9 and the antibiotic resistance gene on separate plasmids. With the improved method, ~ 60% of protoplasts still viable following the transfection procedure show transient resistance to hygromycin and thus have taken up DNA.

We observed that multiple *PHY* gene mutations occurred much more frequently than expected from the incidence of individual mutations. For example, in the sixfold targeting experiment (Table 1d), the projected probability of any quintuple mutant was about 10^{-5}, whereas we found one such mutant in only 74 lines investigated. More convincingly, in the seven-fold targeting experiment using pAL114 (Table 1e), the projected probabilities of sextuple and septuple mutants were about 0.41% and 0.16%, respectively, whereas we obtained 5 and 1, respectively, in only 85 lines. A similar effect was seen in earlier work (Lopez-Obando et al. 2016). The high incidence of multiple mutations might arise from physiological differences between individual protoplasts regarding the effectiveness either of Cas9 in inducing DSB's or of the NHEJ machinery in repairing them, irrespective of the number of sgRNA plasmids present. Thereby, certain cells show much stronger mutagenesis for all targets than others, analogous to the phenomenon of the super-spreader in disease transmission (Lloyd-Smith et al. 2005).

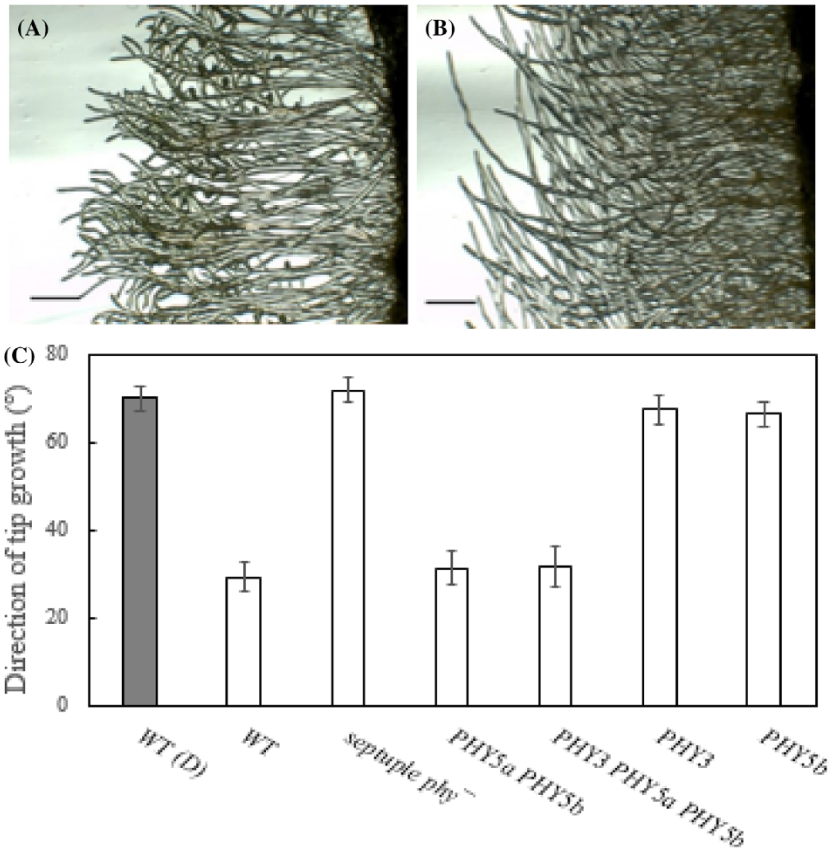

Fig. 5 Phytochrome-mediated abrogation of gravitropism in Physcomitrella. **a** Wild type and **b** septuple KO lines after reorientation in red light. Scale bars: 1.5 mm. **c** Tip growth direction (mean ± SE) of WT in darkness and of WT and five mutant lines in red light (upper case refers to wild-type genes still present), namely *phy1 phy2 phy3 phy4 phy5a phy5b phy5c (the septuple knockout), phy1 phy2 phy3 phy4 PHY5a PHY5b phy5c, phy1 phy2 PHY3 phy4 PHY5a PHY5b phy5c, phy1 phy2 PHY3 phy4 phy5a phy5b phy5c* and *phy1 phy2 phy3 phy4 phy5a PHY5b phy5c*, respectively

The *PHY5b* and *PHY3* sgRNA constructs were least efficient whereas *PHY5a* and *PHY5c* sgRNA constructs were most efficient in both transfections targeting 6 and 7 PHY genes (Fig. 2d, e). Low CG content (< 25%) within the first 10 bp of the sgRNA (distal to the PAM) has been shown to reduce editing activity significantly (Labuhn et al. 2018). However, the PAM-distal CG content for all the sgRNA constructs in our study was > 30% (indeed, the *PHY3*-sgRNA was one of the highest at 60%), thus this character cannot explain the lower efficiency observed (Supplementary Information, Table S2). The constructs also bear none of the sequence motifs such as TT or GCC that commonly reduce CRISPR editing efficiency. On the contrary, the *PHY5c*-sgRNA carried the low efficiency TT-motif near its PAM sequence yet was particularly effective in our experiments. Quite possibly, the factors influencing CRISPR efficiency are different in Physcomitrella from those in human and mouse upon which the usual parameters are based (Graf et al. 2019). On the other hand, we found that the frameshift ratio for each sgRNA predicted by CRISPOR generally corresponded closely to our sequencing results except for the *PHY5b* construct which produced more in-frame mutations than expected (Supplementary Information, Table S1). Frameshift ratio is calculated based on the Lindel algorithm that uses data from mutational events in a human cell line and exploits the bias of NHEJ outcomes towards microhomology mediated events (Chen et al. 2019). The good correspondence observed here is in line with a similar bias observed in Physcomitrella towards microhomology mediated repair of the CRISPR-Cas9 mediated double strand breaks (Collonnier et al. 2017; Mara et al. 2019).

Mallet et al. recently described a cloning method in which ~ 50 bp oligonucleotide pairs corresponding to the protospacer are inserted into a pre-existing Cas9 sgRNA scaffold using Gateway recombination (Mallett et al. 2019). If generally applicable, this procedure would offer an alternative to sgRNA gene synthesis, reducing costs significantly. The authors also reported successful use of multisite Gateway to clone up to four protospacer sequences into a single plasmid, thereby targeting four genes. Thus, using three such plasmids it would theoretically be possible to knock out a dozen genes in one transfection experiment. This elegant

approach might have significant advantages in multiplex targeting, albeit at the expense of flexibility in analysing the functions of individual genes. The Cpf1 (Cas12a) type V (Makarova et al. 2015) programmable endonuclease might be even more effective in gene targeting than Cas9, having been shown to generate threefold multiplex mutations with high efficiency in Physcomitrella (Pu et al. 2019). According to that study, Cpf1 generates large (− 8 to − 33 bp) deletions rather than the small indels (+2 to − 2 bp) seen with Cas9 in our work and that of others. In the case of KO mutagenesis via frame-shift this difference is unimportant, but single (or double) codon deletions which can be useful in particular circumstances are thus unlikely with Cpf1.

Efficient detection of multiplex indels is challenging. The first critical step requires efficient extraction of genomic DNA. Most current gDNA extraction techniques are unsuitable for high-throughput approaches. Additionally, in the case of plants, the cell wall is a literal obstacle for most extraction procedures. We developed an efficient, reliable and inexpensive extraction method to obtain gDNA from just a few milligrams of fresh protonemata appropriate for 96-well microtitre plates without the need of mixer-mill or other specialized equipment. By degrading the cell wall enzymatically rather than breaking it mechanically, we were able to release the content of the cells into the medium. The gDNA was then extracted using CTAB according to conventional methods. The second critical step is to identify indels efficiently. Conventionally, this is achieved by sequencing PCR products spanning each targeted region in each transiently resistant line. In the present work, this would have entailed about 2000 PCR/sequencing procedures. Instead, we devised a PCR-based screening procedure to identify indels prior to sequencing. We amplified a short (~ 100 bp) region flanking each targeted site, paying particular attention to primer specificity in view of the sequence similarities of the 7 *PHY* genes, and analyzed the product on non-denaturing polyacrylamide gels providing a resolution of ± 1 bp, thus allowing all indels to be identified easily (Fig. 4). This mobility-based screen is particularly valuable for large-scale screening in multiplex mutagenesis, providing for efficient identification of higher order mutants. Although the mobility shift can often be judged to represent ± 1, 2 or 3 bp, allowing likely frame-shift mutations to be identified, we invariably sequenced the PCR product. Huge savings in cost, labour and time were achieved nevertheless. We were surprised to find that when using classical Taq DNA polymerase instead of the Phusion DNA polymerase mixture we invariably observed two bands with a mobility difference corresponding to 2 bp (Fig. 2). The longer product probably derives from the well-known addition of unpaired single bases to the 3′ ends of the products of polymerases lacking 3′ → 5′ exonuclease error checking activity (Clark 1988). It is intriguing that, although only about half of the products show reduced mobility, intermediate bands that would correspond to additions to only one of the two strands were never seen. Given that PCR is the single most commonly used method in molecular genetics over the past 30 years, it is quite remarkable that this effect seems not to have been reported earlier. In practice, the dual product can be useful as it allows precise calibration of the electrophoretic mobility in terms of bp lost or gained.

It is possible to introduce larger deletions if a gene is targeted with two sgRNAs (Ermert et al. 2019). Furthermore, the resulting deletion can then be repaired by the HDR pathway when a donor DNA is provided, allowing the whole gene or a section of it to be replaced by another sequence. Widely spaced sgRNAs allow extensive enhancer regions or even gene clusters to be removed or replaced. Very large deletions are possible in principle, 245 kbp deletions having been detected by PCR in rice protoplasts (Zhou et al. 2014). CRISPR-Cas9-mediated fragment deletions of 4.5, 10 and 0.9 kb have been reported in regenerated soybean, rice and *Arabidopsis,* respectively (Cai et al. 2018; Wang et al. 2017; Zhao et al. 2016). ~ 3 kbp deletions have been reported in Physcomitrella (Nomura et al. 2016), extended to ~ 6 kbp for the *PHY4* locus in this study. Surprisingly, we found that the ~ 6 kbp excision was five times *more* efficient than a much shorter (~ 480 bp) fragment using NHEJ (Table 2). Although this might be the result of large differences in the efficiencies of the sgRNA constructs, the sgRNAs used were predicted to be similarly efficient. Whatever the reason for the difference, our results suggest that large deletions mediated by Cas9 might be facile in Physcomitrella.

CRISPR-mediated gene targeting using HDR is challenging in seed plants, with most attempts reporting low success rates (Gil-Humanes et al. 2017; Peng et al. 2020; Shi et al. 2017). The exceptionally high rate of HR in Physcomitrella appears to facilitate Cas9-mediated KO and in particular HDR-mediated gene replacement. We show that CRISPR-induced HDR is highly proficient in removing the whole ~ 6kbp *PHY4* locus with the insertion of an antibiotic cassette (Table 3a). This efficiency is similar to that with NHEJ in our experiments (Table 2b), and nearly tenfold better than CRISPR-mediated single-cut gene targeting with a homologous repair sequence in *Arabidopsis* (Peng et al. 2020). Probably on account of the efficient HR in Physcomitrella we even obtained a single HDR mutant in 63 tested lines without using an insertional marker (Table 3b).

The likely involvement of the MMEJ repair pathway for cleavage products generated through CRISPR editing has been observed in a variety of human cell types (Bae et al. 2014). Our data for Physcomitrella is in line with this, as in previous studies (Mara et al. 2019; Seol et al. 2018). Efficient MH-mediated repair in Physcomitrella might be connected to its potentially particular handling of the DSBs linked also to its unique HR-proficiency, when compared to the

CRISPR-induced mutation pattern in *Arabidopsis*. Indeed, we observed that indels of 1 or 2 bp (which are not repaired with the help of microhomologies) appear much less frequently compared to *Arabidopsis* (Pauwels et al. 2018).

Off-target activity is a perennial problem in gene targeting. We assayed this in the six six- and sevenfold mutants by analyzing all eight of the off-target sites predicted by CRISPOR (Supplementary Information, Table S3). None was found. Although of course other off-target mutations might have arisen, most events of this kind in diverse species involve closely similar sequences. As no off-target mutations were found using similar methods in other Physcomitrella studies (Lopez-Obando et al. 2016; Nomura et al. 2016), we consider that targeting is very specific in this system.

We created this mutant collection to help clarify phytochrome functions in Phydcomitrella, in particular regarding phototropism (Hughes 2013; Mittmann et al. 2004). As proof of principle, we investigated the light-dependent abrogation of gravitropism. Most plants show strong negative gravitropism in darkness, a response that helps them escape from the darkness of the soil, whereas in the light the response is repressed following the formation of Pfr. Accordingly, light repression of gravitropism is weakened in mutants either lacking the appropriate functional phytochrome/s or in which the Pfr signal is blocked. For example, abrogation of gravitropism in *Ceratodon* filaments in light is lost in heme oxygenase null mutants unable to synthesize the phytochrome chromophore (Lamparter et al. 1996). In harmony with that result, here we found that septuple *phy*$^-$ null mutants remained gravitropic in light (Fig. 5b). We then tested the abrogation phenotype in different lower-order KO lines, finding that phy5a is the photoreceptor primarily involved (Fig. 5c). As the approach thus seems to be successful, the mutant library provides a useful resource for the phytochrome community.

In summary, our optimized transfection and targeting methods alongside efficient gDNA extraction, pre-screening for indels via PCR and high-resolution PAGE gels proved effective in CRISPR-based multiplex gene editing in Physcomitrella. We demonstrated the efficacy of the methods by inactivating all seven *PHYTOCHROME* genes and showing the loss of a classical phytochrome-mediated response to light in septuple *PHY* mutants and with the help of lower-order mutants were able to identify the specific phytochromes primarily responsible. We thus expect that our mutant collection will be useful in phytochrome research and that, in general, CRISPR-based genome editing in Physcomitrella will provide unique functional insights into plant biology through efficient genome editing.

Acknowledgements We thank Toshihisa Nomura (RIKEN, Yokohama, Japan) for plasmid pSCOE-fcoCas9.

Author contributions The project was conceived and directed by JH with contributions from FN. The experimental work was carried out by ST, ALE, TG and FS. ST analyzed the data. All authors discussed the results and contributed to the manuscript that was written by ST and JH. All authors approved the submitted version to be published and agree to be accountable for all aspects of the work.

Funding Open Access funding enabled and organized by Projekt DEAL. The work was funded by the *Deutsche Forschungsgemeinschaft* (HU702/5 to JH) and by the French National Research Agency (ANR11-BTBR-0001-GENIUS to FN). The Institut Jean-Pierre Bourgin benefits from the support of the LabEx Saclay Plant Sciences-SPS (ANR-10-LABX-0040-SPS).

Availability of data and materials The plasmids and Physcomitrella mutant library described here are available to the community.

Compliance with ethical standards

Conflict of interest The authors declare no conflict of interest.

References

Anders C, Niewoehner O, Jinek M (2015) In vitro reconstitution and crystallization of Cas9 endonuclease bound to a guide RNA and a DNA target. Methods Enzymol 558:515–537. https://doi.org/10.1016/bs.mie.2015.02.008

Anders C, Niewoehner O, Duerst A, Jinek M (2014) Structural basis of PAM-dependent target DNA recognition by the Cas9 endonuclease. Nature 513:569–573. https://doi.org/10.1038/nature13579

Bae S, Kweon J, Kim HS, Kim JS (2014) Microhomology-based choice of Cas9 nuclease target sites. Nat Methods 11:705–706. https://doi.org/10.1038/nmeth.3015

Cai Y et al (2018) CRISPR/Cas9-mediated deletion of large genomic fragments in soybean. Int J Mol Sci. https://doi.org/10.3390/ijms19123835

Chen W et al (2019) Massively parallel profiling and predictive modeling of the outcomes of CRISPR/Cas9-mediated double-strand break repair. Nucleic Acids Res. https://doi.org/10.1093/nar/gkz487

Clark JM (1988) Novel non-templated nucleotide addition-reactions catalyzed by procaryotic and eukaryotic DNA-polymerases. Nucleic Acids Res 16:9677–9686. https://doi.org/10.1093/nar/16.20.9677

Collonnier C et al (2017) CRISPR-Cas9-mediated efficient directed mutagenesis and RAD51-dependent and RAD51-independent gene targeting in the moss *Physcomitrella patens*. Plant Biotechnol J 15:122–131. https://doi.org/10.1111/pbi.12596

Cove DJ, Perroud PF, Charron AJ, McDaniel SF, Khandelwal A, Quatrano RS (2009a) Isolation and regeneration of protoplasts of the moss *Physcomitrella patens*. CSH Protoc 2:pdb-rot5140

Cove DJ, Perroud PF, Charron AJ, McDaniel SF, Khandelwal A, Quatrano RS (2009b) Transformation of moss *Physcomitrella patens* gametophytes using a biolistic projectile delivery system. CSH Protoc 2:pdb-rpt5145

Cove DJ, Perroud PF, Charron AJ, McDaniel SF, Khandelwal A, Quatrano RS (2009c) Transformation of the moss *Physcomitrella patens* using direct DNA uptake by protoplasts. CSH Protoc 2:pdb-rot5143

Ermert AL, Nogue F, Stahl F, Gans T, Hughes J (2019) CRISPR/Cas9-mediated knockout of *Physcomitrella patens* phytochromes. Methods Mol Biol 2026:237–263. https://doi.org/10.1007/978-1-4939-9612-4_20

Gil-Humanes J et al (2017) High-efficiency gene targeting in hexaploid wheat using DNA replicons and CRISPR/Cas9. Plant J 89:1251–1262. https://doi.org/10.1111/tpj.13446

Graf R, Li X, Chu VT, Rajewsky K (2019) sgRNA sequence motifs blocking efficient CRISPR/Cas9-mediated gene editing. Cell Rep 26:1098–1103. https://doi.org/10.1016/j.celrep.2019.01.024

Haeussler M et al (2016) Evaluation of off-target and on-target scoring algorithms and integration into the guide RNA selection tool CRISPOR. Genome Biol 17:148. https://doi.org/10.1186/s13059-016-1012-2

Horvath M, Steinbiss HH, Reiss B (2016) Gene targeting without DSB induction is inefficient in barley. Front Plant Sci 7:1973. https://doi.org/10.3389/fpls.2016.01973

Hughes J (2013) Phytochrome cytoplasmic signaling. Annu Rev Plant Biol 64:377–402. https://doi.org/10.1146/annurev-arplant-050312-120045

Jenkins GI, Courtice GR, Cove DJ (1986) Gravitropic responses of wild-type and mutant strains of the moss *Physcomitrella patens*. Plant Cell Environ 9:637–644

Jinek M, Chylinski K, Fonfara I, Hauer M, Doudna JA, Charpentier E (2012) A programmable dual-RNA-guided DNA endonuclease in adaptive bacterial immunity. Science 337:816–821. https://doi.org/10.1126/science.1225829

Jinek M et al (2014) Structures of Cas9 endonucleases reveal RNA-mediated conformational activation. Science 343:1247997. https://doi.org/10.1126/science.1247997

Knott GJ, Doudna JA (2018) CRISPR-Cas guides the future of genetic engineering. Science 361(6405):866–869

Labuhn M et al (2018) Refined sgRNA efficacy prediction improves large- and small-scale CRISPR-Cas9 applications. Nucleic Acids Res 46:1375–1385. https://doi.org/10.1093/nar/gkx1268

Lamparter T, Esch H, Cove D, Hughes J, Hartmann E (1996) Aphototropic mutants of the moss *Ceratodon purpureus* with spectrally normal and with spectrally dysfunctional phytochrome. Plant Cell Environ 19:560–568

Lang D et al (2018) The *Physcomitrella patens* chromosome-scale assembly reveals moss genome structure and evolution. Plant J 93:515–533. https://doi.org/10.1111/tpj.13801

Li F-W et al (2015) Phytochrome diversity in green plants and the origin of canonical plant phytochromes. Nat Commun 6:7852. https://doi.org/10.1038/ncomms8852

Lloyd-Smith JO, Schreiber SJ, Kopp PE, Getz WM (2005) Superspreading and the effect of individual variation on disease emergence. Nature 438:355–359. https://doi.org/10.1038/nature04153

Lopez-Obando M et al (2016) Simple and efficient targeting of multiple genes through CRISPR-Cas9 in *Physcomitrella*. G3 (Bethesda) 6:3647–3653. https://doi.org/10.1534/g3.116.033266

Makarova KS et al (2015) An updated evolutionary classification of CRISPR-Cas systems. Nat Rev Microbiol 13:722–736. https://doi.org/10.1038/nrmicro3569

Mallett DR, Chang M, Cheng X, Bezanilla M (2019) Efficient and modular CRISPR-Cas9 vector system for *Physcomitrella patens*. Plant Direct 3:e00168. https://doi.org/10.1002/pld3.168

Mara K, Charlot F, Guyon-Debast A, Schaefer DG, Collonnier C, Grelon M, Nogue F (2019) POLQ plays a key role in the repair of CRISPR/Cas9-induced double-stranded breaks in the moss *Physcomitrella patens*. New Phytol 222:1380–1391. https://doi.org/10.1111/nph.15680

Mittmann F, Brücker G, Zeidler M, Repp A, Abts T, Hartmann E, Hughes J (2004) Targeted knockout in *Physcomitrella* reveals direct actions of phytochrome in the cytoplasm. Proc Natl Acad Sci USA 101:13939–13944

Najera VA, Twyman RM, Christou P, Zhu C (2019) Applications of multiplex genome editing in higher plants. Curr Opin Biotechnol. https://doi.org/10.1016/j.copbio.2019.02.015

Nomura T, Sakurai T, Osakabe Y, Osakabe K, Sakakibara H (2016) Efficient and heritable targeted mutagenesis in mosses using the CRISPR/Cas9 system. Plant Cell Physiol 57:2600–2610. https://doi.org/10.1093/pcp/pcw173

Pauwels L et al (2018) A dual sgRNA approach for functional genomics in *Arabidopsis thaliana*. G3 (Bethesda) 8:2603–2615. https://doi.org/10.1534/g3.118.200046

Peng F, Zhang W, Zeng W, Zhu J-K, Miki D (2020) Gene targeting in *Arabidopsis* via an all-in-one strategy that uses a translational enhancer to aid Cas9 expression. Plant Biotechnol J 18:892–894. https://doi.org/10.1111/pbi.13265

Pu X et al (2019) A CRISPR/LbCas12a-based method for highly efficient multiplex gene editing in *Physcomitrella patens*. Plant J 100:863–872. https://doi.org/10.1111/tpj.14478

Puchta H (2004) The repair of double-strand breaks in plants: mechanisms and consequences for genome evolution. J Exp Bot 56:1–14. https://doi.org/10.1093/jxb/eri025

Rensing SA et al (2008) The *Physcomitrella* genome reveals evolutionary insights into the conquest of land by plants. Science 319:64–69. https://doi.org/10.1126/science.1150646

Sambrook J, Fritsch EF, Maniatis T (1989) Molecular cloning, a laboratory manual, 2nd edn. CSH Press, Cold Spring Harbor

Schaefer DG, Zrÿd J-P (1997) Efficient gene targeting in the moss *Physcomitrella patens*. Plant J 11:1195–1206

Seol J-H, Shim EY, Lee SE (2018) Microhomology-mediated end joining: good, bad and ugly. Mutat Res 809:81–87. https://doi.org/10.1016/j.mrfmmm.2017.07.002

Shi J et al (2017) ARGOS8 variants generated by CRISPR-Cas9 improve maize grain yield under field drought stress conditions. Plant Biotechnol J 15:207–216. https://doi.org/10.1111/pbi.12603

Wang Y et al (2017) Deletion of a target gene in Indica rice via CRISPR/Cas9. Plant Cell Rep 36:1333–1343. https://doi.org/10.1007/s00299-017-2158-4

Zhao Y et al (2016) An alternative strategy for targeted gene replacement in plants using a dual-sgRNA/Cas9 design. Sci Rep 6:23890. https://doi.org/10.1038/srep23890

Zhou H, Liu B, Weeks DP, Spalding MH, Yang B (2014) Large chromosomal deletions and heritable small genetic changes induced by CRISPR/Cas9 in rice. Nucleic Acids Res 42:10903–10914. https://doi.org/10.1093/nar/gku806

Zimmer AD et al (2013) Reannotation and extended community resources for the genome of the non-seed plant *Physcomitrella patens* provide insights into the evolution of plant gene structures and functions. BMC Genomics 14:498. https://doi.org/10.1186/1471-2164-14-498

12.1.1 Supplementary Information

Table 1. List of lines produced in the multiplex *PHY* and *PHOT* mutagenesis using single sgRNA's.

Treatment	**Table**	**Line**	***PHY1***	***PHY2***	***PHY3***	***PHY4***	***PHY5a***	***PHY5b***	***PHY5c***
PHY2 + PHY4	1a	1	-	0	-	deletion	-	-	-
PHY2 + PHY4	1a	5	-	0	-	deletion	-	-	-
PHY2 + PHY4	1a	7	-	0	-	deletion	-	-	-
PHY2 + PHY4	1a	10	-	deletion	-	0	-	-	-
PHY2 + PHY4	1a	14	-	0	-	insertion	-	-	-
PHY2 + PHY4	1a	20	-	-6bp	-	deletion	-	-	-
PHY2 + PHY4	1a	26	-	deletion	-	0	-	-	-
PHY2 + PHY4	1a	27	-	deletion	-	0	-	-	-
PHY2 + PHY4	1a	35	-	0	-	deletion	-	-	-
PHY2 + PHY4	1a	45	-	0	-	deletion	-	-	-
PHY2 + PHY4	1a	49	-	deletion	-	0	-	-	-
PHY2 + PHY4	1a	51	-	0	-	deletion	-	-	-
PHY2 + PHY4	1a	53	-	-10bp	-	deletion	-	-	-
PHY2 + PHY4	1a	60	-	deletion	-	0	-	-	-
PHY2 + PHY4	1a	68	-	deletion	-	0	-	-	-
PHY2 + PHY4	1a	70	-	0	-	deletion	-	-	-
PHY2 + PHY4	1a	135 (WT)	-	0	-	0	-	-	-
PHY2 + PHY4	1a	138 (WT)	-	0	-	0	-	-	-
PHY2 + PHY4	1a	140 (WT)	-	0	-	0	-	-	-
PHY2 + PHY4	1a	141 (WT)	-	0	-	0	-	-	-
PHY2 + PHY4	1a	158 (WT)	-	0	-	0	-	-	-
PHY2 + PHY4	1a	160 (WT)	-	0	-	0	-	-	-
PHY2 + PHY4	1a	165 (WT)	-	0	-	0	-	-	-
PHY2 + PHY4	1a	166 (WT)	-	0	-	0	-	-	-
PHY2 + PHY4	1a	167 (WT)	-	0	-	0	-	-	-
PHY2 + PHY4	1a	194 (WT)	-	0	-	0	-	-	-
PHY2 + PHY4	1a	203	-	deletion	-	deletion	-	-	-
PHY2 + PHY4	1a	204 (WT)	-	0	-	0	-	-	-
PHY2 + PHY4	1a	205 (WT)	-	0	-	0	-	-	-
PHY2 + PHY4	1a	206 (WT)	-	0	-	0	-	-	-
PHY2 + PHY4	1a	207	-	deletion	-	deletion	-	-	-
PHY2 + PHY4	1a	208 (WT)	-	0	-	0	-	-	-
PHY2 + PHY4	1a	209 (WT)	-	0	-	0	-	-	-

PHY2 + PHY4	1a	210 (WT)	-	0	-	0	-	-	-
PHY2 + PHY4	1a	211 (WT)	-	0	-	0	-	-	-
PHY2 + PHY4	1a	212 (WT)	-	0	-	0	-	-	-
PHY2 + PHY4	1a	213 (WT)	-	0	-	0	-	-	-
PHY2 + PHY4	1a	214	-	deletion	-	0	-	-	-
PHY2 + PHY4	1a	216 (WT)	-	0	-	0	-	-	-
PHY2 + PHY4	1a	217 (WT)	-	0	-	0	-	-	-
PHY2 + PHY4	1a	218 (WT)	-	0	-	0	-	-	-
PHY2 + PHY4	1a	219 (WT)	-	0	-	0	-	-	-
PHY2 + PHY4	1a	220 (WT)	-	0	-	0	-	-	-
PHY2 + PHY4	1a	221 (WT)	-	0	-	0	-	-	-
PHY2 + PHY4	1a	222 (WT)	-	0	-	0	-	-	-
PHY2 + PHY4	1a	223 (WT)	-	0	-	0	-	-	-
PHY2 + PHY4	1a	224 (WT)	-	0	-	0	-	-	-
PHY2 + PHY4	1a	225 (WT)	-	0	-	0	-	-	-
PHY2 + PHY4	1a	226 (WT)	-	0	-	0	-	-	-
PHY2 + PHY4	1a	228 (WT)	-	0	-	0	-	-	-
PHY2 + PHY4	1a	230 (WT)	-	0	-	0	-	-	-
PHY2 + PHY4	1a	232 (WT)	-	0	-	0	-	-	-
PHY2 + PHY4	1a	234 (WT)	-	0	-	0	-	-	-
PHY2 + PHY4	1a	235 (WT)	-	0	-	0	-	-	-
PHY2 + PHY4	1a	236 (WT)	-	0	-	0	-	-	-
PHY2 + PHY4	1a	237	-	-8bp	-	-10bp	-	-	-
PHY2 + PHY4	1a	238	-	deletion	-	deletion	-	-	-
PHY2 + PHY4	1a	239	-	deletion	-	0	-	-	-
PHY2 + PHY4	1a	240 (WT)	-	0	-	0	-	-	-
PHY2 + PHY4	1a	241 (WT)	-	0	-	0	-	-	-
PHY2 + PHY4	1a	242	-	deletion	-	0	-	-	-
PHY2 + PHY4	1a	244 (WT)	-	0	-	0	-	-	-
PHY2 + PHY4	1a	245 (WT)	-	0	-	0	-	-	-
PHY2 + PHY4	1a	246 (WT)	-	0	-	0	-	-	-
PHY2 + PHY4	1a	247 (WT)	-	0	-	0	-	-	-
PHY2 + PHY4	1a	248 (WT)	-	0	-	0	-	-	-
PHY2 + PHY4	1a	249	-	deletion	-	0	-	-	-

PHY2 + PHY4	1a	250 (WT)	-	0	-	0	-	-	-
PHY2 + PHY4	1a	252 (WT)	-	0	-	0	-	-	-
PHY2 + PHY4	1a	253 (WT)	-	0	-	0	-	-	-
PHY2 + PHY4	1a	254 (WT)	-	0	-	0	-	-	-
PHY2 + PHY4	1a	255	-	-8bp	-	-13bp	-	-	-
PHY2 + PHY4	1a	256 (WT)	-	0	-	0	-	-	-
PHY2 + PHY4	1a	257 (WT)	-	0	-	0	-	-	-
PHY2 + PHY4	1a	258	-	0	-	deletion	-	-	-
PHY5b + PHY5c	1b	2	-	-	-	-	-	0	-5bp
PHY5b + PHY5c	1b	4	-	-	-	-	-	-2bp	-5bp
PHY5b + PHY5c	1b	9	-	-	-	-	-	+79bp	0
PHY5b + PHY5c	1b	11	-	-	-	-	-	deletion	0
PHY5b + PHY5c	1b	13	-	-	-	-	-	0	insertion
PHY5b + PHY5c	1b	14	-	-	-	-	-	deletion	0
PHY5b + PHY5c	1b	15	-	-	-	-	-	deletion	0
PHY5b + PHY5c	1b	16 (WT)	-	-	-	-	-	0	0
PHY5b + PHY5c	1b	18 (WT)	-	-	-	-	-	0	0
PHY5b + PHY5c	1b	20	-	-	-	-	-	0	+10bp
PHY5b + PHY5c	1b	21 (WT)	-	-	-	-	-	0	0
PHY5b + PHY5c	1b	22	-	-	-	-	-	-6bp	-5bp
PHY5b + PHY5c	1b	24	-	-	-	-	-	deletion	deletion
PHY5b + PHY5c	1b	25 (WT)	-	-	-	-	-	0	0
PHY5b + PHY5c	1b	27	-	-	-	-	-	-12bp	-5bp
PHY5b + PHY5c	1b	28	-	-	-	-	-	0	deletion
PHY5b + PHY5c	1b	29	-	-	-	-	-	0	deletion
PHY5b + PHY5c	1b	30	-	-	-	-	-	0	deletion
PHY5b + PHY5c	1b	32	-	-	-	-	-	0	deletion
PHY5b + PHY5c	1b	33	-	-	-	-	-	0	deletion
PHY5b + PHY5c	1b	35 (WT)	-	-	-	-	-	0	0
PHY5b + PHY5c	1b	44	-	-	-	-	-	deletion	deletion
PHY5b + PHY5c	1b	47	-	-	-	-	-	deletion	0
PHY5b + PHY5c	1b	48 (WT)	-	-	-	-	-	0	0
PHY5b + PHY5c	1b	49 (WT)	-	-	-	-	-	0	0
PHY5b + PHY5c	1b	50	-	-	-	-	-	0	deletion
PHY5b + PHY5c	1b	59	-	-	-	-	-	deletion	Insertion
PHY5b + PHY5c	1b	69	-	-	-	-	-	-2bp	-5bp
PHY5b + PHY5c	1b	98	-	-	-	-	-	deletion	0
PHY5b + PHY5c	1b	99	-	-	-	-	-	deletion	insertion
PHY5b + PHY5c	1b	101	-	-	-	-	-	0	deletion
PHY5b + PHY5c	1b	102	-	-	-	-	-	0	deletion

PHY5b + PHY5c	1b	103	-	-	-	-	-	-2bp	-5bp
PHY5b + PHY5c	1b	104	-	-	-	-	-	0	-5bp
PHY5b + PHY5c	1b	107	-	-	-	-	-	deletion	deletion
PHY5b + PHY5c	1b	109	-	-	-	-	-	0	deletion
PHY5b + PHY5c	1b	110 (WT)	-	-	-	-	-	0	0
PHY5b + PHY5c	1b	112 (WT)	-	-	-	-	-	0	0
PHY5b + PHY5c	1b	113	-	-	-	-	-	0	deletion
PHY5b + PHY5c	1b	118	-	-	-	-	-	deletion	deletion
PHY5b + PHY5c	1b	121	-	-	-	-	-	deletion	insertion
PHY5b + PHY5c	1b	122	-	-	-	-	-	-6bp	0
PHY5b + PHY5c	1b	123	-	-	-	-	-	deletion	0
PHY5b + PHY5c	1b	125	-	-	-	-	-	0	insertion
PHY5b + PHY5c	1b	127	-	-	-	-	-	0	-5bp
PHY5b + PHY5c	1b	134 (WT)	-	-	-	-	-	0	0
PHY5b + PHY5c	1b	137	-	-	-	-	-	deletion	deletion
PHY5b + PHY5c	1b	139	-	-	-	-	-	0	deletion
PHY1-4	1c	37 (WT)	0	0	0	0	-	-	-
PHY1-4	1c	98 (WT)	0	0	0	0	-	-	-
PHY1-4	1c	134 (WT)	0	0	0	0	-	-	-
PHY1-4	1c	139 (WT)	0	0	0	0	-	-	-
PHY1-4	1c	141 (WT)	0	0	0	0	-	-	-
PHY1-4	1c	151 (WT)	0	0	0	0	-	-	-
PHY1-4	1c	180 (WT)	0	0	0	0	-	-	-
PHY1-4	1c	186	-4bp	-8bp	0	-10bp	-	-	-
PHY1-4	1c	187 (WT)	0	0	0	0	-	-	-
PHY1-4	1c	189 (WT)	0	0	0	0	-	-	-
PHY1-4	1c	190 (WT)	0	0	0	0	-	-	-
PHY1-4	1c	192 (WT)	0	0	0	0	-	-	-
PHY1-4	1c	193	0	-4bp	0	-10bp	-	-	-
PHY1-4	1c	194	deletion	0	0	0	-	-	-
PHY1-4	1c	201 (WT)	0	0	0	0	-	-	-
PHY1-4	1c	203 (WT)	0	0	0	0	-	-	-
PHY1-4	1c	204	+4bp	-8bp	0	-10bp	-	-	-
PHY1-4	1c	205 (WT)	0	0	0	0	-	-	-
PHY1-4	1c	206 (WT)	0	0	0	0	-	-	-
PHY1-4	1c	208 (WT)	0	0	0	0	-	-	-
PHY1-4	1c	209 (WT)	0	0	0	0	-	-	-

PHY1-4	1c	211 (WT)	0	0	0	0	-	-	-
PHY1-4	1c	212 (WT)	0	0	0	0	-	-	-
PHY1-4	1c	214 (WT)	0	0	0	0	-	-	-
PHY1-4	1c	215 (WT)	0	0	0	0	-	-	-
PHY1-4	1c	216 (WT)	0	0	0	0	-	-	-
PHY1-4	1c	217 (WT)	0	0	0	0	-	-	-
PHY1-4	1c	218	0	deletion	0	0	-	-	-
PHY1-4	1c	219 (WT)	0	0	0	0	-	-	-
PHY1-4	1c	221 (WT)	0	0	0	0	-	-	-
PHY1-4	1c	224 (WT)	0	0	0	0	-	-	-
PHY1-4	1c	228 (WT)	0	0	0	0	-	-	-
PHY1-4	1c	231 (WT)	0	0	0	0	-	-	-
PHY1-4	1c	233	deletion	0	0	deletion	-	-	-
PHY1-4	1c	234 (WT)	0	0	0	0	-	-	-
PHY1-4	1c	235 (WT)	0	0	0	0	-	-	-
PHY1-4	1c	237 (WT)	0	0	0	0	-	-	-
PHY1-4	1c	238 (WT)	0	0	0	0	-	-	-
PHY1-4	1c	241 (WT)	0	0	0	0	-	-	-
PHY1-4	1c	244 (WT)	0	0	0	0	-	-	-
PHY1-4	1c	246 (WT)	0	0	0	0	-	-	-
PHY1-4	1c	247 (WT)	0	0	0	0	-	-	-
PHY1-4	1c	251	0	deletion	0	0	-	-	-
PHY1-4	1c	253 (WT)	0	0	0	0	-	-	-
PHY1-4	1c	256 (WT)	0	0	0	0	-	-	-
PHY1-4	1c	257 (WT)	0	0	0	0	-	-	-
PHY1-4	1c	261	insertion	0	0	0	-	-	-
PHY1-4	1c	262 (WT)	0	0	0	0	-	-	-
PHY1-4	1c	263	0	insertion	0	0	-	-	-
PHY1-4	1c	264 (WT)	0	0	0	0	-	-	-
PHY1-4	1c	266	insertion	0	0	0	-	-	-
PHY1-4	1c	267 (WT)	0	0	0	0	-	-	-
PHY1-4	1c	268 (WT)	0	0	0	0	-	-	-
PHY1-4	1c	269 (WT)	0	0	0	0	-	-	-
PHY1-4	1c	270	0	0	insertion	0	-	-	-

PHY1-4	1c	273 (WT)	0	0	0	0	-	-	-
PHY1-4	1c	277 (WT)	0	0	0	0	-	-	-
PHY1-4	1c	278 (WT)	0	0	0	0	-	-	-
PHY1-4	1c	281	insertion	insertion	0	deletion	-	-	-
PHY1-4	1c	282 (WT)	0	0	0	0	-	-	-
PHY1-4 + *PHY5b-c*	1d	1 (WT)	0	0	0	0	-	0	0
PHY1-4 + *PHY5b-c*	1d	4 (WT)	0	0	0	0	-	0	0
PHY1-4 + *PHY5b-c*	1d	6 (WT)	0	0	0	0	-	0	0
PHY1-4 + *PHY5b-c*	1d	15 (WT)	0	0	0	0	-	0	0
PHY1-4 + *PHY5b-c*	1d	32 (WT)	0	0	0	0	-	0	0
PHY1-4 + *PHY5b-c*	1d	104 (WT)	0	0	0	0	-	0	0
PHY1-4 + *PHY5b-c*	1d	105	0	0	0	0	-	deletion	0
PHY1-4 + *PHY5b-c*	1d	112	0	0	0	0	-	deletion	0
PHY1-4 + *PHY5b-c*	1d	113	0	0	0	insertion	-	0	deletion
PHY1-4 + *PHY5b-c*	1d	114 (WT)	0	0	0	0	-	0	0
PHY1-4 + *PHY5b-c*	1d	115 (WT)	0	0	0	0	-	0	0
PHY1-4 + *PHY5b-c*	1d	116 (WT)	0	0	0	0	-	0	0
PHY1-4 + *PHY5b-c*	1d	124	-1bp	0	0	-8bp	-	0	-5bp
PHY1-4 + *PHY5b-c*	1d	125 (WT)	0	0	0	0	-	0	0
PHY1-4 + *PHY5b-c*	1d	132 (WT)	0	0	0	0	-	0	0
PHY1-4 + *PHY5b-c*	1d	135 (WT)	0	0	0	0	-	0	0
PHY1-4 + *PHY5b-c*	1d	137 (WT)	0	0	0	0	-	0	0
PHY1-4 + *PHY5b-c*	1d	146 (WT)	0	0	0	0	-	0	0
PHY1-4 + *PHY5b-c*	1d	148 (WT)	0	0	0	0	-	0	0
PHY1-4 + *PHY5b-c*	1d	154 (WT)	0	0	0	0	-	0	0
PHY1-4 + *PHY5b-c*	1d	159 (WT)	0	0	0	0	-	0	0
PHY1-4 + *PHY5b-c*	1d	163 (WT)	0	0	0	0	-	0	0
PHY1-4 + *PHY5b-c*	1d	164	0	0	0	0	-	deletion	0
PHY1-4 + *PHY5b-c*	1d	165	insertion	deletion	insertion	0	-	0	0
PHY1-4 + *PHY5b-c*	1d	169	0	0	0	deletion	-	0	deletion
PHY1-4 + *PHY5b-c*	1d	170 (WT)	0	0	0	0	-	0	0
PHY1-4 + *PHY5b-c*	1d	172 (WT)	0	0	0	0	-	0	0
PHY1-4 + *PHY5b-c*	1d	177 (WT)	0	0	0	0	-	0	0

PHY1-4 + *PHY5b-c*	1d	182	0	0	0	deletion	-	0	0
PHY1-4 + *PHY5b-c*	1d	183 (WT)	0	0	0	0	-	0	0
PHY1-4 + *PHY5b-c*	1d	184 (WT)	0	0	0	0	-	0	0
PHY1-4 + *PHY5b-c*	1d	188 (WT)	0	0	0	0	-	0	0
PHY1-4 + *PHY5b-c*	1d	193	0	0	0	0	-	0	Insertion
PHY1-4 + *PHY5b-c*	1d	199 (WT)	0	0	0	0	-	0	0
PHY1-4 + *PHY5b-c*	1d	200	0	0	0	0	-	0	deletion
PHY1-4 + *PHY5b-c*	1d	207 (WT)	0	0	0	0	-	0	0
PHY1-4 + *PHY5b-c*	1d	208 (WT)	0	0	0	0	-	0	0
PHY1-4 + *PHY5b-c*	1d	209 (WT)	0	0	0	0	-	0	0
PHY1-4 + *PHY5b-c*	1d	213 (WT)	0	0	0	0	-	0	0
PHY1-4 + *PHY5b-c*	1d	215 (WT)	0	0	0	0	-	0	0
PHY1-4 + *PHY5b-c*	1d	216	0	deletion	insertion	0	-	0	deletion
PHY1-4 + *PHY5b-c*	1d	218	0	0	0	0	-	deletion	0
PHY1-4 + *PHY5b-c*	1d	220 (WT)	0	0	0	0	-	0	0
PHY1-4 + *PHY5b-c*	1d	222 (WT)	0	0	0	0	-	0	0
PHY1-4 + *PHY5b-c*	1d	225	0	0	0	0	-	0	insertion
PHY1-4 + *PHY5b-c*	1d	226	0	0	-2bp	0	-	0	0
PHY1-4 + *PHY5b-c*	1d	228	-28bp	-4bp	+37bp	-10bp	-	0	-5bp
PHY1-4 + *PHY5b-c*	1d	232 (WT)	0	0	0	0	-	0	0
PHY1-4 + *PHY5b-c*	1d	233 (WT)	0	0	0	0	-	0	0
PHY1-4 + *PHY5b-c*	1d	234	0	0	0	0	-	0	deletion
PHY1-4 + *PHY5b-c*	1d	235 (WT)	0	0	0	0	-	0	0
PHY1-4 + *PHY5b-c*	1d	236	0	0	0	0	-	0	-5bp
PHY1-4 + *PHY5b-c*	1d	237	0	0	0	0	-	0	deletion
PHY1-4 + *PHY5b-c*	1d	238 (WT)	0	0	0	0	-	0	0
PHY1-4 + *PHY5b-c*	1d	239 (WT)	0	0	0	0	-	0	0
PHY1-4 + *PHY5b-c*	1d	240	0	0	0	0	-	0	deletion
PHY1-4 + *PHY5b-c*	1d	242 (WT)	0	0	0	0	-	0	0
PHY1-4 + *PHY5b-c*	1d	244	0	-38bp	0	0	-	0	0
PHY1-4 + *PHY5b-c*	1d	246	insertion	0	0	0	-	0	0
PHY1-4 + *PHY5b-c*	1d	247	insertion	0	0	0	-	0	0

PHY1-4 + *PHY5b-c*	1d	248	insertion	0	0	0	-	0	0
PHY1-4 + *PHY5b-c*	1d	249 (WT)	0	0	0	0	-	0	0
PHY1-4 + *PHY5b-c*	1d	250 (WT)	0	0	0	0	-	0	0
PHY1-4 + *PHY5b-c*	1d	251	0	0	0	0	-	0	deletion
PHY1-4 + *PHY5b-c*	1d	252 (WT)	0	0	0	0	-	0	0
PHY1-4 + *PHY5b-c*	1d	256 (WT)	0	0	0	0	-	0	0
PHY1-4 + *PHY5b-c*	1d	258 (WT)	0	0	0	0	-	0	0
PHY1-4 + *PHY5b-c*	1d	260	0	deletion	0	0	-	0	0
PHY1-4 + *PHY5b-c*	1d	261 (WT)	0	0	0	0	-	0	0
PHY1-4 + *PHY5b-c*	1d	262	insertion	0	0	0	-	0	0
PHY1-4 + *PHY5b-c*	1d	263	0	0	0	deletion	-	0	0
PHY1-4 + *PHY5b-c*	1d	265	0	0	0	deletion	-	insertion	insertion
PHY1-4 + *PHY5b-c*	1d	266 (WT)	0	0	0	0	-	0	0
PHY1-4 + *PHY5b-c*	1d	272 (WT)	0	0	0	0	-	0	0
all *PHYs*	1e	1	deletion	0	-5bp	-10bp	-7bp	0	-5bp
all *PHYs*	1e	2	0	0	0	0	deletion	0	0
all *PHYs*	1e	3	deletion	0	0	0	deletion	0	0
all *PHYs*	1e	4	0	0	0	deletion	deletion	0	0
all *PHYs*	1e	5	0	0	0	deletion	0	0	0
all *PHYs*	1e	6	insertion	0	0	0	insertion	deletion	-5bp
all *PHYs*	1e	7	0	0	0	0	0	0	deletion
all *PHYs*	1e	8	0	0	0	0	deletion	0	0
all *PHYs*	1e	9	0	0	0	0	deletion	0	0
all *PHYs*	1e	10	0	-8bp	-6bp	-5bp	-7bp	0	-5bp
all *PHYs*	1e	11	+14bp	+1bp	0	-5bp	-2bp	-6bp	-5bp
all *PHYs*	1e	12	0	0	0	0	deletion	0	0
all *PHYs*	1e	13	deletion	0	0	deletion	deletion	0	0
all *PHYs*	1e	14	0	deletion	0	0	insertion	0	deletion
all *PHYs*	1e	15	deletion	0	0	deletion	deletion	0	deletion
all *PHYs*	1e	16	-7bp	-321bp	-11bp	-10bp	+2bp	0	-5bp
all *PHYs*	1e	17	0	deletion	0	deletion	deletion	0	0
all *PHYs*	1e	18	deletion	0	0	0	deletion	0	0
all *PHYs*	1e	19	0	0	0	0	deletion	0	0
all *PHYs*	1e	20	0	-4bp	0	+111bp	-4bp	0	-5bp
all *PHYs*	1e	21	0	deletion	0	0	0	0	deletion
all *PHYs*	1e	22	deletion	deletion	0	deletion	deletion	0	deletion
all *PHYs*	1e	23	+14bp	-8bp	-14bp	-5bp	-9bp	-6bp	-5bp
all *PHYs*	1e	24	0	0	0	0	insertion	0	deletion
all *PHYs*	1e	25	0	deletion	0	deletion	deletion	0	deletion

all *PHYs*	1e	26	insertion	0	deletion	-5bp	-6bp	-9bp	-5bp
all *PHYs*	1e	27	deletion	0	0	deletion	deletion	0	deletion
all *PHYs*	1e	28	0	0	0	0	deletion	0	0
all *PHYs*	1e	29	0	0	0	0	deletion	0	0
all *PHYs*	1e	30	0	0	0	insertion	0	0	0
all *PHYs*	1e	31	0	insertion	0	deletion	deletion	deletion	deletion
all *PHYs*	1e	32	deletion	0	deletion	0	deletion	0	0
all *PHYs*	1e	33	+136bp	-8bp	0	+21bp	-13bp	-2bp	-5bp
all *PHYs*	1e	35	deletion	0	0	0	deletion	0	0
all *PHYs*	1e	36	insertion	0	deletion	deletion	0	0	deletion
all *PHYs*	1e	37	0	deletion	0	deletion	deletion	0	0
all *PHYs*	1e	39 (WT)	0	0	0	0	0	0	0
all *PHYs*	1e	40	0	0	0	deletion	deletion	0	0
all *PHYs*	1e	41	0	0	0	-1bp	deletion	deletion	-5bp
all *PHYs*	1e	42 (WT)	0	0	0	0	0	0	0
all *PHYs*	1e	43	insertion	deletion	0	0	deletion	0	deletion
all *PHYs*	1e	46	deletion	deletion	0	deletion	deletion	0	deletion
all *PHYs*	1e	47	deletion	deletion	0	0	insertion	0	0
all *PHYs*	1e	48	0	0	0	deletion	deletion	0	0
all *PHYs*	1e	49	deletion	0	0	0	insertion	0	0
all *PHYs*	1e	50 (WT)	0	0	0	0	0	0	0
all *PHYs*	1e	51 (WT)	0	0	0	0	0	0	0
all *PHYs*	1e	52	0	0	0	deletion	deletion	0	deletion
all *PHYs*	1e	54	0	0	0	deletion	deletion	0	deletion
all *PHYs*	1e	55	deletion	0	0	0	deletion	0	0
all *PHYs*	1e	56	0	deletion	0	deletion	0	0	deletion
all *PHYs*	1e	57	0	0	0	deletion	0	0	0
all *PHYs*	1e	58	insertion	0	0	0	0	0	0
all *PHYs*	1e	59	0	deletion	0	deletion	deletion	0	deletion
all *PHYs*	1e	60	0	0	0	0	0	0	deletion
all *PHYs*	1e	61	0	deletion	deletion	deletion	0	0	deletion
all *PHYs*	1e	62	0	deletion	0	0	deletion	0	0
all *PHYs*	1e	63	0	insertion	0	0	0	deletion	deletion
all *PHYs*	1e	64	deletion	0	0	0	0	0	0
all *PHYs*	1e	65	deletion	0	0	0	insertion	deletion	deletion
all *PHYs*	1e	66	0	0	0	insertion	0	0	deletion
all *PHYs*	1e	67	0	insertion	0	0	deletion	0	deletion
all *PHYs*	1e	69	0	0	0	0	deletion	0	0
all *PHYs*	1e	70	0	0	0	0	deletion	0	0
all *PHYs*	1e	71	0	0	0	0	deletion	0	deletion
all *PHYs*	1e	73	0	deletion	0	deletion	insertion	0	deletion
all *PHYs*	1e	74	0	0	deletion	0	0	0	deletion
all *PHYs*	1e	75	0	deletion	0	0	0	deletion	deletion
all *PHYs*	1e	76	0	0	0	0	0	deletion	deletion
all *PHYs*	1e	77	0	0	0	0	0	0	deletion

all *PHYs*	1e	78	0	0	0	0	insertion	0	0
all *PHYs*	1e	79	0	0	0	0	0	deletion	deletion
all *PHYs*	1e	80	0	0	0	0	insertion	0	deletion
all *PHYs*	1e	83	0	0	insertion	deletion	deletion	0	deletion
all *PHYs*	1e	84	0	deletion	deletion	deletion	0	0	0
all *PHYs*	1e	85	deletion	0	0	deletion	deletion	0	deletion
all *PHYs*	1e	87	deletion	0	0	0	deletion	0	0
all *PHYs*	1e	88	0	0	0	0	deletion	0	0
all *PHYs*	1e	89	insertion	0	0	0	deletion	0	deletion
all *PHYs*	1e	90 (WT)	0	0	0	0	0	0	0
all *PHYs*	1e	91	0	0	0	0	0	0	deletion
all *PHYs*	1e	92	insertion	0	0	deletion	insertion	deletion	deletion
all *PHYs*	1e	93	0	0	0	0	deletion	0	0
all *PHYs*	1e	94	deletion	0	0	deletion	insertion	deletion	0
all *PHYs*	1e	95	0	0	insertion	0	0	0	0
PHY5a + *PHY5b* in d	1f	2	-28bp	-4bp	+37bp	-10bp	0	0	-5bp
PHY5a + *PHY5b* in d	1f	3	-28bp	-4bp	+37bp	-10bp	deletion	0	-5bp
PHY5a + *PHY5b* in d	1f	4	-28bp	-4bp	+37bp	-10bp	0	0	-5bp
PHY5a + *PHY5b* in d	1f	5	-28bp	-4bp	+37bp	-10bp	deletion	0	-5bp
PHY5a + *PHY5b* in d	1f	6	-28bp	-4bp	+37bp	-10bp	insertion	0	-5bp
PHY5a + *PHY5b* in d	1f	7	-28bp	-4bp	+37bp	-10bp	deletion	0	-5bp
PHY5a + *PHY5b* in d	1f	8	-28bp	-4bp	+37bp	-10bp	0	insertion	-5bp
PHY5a + *PHY5b* in d	1f	11	-28bp	-4bp	+37bp	-10bp	-5bp	0	-5bp
PHY5a + *PHY5b* in d	1f	12	-28bp	-4bp	+37bp	-10bp	insertion	0	-5bp
PHY5a + *PHY5b* in d	1f	13	-28bp	-4bp	+37bp	-10bp	-2bp	-6bp	-5bp
PHY5a + *PHY5b* in d	1f	16	-28bp	-4bp	+37bp	-10bp	-6bp	0	-5bp
PHY5a + *PHY5b* in d	1f	17	-28bp	-4bp	+37bp	-10bp	-23bp	-17bp	-5bp
PHY5a + *PHY5b* in d	1f	18	-28bp	-4bp	+37bp	-10bp	insertion	0	-5bp
PHY5a + *PHY5b* in d	1f	19	-28bp	-4bp	+37bp	-10bp	-13bp	-6bp	-5bp
PHY5a + *PHY5b* in d	1f	20	-28bp	-4bp	+37bp	-10bp	deletion	0	-5bp
PHY5a + *PHY5b* in d	1f	21	-28bp	-4bp	+37bp	-10bp	deletion	0	-5bp
PHY5a + *PHY5b* in d	1f	22	-28bp	-4bp	+37bp	-10bp	deletion	0	-5bp
PHY5a + *PHY5b* in d	1f	23	-28bp	-4bp	+37bp	-10bp	deletion	0	-5bp
PHY5a + *PHY5b* in d	1f	24	-28bp	-4bp	+37bp	-10bp	0	deletion	-5bp
PHY5a + *PHY5b* in d	1f	29	-28bp	-4bp	+37bp	-10bp	0	0	-5bp
PHY5a + *PHY5b* in d	1f	30	-28bp	-4bp	+37bp	-10bp	-11bp	0	-5bp
PHY5a + *PHY5b* in d	1f	31	-28bp	-4bp	+37bp	-10bp	-8bp	0	-5bp

PHY5a + *PHY5b* in d	1f	32	-28bp	-4bp	+37bp	-10bp	deletion	0	-5bp
PHY5a + *PHY5b* in d	1f	33	-28bp	-4bp	+37bp	-10bp	deletion	deletion	-5bp
PHY5a + *PHY5b* in d	1f	34	-28bp	-4bp	+37bp	-10bp	insertion	0	-5bp
PHY5a + *PHY5b* in d	1f	35	-28bp	-4bp	+37bp	-10bp	deletion	0	-5bp
PHY5a + *PHY5b* in d	1f	37	-28bp	-4bp	+37bp	-10bp	-13bp	-6bp	-5bp
PHY5a + *PHY5b* in d	1f	38	-28bp	-4bp	+37bp	-10bp	deletion	0	-5bp
PHY5a + *PHY5b* in d	1f	39	-28bp	-4bp	+37bp	-10bp	deletion	0	-5bp
PHY5a + *PHY5b* in d	1f	43	-28bp	-4bp	+37bp	-10bp	+5bp	-3bp	-5bp
PHY5a + *PHY5b* in d	1f	45	-28bp	-4bp	+37bp	-10bp	deletion	0	-5bp
PHY5a + *PHY5b* in d	1f	46	-28bp	-4bp	+37bp	-10bp	-10bp	0	-5bp
PHY5a + *PHY5b* in d	1f	47	-28bp	-4bp	+37bp	-10bp	0	0	-5bp
PHY5a + *PHY5b* in d	1f	49	-28bp	-4bp	+37bp	-10bp	deletion	0	-5bp
PHY5a + *PHY5b* in d	1f	50	-28bp	-4bp	+37bp	-10bp	0	0	-5bp
PHY5a + *PHY5b* in d	1f	51	-28bp	-4bp	+37bp	-10bp	-9bp	-6bp	-5bp
PHY5a + *PHY5b* in d	1f	52	-28bp	-4bp	+37bp	-10bp	deletion	0	-5bp
PHY5a + *PHY5b* in d	1f	55	-28bp	-4bp	+37bp	-10bp	-3bp	+3bp	-5bp
PHY5a + *PHY5b* in d	1f	56	-28bp	-4bp	+37bp	-10bp	insertion	0	-5bp
PHY5a + *PHY5b* in d	1f	57	-28bp	-4bp	+37bp	-10bp	-4bp	-6bp	-5bp
PHY5a + *PHY5b* in d	1f	58	-28bp	-4bp	+37bp	-10bp	-9bp	deletion	-5bp
PHY5a + *PHY5b* in d	1f	59	-28bp	-4bp	+37bp	-10bp	-9bp	deletion	-5bp
PHY5a + *PHY5b* in d	1f	61	-28bp	-4bp	+37bp	-10bp	-3bp	deletion	-5bp
PHY5a + *PHY5b* in d	1f	62	-28bp	-4bp	+37bp	-10bp	-6bp	-6bp	-5bp
PHY5a + *PHY5b* in d	1f	63	-28bp	-4bp	+37bp	-10bp	0	deletion	-5bp
PHY5a + *PHY5b* in d	1f	64	-28bp	-4bp	+37bp	-10bp	deletion	0	-5bp
PHY5a + *PHY5b* in d	1f	65	-28bp	-4bp	+37bp	-10bp	insertion	0	-5bp
PHY5a + *PHY5b* in d	1f	66	-28bp	-4bp	+37bp	-10bp	deletion	0	-5bp
PHY5a + *PHY5b* in d	1f	67	-28bp	-4bp	+37bp	-10bp	-2bp	-2bp	-5bp
PHY5a + *PHY5b* in d	1f	68	-28bp	-4bp	+37bp	-10bp	deletion	0	-5bp
PHY5a + *PHY5b* in d	1f	70	-28bp	-4bp	+37bp	-10bp	0	0	-5bp
PHY5a + *PHY5b* in d	1f	71	-28bp	-4bp	+37bp	-10bp	deletion	0	-5bp
PHY5a + *PHY5b* in d	1f	72	-28bp	-4bp	+37bp	-10bp	deletion	0	-5bp

Treatment	Line	*PHOTA1*	*PHOTA2*	*PHOTA3*	*PHOTB1*	*PHOTB2*
All *PHOTs*	1	-18bp	0	0	-11bp	-8bp
All *PHOTs*	4	0	0	0	deletion	deletion
All *PHOTs*	5	-4bp	0	0	-2bp	+10bp
All *PHOTs*	6	0	0	0	deletion	deletion
All *PHOTs*	7	0	0	0	0	deletion
All *PHOTs*	8	deletion	0	0	0	deletion
All *PHOTs*	9	0	0	0	deletion	insertion
All *PHOTs*	10	0	0	0	deletion	deletion
All *PHOTs*	11	0	0	0	deletion	deletion
All *PHOTs*	12	0	0	deletion	insertion	deletion
All *PHOTs*	13	0	0	0	no product	deletion
All *PHOTs*	14	0	0	0	insertion	deletion
All *PHOTs*	15	0	0	0	deletion	deletion
All *PHOTs*	17	0	0	0	deletion	no product
All *PHOTs*	18	insertion	0	0	insertion	deletion
All *PHOTs*	19	deletion	0	0	-2bp	no product
All *PHOTs*	20	deletion	0	0	deletion	deletion
All *PHOTs*	21	-25bp	0	0	-6bp	deletion
All *PHOTs*	22	no product	0	0	insertion	deletion
All *PHOTs*	23	0	0	0	deletion	deletion
All *PHOTs*	25	0	0	0	deletion	insertion
All *PHOTs*	26	no product	0	0	deletion	deletion
All *PHOTs*	29	0	0	0	deletion	deletion
All *PHOTs*	31	no product	0	0	insertion	deletion
All *PHOTs*	34	-4bp	0	12bp	-1bp	-8bp
All *PHOTs*	35	0	0	0	insertion	deletion
All *PHOTs*	36	0	0	0	0	insertion
All *PHOTs*	37	0	0	0	0	deletion
All *PHOTs*	38	0	0	0	0	deletion
All *PHOTs*	39	0	0	0	0	deletion
All *PHOTs*	40	0	0	0	0	deletion
All *PHOTs*	41	-18bp	0	0	0	deletion
All *PHOTs*	42	0	0	0	no product	0
All *PHOTs*	43	insertion	0	0	deletion	deletion
All *PHOTs*	44	0	0	0	deletion	deletion
All *PHOTs*	45	0	0	0	deletion	deletion
All *PHOTs*	46	0	0	0	deletion	deletion
PHOTA2+A3	1	-4bp	-13bp	+2bp, +2bp	-2bp	+10bp
PHOTA2+A3	2	-4bp	+4bp	-10bp	-2bp	+10bp
PHOTA2+A3	3	-4bp	+15bp, -1 bp	-39bp, 1SNP	-2bp	+10bp
PHOTA2+A3	4	-4bp	-44bp	-10bp	-2bp	+10bp
PHOTA2+A3	6	-4bp	-6bp	-10bp, + 1bp	-2bp	+10bp
PHOTA2+A3	8	-4bp	insertion	insertion	-2bp	+10bp

PHOTA2+A3	12	-4bp	insertion	deletion	-2bp	+10bp
PHOTA2+A3	13	-4bp	deletion	deletion	-2bp	+10bp
PHOTA2+A3	14	-4bp	-39bp	-10bp	-2bp	+10bp
PHOTA2+A3	16	-4bp	deletion	deletion	-2bp	+10bp
PHOTA2+A3	17	-4bp	0	-10bp, +1bp	-2bp	+10bp
PHOTA2+A3	20	-4bp	+8bp, +2bp, 3SNPs	-10bp	-2bp	+10bp
PHOTA2+A3	23	-4bp	deletion	-10bp, +1bp	-2bp	+10bp
PHOTA2+A3	24	-4bp	deletion	no product	-2bp	+10bp
PHOTA2+A3	25	-4bp	deletion	0	-2bp	+10bp
PHOTA2+A3	27	-4bp	deletion	deletion	-2bp	+10bp
PHOTA2+A3	29	-4bp	0	deletion	-2bp	+10bp
PHOTA2+A3	34	-4bp	deletion	deletion	-2bp	+10bp
PHOTA2+A3	40	-4bp	0	0	-2bp	+10bp
PHOTA2+A3	41	-4bp	deletion	deletion	-2bp	+10bp
PHOTA2+A3	45	-4bp	deletion	deletion	-2bp	+10bp
PHOTA2+A3	46	-4bp	deletion	deletion	-2bp	+10bp
PHOTA2+A3	48	-4bp	deletion	deletion	-2bp	+10bp
PHOTA2+A3	50	-4bp	insertion	deletion	-2bp	+10bp
PHOTA2+A3	52	-4bp	deletion	deletion	-2bp	+10bp
PHOTA2+A3	53	-4bp	0	deletion	-2bp	+10bp
PHOTA2+A3	54	-4bp	0	deletion	-2bp	+10bp
PHOTA2+A3	55	-4bp	0	deletion	-2bp	+10bp
PHOTA2+A3	58	-4bp	insertion	deletion	-2bp	+10bp
PHOTA2+A3	60	-4bp	0	deletion	-2bp	+10bp
PHOTA2+A3	61	-4bp	0	deletion	-2bp	+10bp
PHOTA2+A3	63	-4bp	0	0	-2bp	+10bp

Table 2. Target genes and crRNA sequences for members of the *Physcomitrella PHY* gene family used in the multiplex gene editing via single-cut.

Gene[a]	crRNA sequence	Specificity Score[b] (%)
Pp3c25_2610V1.1 (PHY1)	GACCCTCACACTATGCGCCT **TGG**	100
Pp3c16_20280V1.1 (PHY2)	GTCAAAGCATAGTGTCCGGG **TGG**	100
Pp3c16_18760V3.1 (PHY3)	AGTCGAAGGCCCACAGCGTG **AGG**	100
Pp3c27_7830V3.3 (PHY4)	GGCAGCCTATTAGTCTGGCC **GGG**	100
Pp3c3_23790V1.1 (PHY5a)	CACAAGCTGTACCGAGTGTG **GGG**	100
Pp3c12_9240V3.1 (PHY5b)	ACTTCCTTTAGACCGACACT **TGG**	100
Pp3c4_15350V3.1 (PHY5c)	GCGCGGCTACAATCCCTTCC **CGG**	99

[a]: Identifier and name (in brackets) of genes from Phytozome V11 - *P. patens* genome.
[b]: Specificity Score data from CRISPOR (Hsu *et al.*, 2013).

Table 3. Selected predicted off-targets against members of the *Physcomitrella PHY* gene family for the evaluation of off-target activity in the multiplex gene editing via single-cut.

On-target gene	Predicted off-targets sequence[a]	Off-target annotation
PHY1	GACTCTCACAGTCTGCCCCT **CGG**	Off-T1: Non-coding DNA region
	GACTCTCACAGTATGGCCCT **CGG**	*Off-T2: Non-coding DNA region
	GACTCTCACACTCTGGCCCT **TGG**	Off-T3: Scaffold38
PHY2	GTCAAAGCATTGTGACAGGT **CGG**	Off-T1: Non-coding DNA region
	GTCACGGCTTAGTTTCCGGG **AGG**	*Off-T2: *Pp3c1_35220*
	GTCAAAGCAGAGGTTCCGGT **AGG**	*Off-T3: *Pp3c14_9939*
PHY3	AGTCCAAGGCGCATAGTGTG **AGG**	Off-T1: Exon of *Pp3c25_2610*
PHY5a	AACAAGCTGAACTGAGTGAG **GGG**	*Off-T1: *Pp3c20_21890*
	CAAAAGATATACCTAGTGTG **TGG**	Off-T2: Non-coding DNA region
PHY5b	ACTTCCTGCTGACCCACACT **GGG**	*Off-T1: Exon of *Pp3c27_7830*
	ACTTCCTGTTGGCCCACACT **TGG**	*Off-T2: 5' UTR of *Pp3c27_7830*
	ACTTCCTTTAGCCAGCCATT **TGG**	*Off-T3: 5' UTR of *Pp3c7_6260*
PHY5c	TCGCGGTTGCAATCCCTTCC **CGG**	*Off-T1: Exon of *Pp3c12_9240*

[a]: Mismatch of off-target sequence with respect to the crRNA sequence is shown in yellow.
*: Off-targets for which the activity of the sgRNA was analyzed through PCR screening and high-resolution PAGE gels in six mutants.

Table 4. List of primers used in the multiplex *PHY* gene editing via single-cut.

Name	Primer sequence	Description
FST5 FW	CCCAAGAAGACATACTCCTCAAC	*(Pp.PHY1)*PCR screening
FST6 RV	GAAGTGCTGCATCTGCGGTT	*(Pp.PHY1)*PCR screening
FST7 FW	GTCAGGGAGTTCTGTGAAGTCA	(*Pp.PHY2)* PCR screening
FST8 RV	TCCAGATTCTTCGTACACAGCC	(*Pp.PHY2)* PCR screening
FST11 FW	CTTACTCCTCCACAAGTTCG	*(Pp.PHY3)* PCR screening
FST12 RV	TTTCAAACACAGCATGAAGG	*(Pp.PHY3)* PCR screening
FST13 FW	AAAGTGGTTCAGGACAAGGAT	(*Pp.PHY4)* PCR screening
FST14 RV	GAGTTCATGTTGCCCATGTAT	(*Pp.PHY4)* PCR screening
ST15 FW	GCTTACAGCGAGAATGCTCT	(*Pp.PHY5a)* PCR screening
ST16 RV	CAATGATCTCGAGTCGGTTCC	(*Pp.PHY5a)* PCR screening
FST17 FW	ACAGTGAGAATGCGCCCGAA	(*Pp.PHY5b)* PCR screening
FST18 RV	CATCGGTTCCGATTCCGAGG	(*Pp.PHY5b)* PCR screening
FST19 FW	ATTCCCACAAATTGGCAGCT	(*Pp.PHY5c)* PCR screening
FST20 RV	CCACAACTGCATCACACAGT	(*Pp.PHY5c)* PCR screening
FST37 FW	GCTACCGGATCTCGGAGTTG	(*Pp.PHY1)* Sequencing reaction
FST38 RV	GAGAGGCGACACTTGAAGCT	(*Pp.PHY1)* Sequencing reaction
FST23 FW	GAGCTGCCTGGTTTAGTGAC	(*Pp.PHY2)* Sequencing reaction
FST24 RV	TCAGCATAGTCACATCCACA	(*Pp.PHY2)* Sequencing reaction
FST35 FW	ACACTCGGCTACAGTTCTGC	(*Pp.PHY3)* Sequencing reaction
FST36 RV	GTCCCGATTCCTAGCGTGTTTAT	(*Pp.PHY3)* Sequencing reaction
FST26 FW	ATGCCGTTGTGTCCTCCGCA	(*Pp.PHY4)* Sequencing reaction
FST27 RV	GTGTGATTCCCAAAAGCCAAAACCT	(*Pp.PHY4)* Sequencing reaction
ST33 FW	GAATCAAACGACTCTGGGGA	(*Pp.PHY5a)* Sequencing reaction
ST34 RV	CTGTTGCAGGATAATGTAGCC	(*Pp.PHY5a)* Sequencing reaction
FST31 FW	ACACCTCATAGCGGTTTTGG	(*Pp.PHY5b)* Sequencing reaction
FST32 RV	ACTTCCTCCACAACTGCGTC	(*Pp.PHY5b)* Sequencing reaction
FST29 FW	GTCAAGCTGCCAAAGCAACC	(*Pp.PHY5c)* Sequencing reaction
FST30 RV	CAAGAGTGATTGGCTGACGC	(*Pp.PHY5c)* Sequencing reaction
PHY1_OFFT2 FW	GCTTGCCGACGGATCATCTT	Off-target analysis
PHY1_OFFT2 RV	TCCTCAATAGCGGCACCAAAA	Off-target analysis
PHY2_OFFT2 FW	AAGCAGACAAGGCTGATCCC	Off-target analysis
PHY2_OFFT2 RV	TAGTCATCATCAGCGCGGTC	Off-target analysis
PHY2_OFFT3 FW	CTTGGGACGGAGAGAAGGTG	Off-target analysis
PHY2_OFFT3 RV	ACTGCTTTCCTGCAAATCGC	Off-target analysis
PHY5a_OFFT1 FW	GGTAAACGCGCGCAAAAGAT	Off-target analysis
PHY5a_OFFT1 RV	CACTCTTCTGGCGGTACGTC	Off-target analysis
PHY5b_OFFT1 FW	GAATGCGCCAGAGATGCTTG	Off-target analysis
PHY5b_OFFT1 RV	AAAGGAGGCCAATGTCTCCG	Off-target analysis
PHY5b_OFFT2 FW	TAAGGGCGTGTCGGATTGTT	Off-target analysis
PHY5b_OFFT2 RV	AAGACCTCACCGTGTTCGTC	Off-target analysis
PHY5b_OFFT3 FW	AGCTTCCTCACCTCGCCTTC	Off-target analysis
PHY5b_OFFT3 RV	CCGAACCCTGTCCCAAATGT	Off-target analysis

Table 5. Percentage of frameshift mutations per gene compared to Lindel frameshift predictions available at CRISPOR website.

Target gene	Lindel prediction (%)	Frameshift mutations (%)*
Pp.PHY1	81	83
Pp.PHY2	80	87
Pp.PHY3	79	83
Pp.PHY4	85	93
Pp.PHY5a	87	75
Pp.PHY5b	77	23
Pp.PHY5c	89	100

*:(∑ frameshift mutations by gene in the multiplex gene editing/∑ mutations by gene in the multiplex gene editing) x100

Acknowledgements

I am deeply grateful to Prof. Jon Hughes for giving me the opportunity to work on this fascinating research project. His invaluable guidance, enthusiasm and stoic patience helped me immensely throughout the course of my Ph.D..

I would like to thank Prof. Mathias Zeidler for his insightful comments and suggestions during our group seminars, which helped to shape this project.

I would like to thank Tanja from the bottom of my heart, not only for her excellent technical assistance, but also for her unwavering support, motivation and precious friendship.

I would also like to thank all the other members of the Institute of Plant Physiology: Christina Lang, Sonja Graf, Anette Mündelein, Roland Kürschner, Soshichiro Nagano, Peng-Yuan Chen, Kaoling Guan, Nicole Bazant, for the kind help and support that have made my work and life in Germany a wonderful experience.

Finally, I would like to thank my family for their great understanding and encouragement throughout my studies.

I declare that I have completed this dissertation single-handedly without the unauthorized help of a second party and only with the assistance acknowledged therein. I have appropriately acknowledged and cited all text passages that are derived verbatim from or are based on the content of published work of others, and all information relating to verbal communications. I consent to the use of an anti-plagiarism software to check my thesis. I have abided by the principles of good scientific conduct laid down in the charter of the Justus Liebig University Giessen "Satzung der Justus-Liebig-Universität Gießen zur Sicherung guter wissenschaftlicher Praxis" in carrying out the investigations described in the dissertation.

Place and Date: Signature: